ISSN 0503-1540

Tome 32 *Août* *1994* Numéro 3

La mer

うみ

1994 年 8 月

日 仏 海 洋 学 会

La Société franco-japonaise
d'océanographie
Tokyo, Japon

Note pour la présentation des manuscrits

La mer, organe de la Société franco-japonaise d'océanographie, publie des articles et notes originaux, des articles de synthèse, des analyses d'ouvrages et des informations intéressant les membres de la société. Les sujets traités doivent avoir un rapport direct avec l'océanographie générale, ainsi qu'avec les sciences halieutiques.

Les manuscrits doivent être présentés avec un double, et dactylographiés, en *double interligne*, et au recto exclusivement, sur du papier blanc de format A4 (21×29,7 cm). Les tableaux et les légendes des figures seront regroupés respectivement sur des feuilles séparées à la fin du manuscrit.

Le manuscrit devra être présenté sous la forme suivante:

1° Il sera écrit en japonais, français ou anglais. Dans le cadre des articles originaux, il comprendra toujours le résumé en anglais ou français de *200 mots* environs. Pour les textes en langues européennes, il faudra joindre en plus le résumé en japonais de *500 lettres* environs. Si le manuscrit est envoyé par un non-japonophone, le comité sera responsable de la rédaction de ce résumé.

2° La présentation des articles devra être la même que dans les numéros récents; le nom de l'auteur précédé du prénom *en entier*, en minuscules; les symboles et abréviations standards autorisés par le comité; les citations bibliographiques seront faites selon le mode de publication: article dans une revue, partie d'un livre, livre entier, etc.

3° Les figures ou dessins originaux devront être parfaitement nettes en vue de la réduction nécessaire. La réduction sera faite dans le format 14,5×20,0 cm.

La première épreuve seule sera envoyée à l'auteur pour la correction.

Les membres de la Société peuvent publier 7 pages imprimées sans frais d'impression dans la mesure à leur manuscrit qui ne demande pas de frais d'impression excessifs (pour des photos couleurs, par exemple). Dans les autres cas, y compris la présentation d'un non-membre, tous les frais seront à la charge de l'auteur.

Cinquante tirés-à-part peuvent être fournis par article aux auteurs à titre gratuit. On peut en fournir aussi un plus grand nombre sur demande, par 50 exemplaires.

Les manuscrits devront être adressés directement au directeur de publication de la Société: Y. YAMAGUCHI, Université des Pêches de Tokyo, Konan 4-5-7, Minato-ku, Tokyo, 108 Japon; ou bien au rédacteur étranger le plus proche: H. J. CECCALDI, EPHE, Station marine d'Endoume, rue Batterie-des-Lions, 13007 Marseille, France; E. D. GOLDBERG, Scripps Institution of Oceanography, La Jolla, California 92093, Etats-Unis; T. ICHIYE, Department of Oceanography, Texas A & M University, College Station, Texas 77843, Etats-Unis; ou T. R. PARSONS, Department of Oceanography, University of British Columbia, Vancouver, B. C. V6T 1W5, Canada.

La mer 32: 153–165, 1994
Société franco-japonaise d'océanographie, Tokyo

Tide and Tidal Current in the Yellow/East China Seas*

Tetsuo YANAGI** and Kouichi INOUE**

Abstract: The four major components of tides and tidal currents, M_2, S_2, K_1 and O_1 in the Yellow/East China Seas are well reproduced except amphidromic points of M_2 and S_2 in Liautung Bay with use of the horizontal two-dimensional numerical model with a cartesian coordinate of β-plane. The curvature of the earth does not affect the tidal phenomena there. The characteristics of tides and tidal currents in the Yellow/East China Seas are discussed.

1. Introduction

The Yellow/East China Seas (including Bohai Sea) are one of the largest shelf sea in the world (Fig. 1). Much land-derived materials flow into this shelf sea from large rivers such as Huanghe, Changjiang and so on. They are advected by residual flow and dispersed mainly by tidal current, which is the most dominant flow there, and some of them deposit to the bottom of this shelf sea and others flow out to the Pacific Ocean through the shelf edge or to the Japan Sea through the Tsushima Strait. It is very important to reveal the characteristics of tidal current in the Yellow/East Chian Seas in order to clarify the material transport there.

AN (1977) carried out a numerical experiment with the cartesian co-ordinate of f-plane including the tide-generating potentials on M_2 tide in the Yellow Sea. CHOI (1980) revealed the characteristics of four major tidal components, M_2, S_2, K_1 and O_1 in the Yellow/East Chian Seas with use of the horizontal two-dimensional numerical model under the spherical co-ordinate of β-plane neglecting the tide-generating potentials. Moreover, CHOI (1984) revealed the three-dimensional structure of M_2 tidal current in the Yellow/East Chian Seas with use of linear numerical model except a quadratic bottom friction.

As for field observation of tides there, the work by OGURA (1933) is very famous and it has been used for the verification of numerical experiments. Recently, NISHIDA (1980) reconstructed the co-tidal and co-range charts of four major tidal components there with new tidal data.

Here we try to reveal the characteristics of tides and tidal currents in the Yellow/East Chian Seas with use of two-dimensional numerical model under the cartesian co-ordinate of β-plane. The aim of this paper is to compare our results with those by CHOI (1980) under the spherical co-ordinate and to investigate the effect of earth's curvature to the tidal phenomena in the Yellow/East Chian Seas.

2. Field date

The amplitude spectra of tides at two representative stations (OGURA, 1941) are shown in Fig. 2. M_2 tide is the most dominant and S_2, N_2, K_1, and O_1 components are dominant. Though Sa component is also dominant, we do not treat it in this paper, because it is mainly governed by meteorological effects, that is, by the seasonal variations in water temperature, air pressure and sea surface wind. Such meteorological effects on the currents there were already investigated by YANAGI and TAKAHASHI (1993). Therefore, we try to reproduce major components of M_2, S_2, N_2, K_1 and O_1 tides and tidal currents in the Yellow/East Chian Seas in this paper.

3. Numerical model

The horizontal two-dimensional momentum and continuity equations for tide and tidal current in the homogeneous fluid under the cartesian co-ordinate are as follows (YANAGI and OKAMOTO, 1985),

* Received May 4, 1994
** Department of Civil and Ocean Engineering, Ehime University, Bunkyo 3 Matsuyama 790, Japan

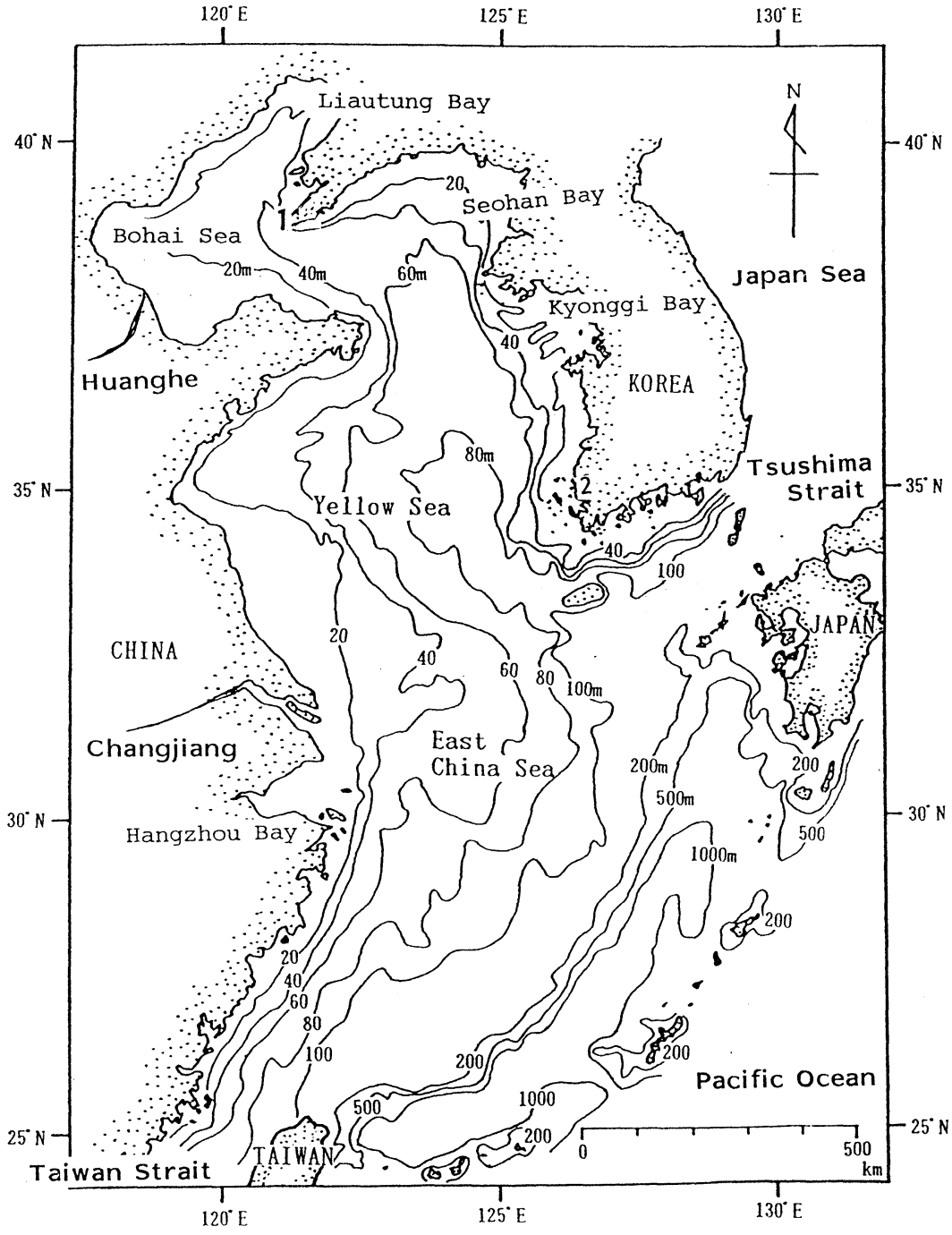

Fig. 1. Yellow/East China Seas. Numbers 1 (Ryozyun), 2 (Gunsan) show the tidal stations.

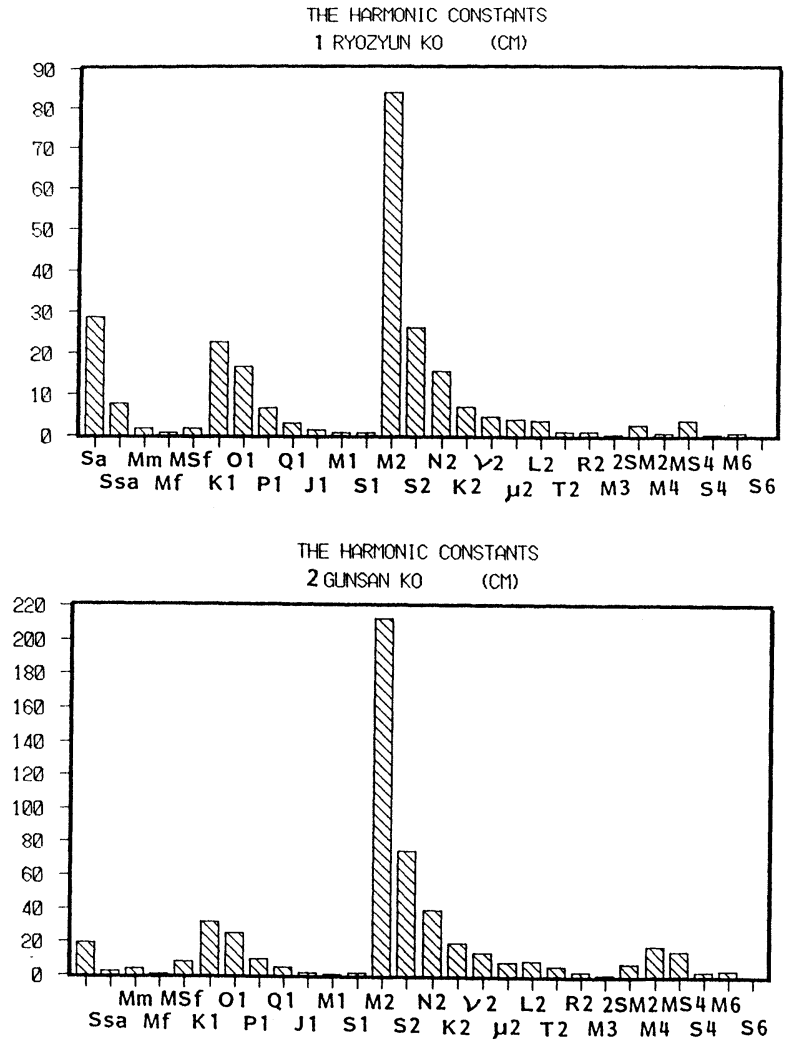

Fig. 2. Tidal amplitude spectra at representative two stations 1 (Ryozyun) and 2 (Gunsan).

$$\frac{\partial u}{\partial t}+(u\cdot\nabla)u+fK\times u= -g\nabla\eta-\frac{\gamma_b{}^2|u|u}{H+\eta}+\nu\nabla^2u \qquad (1)$$

$$\frac{\partial \eta}{\partial t}+\nabla\cdot\{(H+\eta)u\}=0 \qquad (2)$$

Here u is the depth-avereged velocity vector, t time, ∇ the horizontal differential operator, f the Coriolis parameter and $f=f_0+\beta$ ($f_0=7.7\times10^{-5}\mathrm{s}^{-1}$ at 33° N and $\beta=0.23\times10^{-5}\mathrm{s}^{-1}\mathrm{degree}^{-1}$), y the difference of latitude from 33° N, K the locally vertical unit vector, g (=980cm s^{-2}) the gravitational acceralation, η the sea surface elevation above the mean sea surface, $\gamma_b{}^2$ (=0.0026) the bottom frictional coefficient, ν (=10^7 cm^2 s^{-1}) the horizontal eddy viscosity, and H the local water depth.

Equations (1) and (2) are approximated by finite-differences and are solved by the primitive method. The grid size is 25 km × 25 km. The observed tidal amplitude and phase lag are given along three open boundaries, Tsushima Strait, 300 m iso-bath and Taiwan Strait shown in Fig. 3, on the basis of co-tidal and co-range

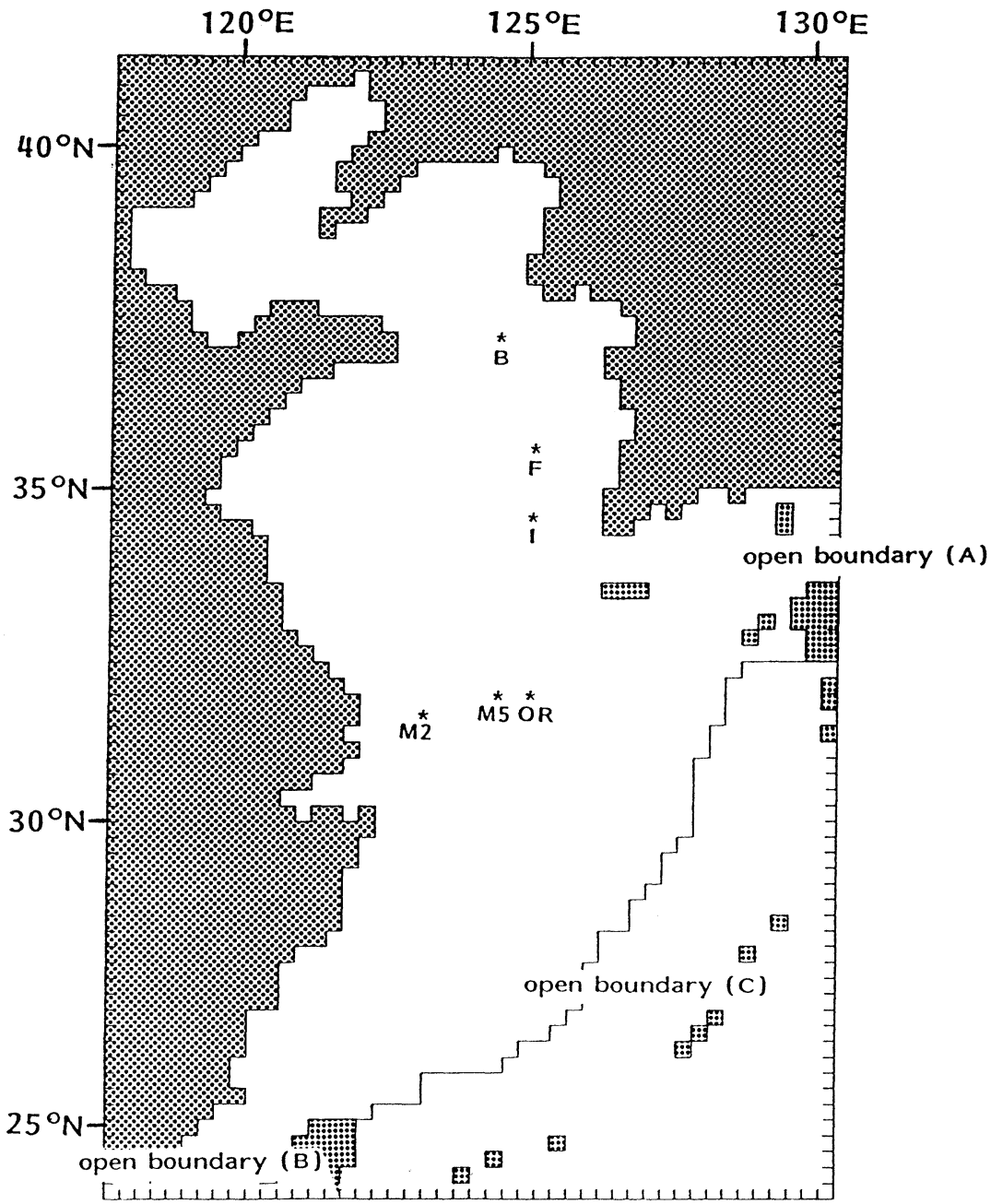

Fig. 3. Numerical model with open boundaries. The symbol shows the observation station of tidal current and its result is shown in Fig. 6.

charts by NISHIDA (1980). The quasi-steady state is obtained four tidal cycles after the beginning of the calculation and the harmonic analysis of sea surface elevation and current field is carried out at the 5th tidal cycle.

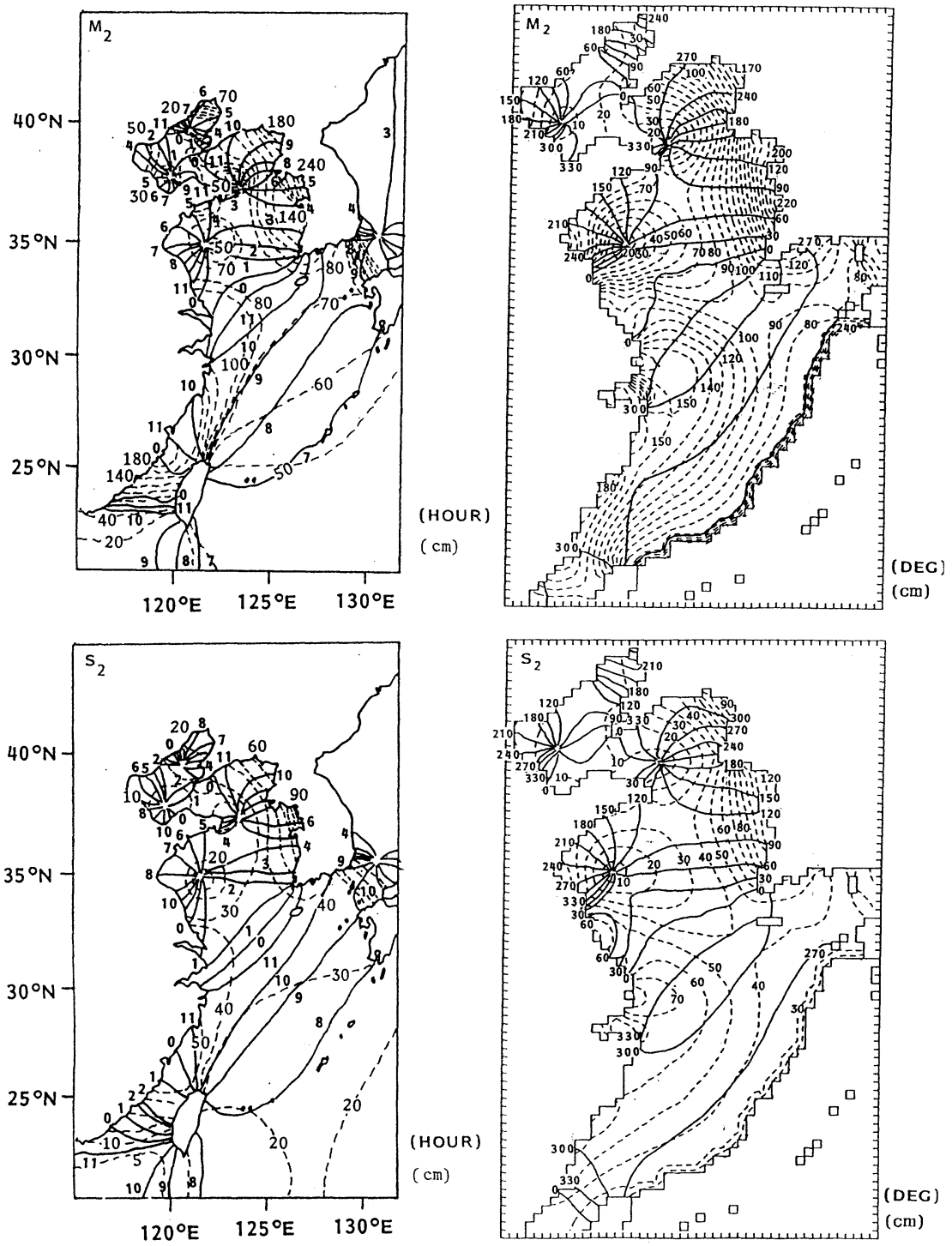

Fig. 4. Observed co-tidal (full line) and co-range (broken line) charts (left) and calculated ones right of M_2 and tides in the Yellow/East China Seas.

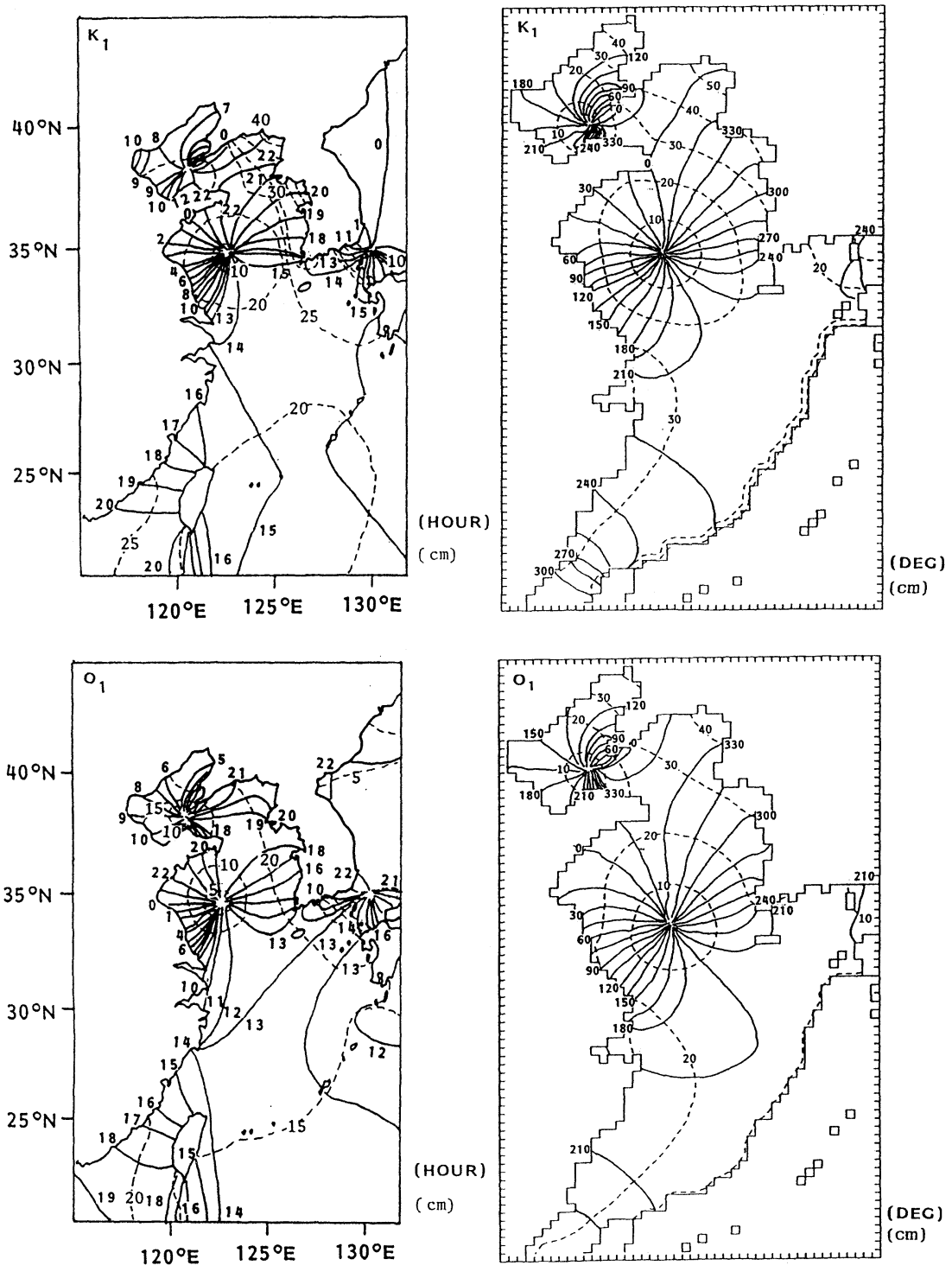

Fig. 4. Observed co-tidal (full line) and co-range (broken line) charts (left) and calculated ones right of K_1 and O_1 tides in the Yellow/East China Seas.

4. Results

4.1. Tides

The calculated co-tidal and co-range charts of four major component tides are shown in Fig. 4 with the observational results by NISHIDA (1980). As for N_2 tide, its co-tidal and co-rauge charts are very similar to those of M_2 and S_2 except the absolute values and they are not shown here. Calculated result of M_2 tide well coincides with the observed ones except an amphidromic point in Liautung Bay. The numerical experiment by AN (1977), which includes the tide-generating potential in the Yellow Sea and Bohai Sea, could not reproduce an amphidromic point of M_2 tide in Liautung Bay. AN (1977) showed that the tidal amplitude due to tide-generating potential was only about 3 % compared to that due to the incident tidal wave from the Pacific Ocean. Therefore, the disagreement of an amphidromic point of M_2 tide in Liautung Bay between the prototype and our numerical model is not due to the neglect of tide-generating potential. Also, such disagreement is not due to the employment of cartesian coordinate of our model because an amphidromic point of M_2 tide in Liautung Bay was not reproduced by CHOI (1980) with the spherical coordinate neglecting the tide-generating potential. The amphidromic point of S_2 tide in Liautung Bay is also not reproduced as shown in Fig. 4. The formation of amphidromic point is the problem of reflection of Kelvin wave at the back of the bay. LARSEN *et al.* (1985) inferred that such discrepancy of amphidromic point between the prototype and the numerical model might be due to poor grid resolution and the unnatural orientation of the grid system with respect to the coastal shape. Anyway, the reproduction of amphidromic point of semi-diurnal tides in Liautung Bay will be a future problem to be solved.

The amplitude of M_2 tide is over 160 cm at Seohan Bay, Kyonggi Bay (Inchon Bay is situated at the head of Kyonggi Bay) and Hangzhou Bay. The amplitude of S_2 tide exceeds 80 cm at the same places. AN (1977) showed that the resonance of semi-diurnal tide occurred in Kyonggi Bay, where the period of normal oscillation $T = 4L/(gH)^{1/2}$ (L : length of the bay $=100$ km and H : the depth of the bay $=10$ m) was about 10 hours and it was very near that of semi-diurnal tides, and the tidal range was unstably amplified in the frictionless case. CHOI (1980) showed that such resonance was not occurred in the case of no Coriolis force because the propagation characteristic of M_2 tidal wave in the Yellow Sea was completely changed.

As for K_1 and O_1 tides, the calculated results well reproduce the observed one as shown in Fig. 4. The amplitude of K_1 and O_1 tides are ovre 40 cm and 30 cm, respectively, at the head of Liautung Bay and in Seohan and Kyonggi Bays. Amphidromic points of K_1 and O_1 tides are situated in the central part of the Yellow Sea while those of M_2 and S_2 tides near the Chinese Coast. Such facts suggest that the friction to diurnal tide is smaller than that to semi-diurnal tide in the Yellow Sea.

4.2. tidal currents

The current patterns of M_2 tidal current at the times of maximum flood and maximum ebb near the mouth of Changjiang are shown in Fig. 5 (a). The phase lag of M_2 tidal current between southern Chinese coast and Kyonggi Bay is about 180 degree, that is, the maximum flood current occurs in Kyonggi Bay when the maximum ebb current along the southern Chinese coast. The phase lag between Kyonggi Bay and Seohan Bay is also about 180 degree as shown later. S_2 tidal current has nearly the same pattern as M_2 tidal current except the maximum current speed of 40 to 50 cm s^{-1} (not shown). The current patterns of K_1 tidal component at the times of maximum flood and maximum ebb near the mouth of Changjiang are shown in Fig. 5 (b). The maximum current speed is about 20 cm s^{-1} and the strong current does not occur along the Korean coast. This may be due to the near-resonant responese is only occurred in the period of M_2 or S_2 tidal components in Kyonggi Bay.

The comparisons of calculated tidal current ellipses and observed ones (CHOI, 1986) at some representative stations, shown in Fig. 3, are shown in Fig. 6 (a) and (b). The full circle in the left part shows the observational result, the dotted one in the left the calculated one by CHOI (1986) and the full circle in the right our result. The calculated M_2 and K_1 tidal current ellipses

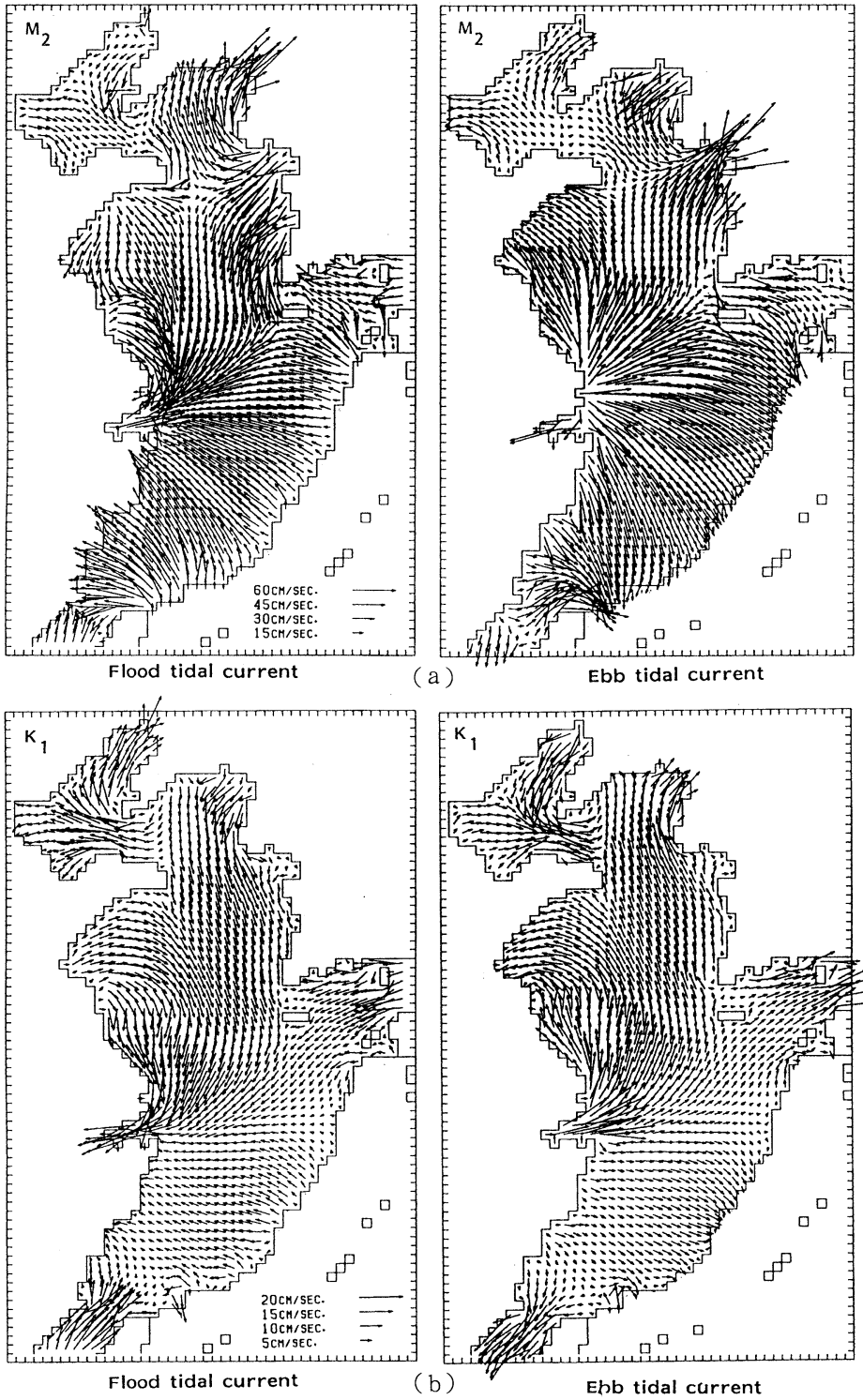

Fig. 5. Maximum flood (left) and ebb (right) tidal current at the river mouth of Changjiang in M_2 (a) and K_1 (b) components.

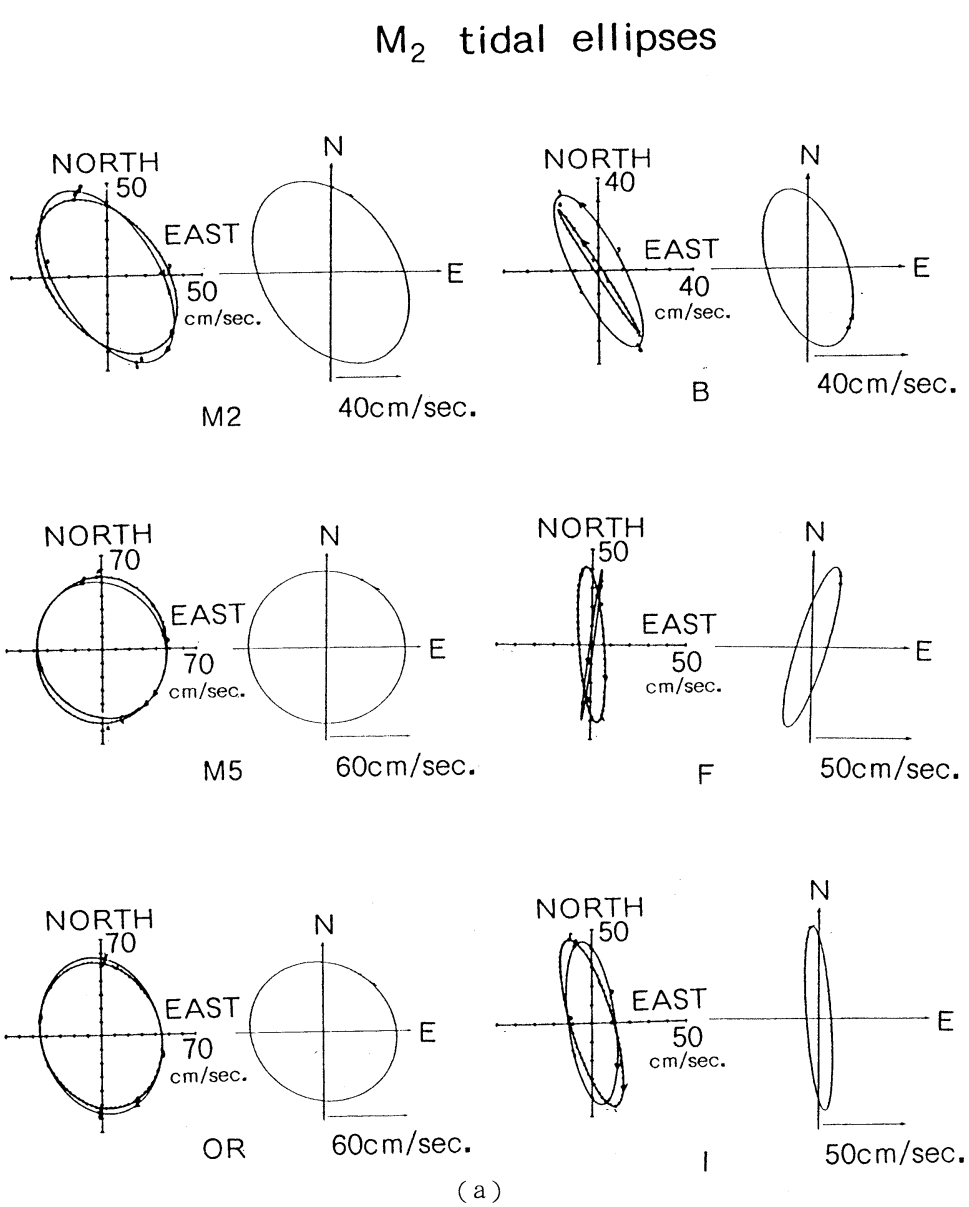

Fig. 6. Observed (full line in the left), calculated by CHOI (1986) (dotted line in the left) and calculated in the present model (full line in the right) M_2 (a) and K_1 (b) tidal current ellipses at representative stations shown in Fig. 3.

by our model well reproduce the observed ones and they are similar to those by CHOI (1986) as shown in Fig. 6.

The co-tidal and co-amplitude charts of four major tidal current components are shown in Fig. 7. The amplitudes of M_2 and S_2 tidal currents are over 80 cm s^{-1} and 50 cm s^{-1}, respectively, in Seohan, Kyonggi and Hangzhou Bays and at the southwestern tip of Korea Peninsula. The amplitudes of K_1 and O_1 tidal currents are over 20 cm s^{-1} at the mouth of Bohai Sea and in Hangzhou Bay.

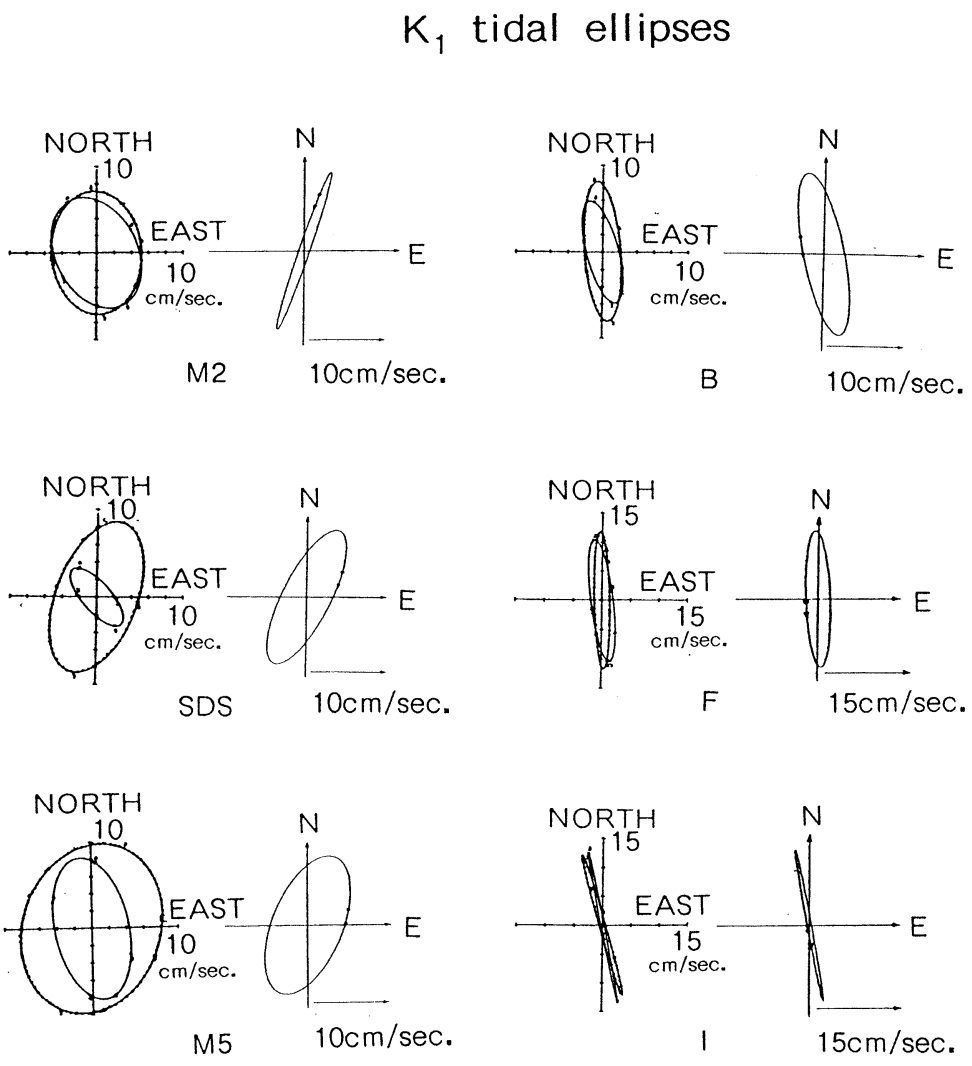

(b)

Fig. 6. Observed (full line in the left), calculated by CHOI (1986) (dotted line in the left) and calculated in the present model (full line in the right) M_2 (a) and K_1 (b) tidal current ellipses at representative stations shown in Fig. 3.

4.3. Tide-induced residual currents

The calculated tide-induced residual currents by M_2 and K_1 tides, which were obtained by averaging calculated tidal currents over one-tidal cycle, are shown in Fig. 8. The speed of tide-induced residual currents are very weak, that is, they are less than 2 cm s^{-1} in the central part of Yellow/East China Seas except the particular reginos, e.g. at the mouth of Bohai Sea in the case of K_1 tide and at the south-western tip of Korea Peninsula in the case of M_2 tide. We cannot find the remarkable large-scale tide-induced residual circulations in the central part of Yellow/East China Seas from Fig. 8.

We carried out the same experiments with the cartesian co-ordinate of f-plane (that is, the

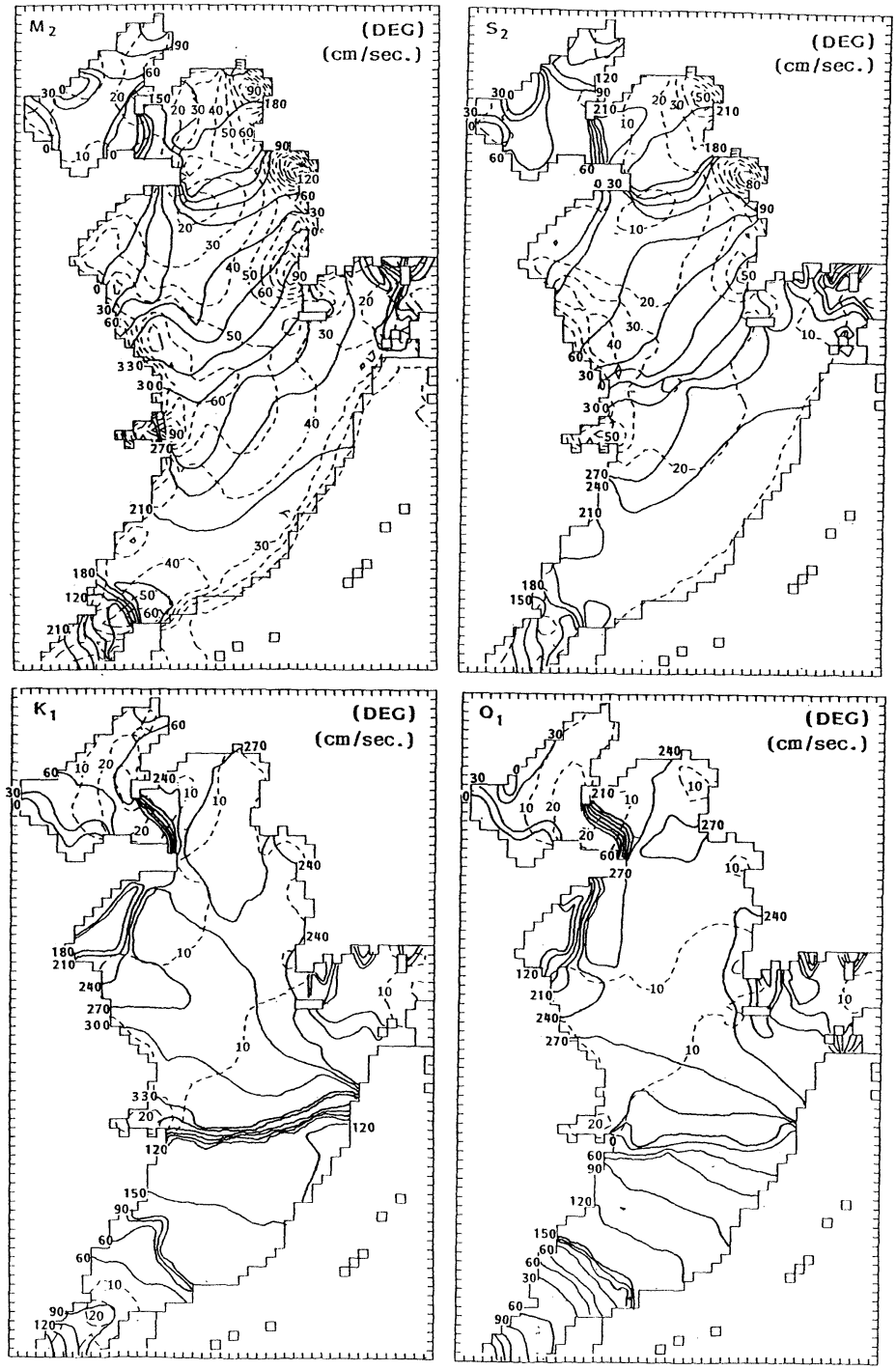

Fig. 7. Calculated co-tidal (full line) and co-amplitude (broken line) charts of M_2, S_2, K_1 and O_1 tidal currents.

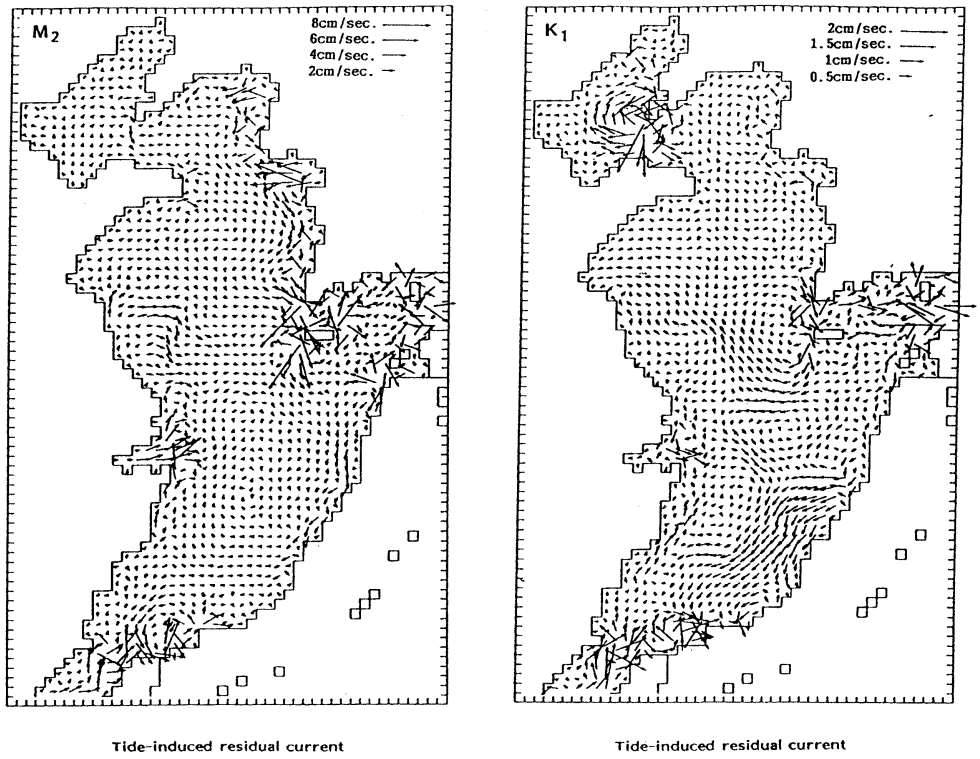

Fig. 8. Calculated tide-induced residual current of M_2 (left) and K_1 (right) tidal component.

Coriolis parameter is constant), but the results were nearly the same (not shown).

5. Conclusion

We developed two-dimensional numerical model under the cartesian co-ordinate of β-plane in the Yellow/East China Seas and compared its results with those of field observations and those of CHOI (1980 and 1986). The calculated tides and tidal currents of four major tidal components by our model well reproduce the observed ones and they are nearly the same as those of CHOI (1980 and 1986) which used the spherical co-ordinate of β-plane. We also carried out the numerical experiments with f-plane, but the calculated results are nearly the same as those with β-plane. Such recults suggest that the curvature of the earth (spherical co-ordinate and β-effect) dose not affect the tidal phenomena in the Yellow/East China Seas.

Acknowledgments

The authors express their sincere thanks to Dr. H. TAKEOKA of Ehime University for his useful discussions, to Mr.S.TAKAHASHI for his help in numerical experiments and to Prof.B. H. CHOI for sending many valuable reprints. This study is a part of MASFLEX funded by the Agency of Science and Technology, Japan.

References

AN, H.S. (1977): A numerical experiment of the M_2 tide in the Yellow Sea. J. Oceanogr. Soc. Japan, **33**, 103–110.

CHOI, B.H. (1980) : A tidal model of the Yellow Sea and the eastern China Sea. KORDI Report 80-02, 72p.

CHOI, B.H. (1984): A three-dimensional model of the East China Sea. *In* "Ocean Hydrodynamics of the Japan and East China Seas" T. ICHIE (ed), Elsevier, Amsterdam, 209–224.

CHOI, B.H. (1986): Predictions of sand transport directions of the offshore tidal sand banks in

the Yellow Sea. 5th Congress Asian and Pacific Regional Division International Association for Hydraulic Research, 231–247.
LARSEN, L.H., G.A. CANNON and B.H. CHOI (1985) East China Sea tidal currents. Cont. Shelf Res., **4**, 77–103.
NISHIDA, H. (1980): Improved tidal charts for the western part of the north Pacific Ocean. Report of Hydrographic Researches, **15**, 55–70.
OGURA, S. (1933): The tides in the sea adjacent to Japan. Bulletin of the Hydrographic Department, Imperial Japanese Navy, **7**, 1–189.
OGURA, S. (1941): Tides. Iwanami Co., Tokyo, 252 pp. (in Japanese).
YANAGI, T. and Y. OKAMOTO (1985): A numerical simulation of oil spreading on the sea surface. La mer, **22**, 137–146.
YANAGI, T. and S. TAKAHASHI (1993): Seasonal variation of circulations in the East China Sea and the Yellow Sea. J. Oceanogr., **49**, 503–520.

黄海・東シナ海の潮汐・潮流

柳　哲雄・井上康一

要旨：水平2次元β平面デカルト座標を用いた数値モデルで黄海・東シナ海の潮汐・潮流を計算した。Liautung湾の半日周潮の無潮点が計算により再現されないことを除けば4大分潮の計算結果は観測結果をよく再現した。又この計算結果はf平面の結果やCHOI（1980）の水平2次元球面座標の結果とほとんど同一である。このことは地球の曲率は黄海・東シナ海の潮汐潮流現象にほとんど影響していないことを示唆している。

La mer 32: 167–172, 1994
Société franco-japonaise d'océanographie, Tokyo

Some Indications of Excess CO_2 Penetration near Cape Adare off the Ross Sea*

Chen-Tung Arthur CHEN

Abstract: The Antarctic Bottom Water (AABW) is generally believed to be formed in the Weddell Sea. It contains little anthropogenic CO_2. The role of the Ross Sea as a sink for excess CO_2 is perhaps even smaller as it contributes much less to AABW than does the Weddell Sea. On the other hand, I have reported earlier that excess CO_2 is found on the shelf around the Antarctica. Excess CO_2 is also found to penetrate rather deeply off Cape Adare at the northwest corner of the Ross Sea. I report here more detailed analysis using the GEOSECS, International Geophysical Year and the R/V Polar Sea data.

1. Introduction

Thermohaline circulation transports warm water poleward from low latitudes. As surface waters cool, their capacity to absorb CO_2 from the atmosphere increases and they act as a sink for anthropogenic CO_2. The ability of the North Atlantic Deep Water to absorb the excess CO_2 has been demonstrated (CHEN, 1982, 1987) but the situation is somewhat different in the Southern Ocean where the Antarctic Bottom Water (AABW) plays a mojor role. The AABW is generally believed to be formed in the Weddell Sea. Sea ice, however, blocks the air-sea exchange of gases thus limits the influx of excess CO_2 to the surface water. The upwelled Weddell Sea Deep Water (WSDW) dilutes the anthropogenic CO_2 concentration in the surface water, which then mixes with the Weddell Sea Shelf Water and more WSDW to from AABW. Since the WSDW probably was formed before industrialization and the surface water is also deficient in excess CO_2, the AABW contains little anthropogenic CO_2 (6 ± 5 μmol kg^{-1}) (CHEN and POISSON, 1984, POISSON and CHEN, 1987). As a result, the Weddell Sea is not a major sink for excess CO_2 (CHEN and RODMAN, 1990; CHEN, 1991).

The role of the Ross Sea as a sink for excess CO_2 is perhaps even smaller as it contributes much less to AABW than does the Weddell Sea. Recent data, however, indicates that freons have penetrated throughout the shelf area and have even appeared near the base of the continental slope at depths of 2.5 to 3.0 km. This is a good indication of newly formed AABW (MICHEL *et al.*, 1985; TRUMBORE *et al.*, 1991) which may carry some excess CO_2.

CHEN (1982) reported earlier that excess CO_2 is found on the shelf around the Antarctica. Excess CO_2 is also found to penetrate rather deeply off Cape Adare at the northwest corner of the Ross Sea (CHEN, 1987; 1993a). I report here more detailed analysis using the GEOSECS and International Geophysical Year (IGY) data. The R/V Polar Sea (JACOBS *et al.*, 1989) CO_2 data are spaced too far apart vertically and can not be used to estimate the excess CO_2 signal. The chlorofluorocarbons (CFCs) collected during the R/V Polar Sea cruise are, however, quite usefull for tracing newly formed waters. To my knowledge no other CO_2 or tracer data are available. The station locations are given in Fig. 1.

2. Method

The method of excess CO_2 computation and its limitations have been described in detail elsewhere (CHEN and MILLERO, 1979; CHEN and PYTKOWICZ, 1979; CHEN *et al.*, 1982: CHEN, 1982, 1984: CLINE *et al.*, 1985). The method involves a back-calculation of the CO_2 concentration of a parcel of seawater to its initial concentration at the sea surface by correcting

* Received June 30, 1994
** Institute of Marine Geology, National Sun Yat-Sen University, Kaohsiung, Taiwan, R.O.C.

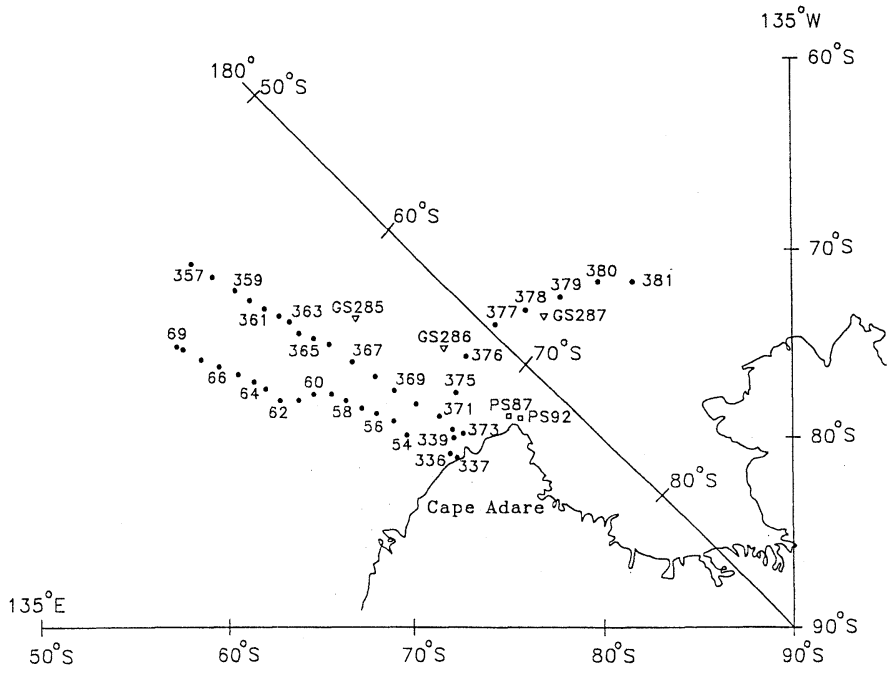

Fig. 1. Station locations in the study area (▽ GEOSECS; ● IGY; □ Polar Sea).

for changes due to the decomposition of organic material and dissolution of carbonate tests.

Specifically, the method assumes that a water parcel maintains a fixed degree of saturation with respect to atomospheric CO_2 at the sea surface. Respiration and carbonate dissolution add carbon dioxide to the water parcel after it sinks. The respiration induced increase in CO_2 can be calculated from the oxygen data using Redfield ratio (REDFIELD *et al.*, 1963) while CO_2 changes due to carbonate dissolution can be calculated from the alkalinity changes. By correcting the CO_2 data for these changes, estimates can be made of the CO_2 concentration of the water parcel when it was last in contact with the atmosphere. These back calculated CO_2 concentrations of waters with various ages are then compared with each other and with the contemporary surface CO_2 concentrations to obtain the oceanic CO_2 increase.

3. Results and Discussion

Fig. 2 shows the north-south cross-section of excess CO_2 centered along 160° E based on IGY data. The lower boundary of penetration is taken as the level where the excess CO_2 signal equals to $5 \pm 10\,\mu$mol/kg. The depth could be up to 100 m to deep or 300 m to shallow because of the vertical sample spacing and because of the uncertainty in the method.

The thin broken line shows the minimum temperature layer which is probably the modified remnant of the isothermal layer produced during the previous winter (FOSTER and CARMACK, 1976: WEISS *et al.*, 1979). The excess CO_2 content falls between 20 and $30\,\mu$mol/kg with an average of $25\,\mu$mol/kg in this layer.

The maximum temperature contour (broken lines) is near the core of the Circumpolar Deep Water (CDW) which is also at approximately the same level as the maximum AOU (apparent oxygen utilization) layer. Excess CO_2 does not appear to penetrate deeply enough to reach the core of the warm, old CDW. Also the deep and bottom waters do not appear to contain significant amounts of anthropogenic CO_2.

Temperature contours indicate that IGY 62 (at 60° S) is north of the Polar Front. Antarctic Intermediate Water (AAIW), formed by strong vertical convection, apparently carries anthropogenic CO_2 with it more deeply north of the Polar Front. The anthropogenic CO_2 penetrates

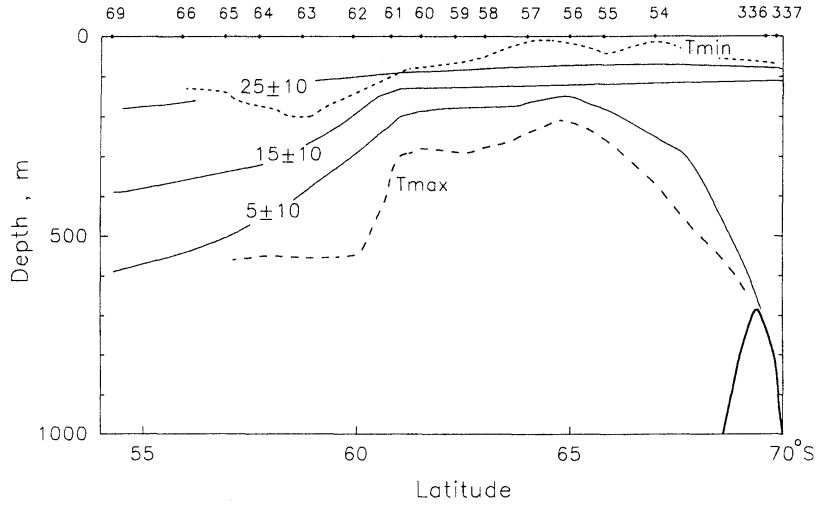

Fig. 2. Excess CO_2 cross-section along 160° E.

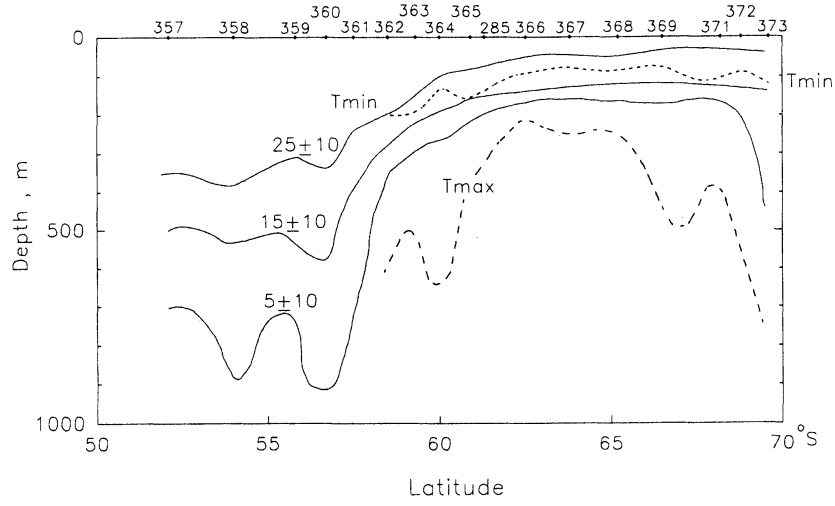

Fig. 3. Excess CO_2 cross-section along 166° E.

less deeply at the more southerly stations due to the upwelling of the old CDW, evidenced by the upwardly concaved structure of the maximum temperature contour. The CDW pushes upward on and disperses the younger Antarctic Surface Water (GORDON *et al.*, 1977, 1984). As a result, the excess CO_2 penetrates less than 300 m between 61 and 66 °S.

South of IGY 54, however, the maximum temperature contour deepens again and intersects the bottom at IGY 336 and 337 near Cape Adare. This is an indication of some downwelling of the fresher, newly cooled seawater. Excess CO_2 also penetrates to near the bottom at these stations which are located on the upper continental slope.

Figure 3 shows the excess CO_2 values at roughly 166° E based on IGY and GEOSECS data. Excess CO_2 penetrates deeper north of the Polar Front near IGY 365. South of the Polar Front the contour concaves upward due to upwelling of CDW but deepens at the southernmost sation, IGY 373. No excess CO_2 is evident in the bottom layer.

Figure 4 shows the west-east cross-section of

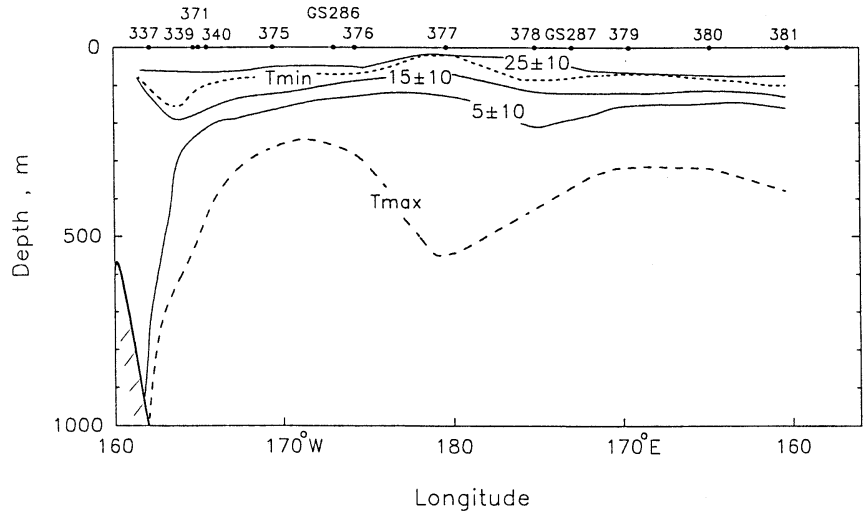

Fig. 4. Excess CO_2 cross-section along 69 °S.

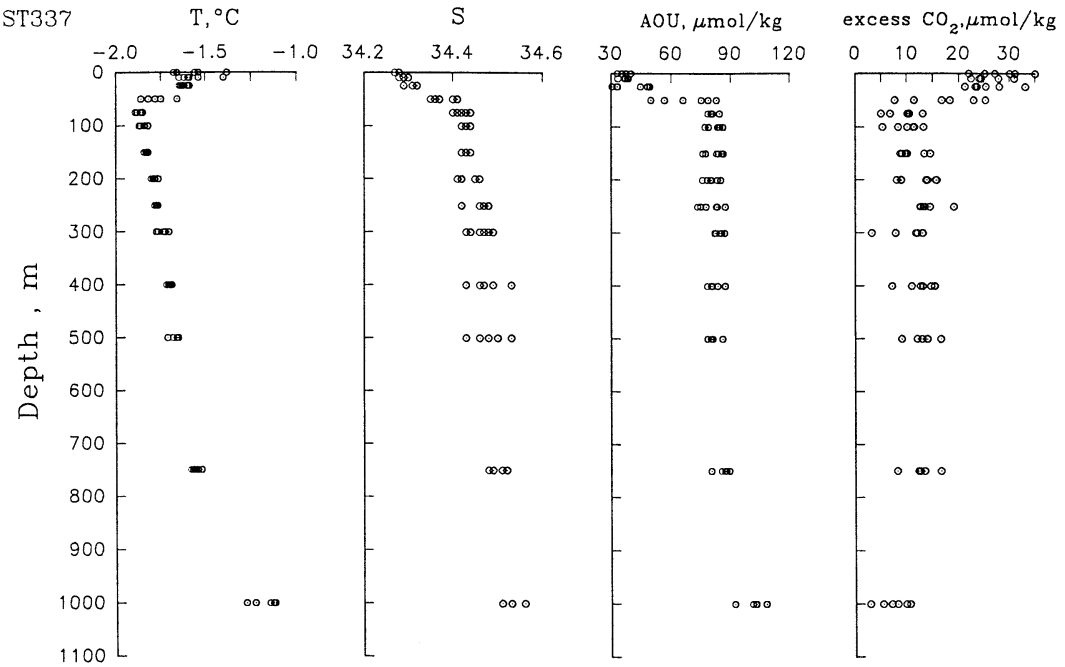

Fig. 5. Temperature, salinity, AOU and excess CO_2 at IGY 337.

excess CO_2 concentration along roughly 69° S based on IGY and GEOSECS data. All stations are south of the Polar Front, and all stations, except for IGY 337, have a water depth deeper than 1000 m. As mentioned earlier, the excess CO_2 penetrates to near the bottom at IGY 337 on the upper continental slope.

IGY 339 sits on the lower continental slope with a water depth of 3350 m. No excess CO_2 could be detected below 250 m at this station (Fig. 4). In fact, all stations except IGY 337 in the cross-section show rather shallow excess CO_2 penetration.

Circulation and hydrography in the vicinity of

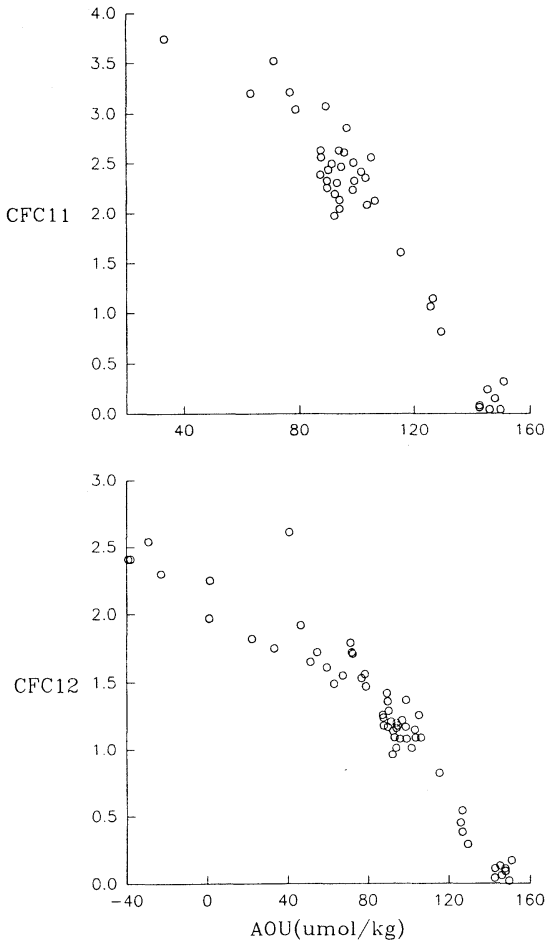

Fig. 6. CFC 11 and CFC 12 concentrations plotted vs. AOU based on the Polar Sea data (JACOBS *et al.*, 1989).

the Ross Sea continental shelf have been reviewed by JACOBS *et al.* (1985). Water on the continental shelf is ultimately derived from CDW, which has upwelled over the continental slope north and east of the Ross Sea, and has been modified by mixing with surface and slope waters. Subsequent interactions with the atmosphere, sea ice and glacial ice cool and reduce the salinities of the shelf waters. These waters eventually become cold and dense enough to move back into and under the CDW to ventilate the deep ocean much like the situation in the Weddell Sea (WEISS *et al.*, 1979; CHEN, 1984). Partial equilibration with atmospheric CO_2 can also occur through gas exchange and mixing with surface and other shelf waters. Direct gas exchange with the atmosphere, however, is limited in winter to breaks and polynyas in the sea ice canopy (TRUMBORE *et al.*, 1991) as sea ice is not entirely permeable to gases (CHEN, 1988). Aa a result, only limited amount of excess CO_2 moves into the winter-formed deep waters on the shelf. The partially ventilated deep water mixes with the surrounding waters as it flows out near the bottom, further diluting the excess CO_2. Finally, the excess CO_2 becomes undetectable excpet in shallow waters or near an area where vertical mixing of the water column occurs quickly.

IGY 337 is an example where vertical mixing occurrs quickly as evidenced by its uniformly low temperature throughout the water column, all between -1.2 and -1.8°C. The salinity varies only between 34.4 and 34.5 below 100 m. AOU varies between 80 and 105 μmol/kg below 100 m (Fig. 5). The relatively low temperature and AOU are indications of rapid turnover.

Earlier work elsewhere has shown a correlation between CFC-11 and excess CO_2 (CLINE *et al.*, 1985; CHEN, 1993b). The Polar Sea stations 87 and 92 sit on the continental slope (Fig. 1). CFCs 11 and 12 are found throughout the water column (to 339 m for PS 92 and to 2058 m for PS 87). Excess CO_2 probably also exists where CFCs are found. The combined Polar Sea CFCs show a decreasing trend when plotted vs. AOU (Fig. 6), reaching zero at an AOU of only about 150 μmol/kg. The IGY and GEOSECS excess CO_2 signals disappear at an AOU of only about 120 μmol/kg. Because of the poor precision of the excess CO_2 signal, it can not be judged whether the difference is because the excess CO_2 (and CFCs) has penetrated deeper during the Polar Sea expedition, reaching older, higher AOU waters.

4. Conclusion

The excess CO_2 does not penetrate more than a few hundred meters south of the Polar Front near the Ross Sea except for a small area near Cape Adare. As a result, the Ross Sea probably has not been a significant excess CO_2 sink.

Acknowledgements

This research was supported by the National

Science Council (NSC 83-0209-M110-002K). I thank S.S. JACOBS for providing the Polar Sea data.

References

CHEN, C.T. (1982): On the distribution of anthropogenic CO_2 in The Atlantic and the Southern Oceans, Deep-Sea Res., **29**, 563–580.

CHEN, C.T. (1984): Carbonate chemistry of the Weddell Sea, Department of Energy DOE/EV/10611-4, 118pp.

CHEN, C.T. (1987): On the depth of anthropogenic CO_2 penetration in the Atlantic and Pacific Oceans. Oceanologica Acta, sp., 97–102.

CHEN, C.T. (1988): Summer-winter comparisons of oxygen, nutrients and carbonates in the polar seas, La mer, **26**: 1–11.

CHEN, C.T.A.(1991): Descriptive chemical oceanography of the Weddell Sea , Proceedings, National Science Council, **15**, 2, 133–142.

CHEN, C.T.A. (1993a): The oceanic anthropogenic CO_2 sink, Chemosphere, **27**, 1041–1064.

CHEN, C.T.A. (1993b): Anthropogenic CO_2 distribution in the North Pacific Ocean, J. Oceanogr. **49**, 257–270.

CHEN, C.T. and F.J. MILLERO (1979): Gradual increase of oceanic carbon dioxide, Nature, **277**, 205–206.

CHEN, C.T. and R.M. PYTKOWICZ (1979): On the total, CO_2-titration alkalinity-oxygen system in the Pacific Ocean, Nature, **281**, 362–365.

CHEN, C.T., F.J. MILLERO and R.M. PYTKOWICZ (1982): Comment on "calculating the oceanic CO_2 increase: a need for caution", by A.M. SHILLER, J. Geophys. Res., **87**, 2083–2085.

CHEN, C.T. and A. POISSON (1984): Excess carbon dioxide in the Weddell Sea, U.S. Antarctic J., Review, 74–75.

CHEN, C.T.A. and M.R. RODMEN (1990): The inhomogeneous distribution of tritium and radiocarbon in the abyssal Southern Ocean, Terrestrial Atmospheric and Oceanic Sciences, **1**, 91–109.

CLINE, J.D., R.A. FEELY, K. KELLY-HANSEN, J.F. GENDRON, D.P. WISEGARVER and C.T. CHEN (1985): Current inventory of anthropogenic carbon dioxide in the North Pacific gyre. NOAA Technical Memorandum, ERL PMEL-60, 46pp.

FOSTER T.D. and E.C. CARMACK (1976): Frontal zone mixing and Antarctic Bottom Water formation in the Southern Weddell Sea. Deep-Sea Res., **23**, 301–317.

GORDON A.L., D.T. GEORGI and H.W. TAYLOR (1977): Antarctic polar front zone in the Western Scotia Sea - summer 1975, J. Phys. Oceanogr., **7**, 309–328.

GORDON A.L., C.T. CHEN and W.G. METCALF (1984): Winter mixed layer entrainment of the Weddell deep water, J.Geophys. Res., **89**, 637–640.

JACOBS S.S., R.G. FAIRBANKS and Y. HORIBE (1985): Origin and evolution of the water masses near the Antarctic Continental Margin: evidence from $H_2{}^{18}O/H_2{}^{16}O$ ratios. *In*: Oceanol. Ant. Cont. Shelf, Ant. Res. Ser. 43, AGU, 59–85.

JACOBS S., W. HAINES, J.L. ARDAI Jr and P. MELE (1989): Ross Sea Oceanographic Data, 1983–1987, LDGO 89-4, Lamont-Doherty Geological Observatory of Columbia University, Palisades, NY.

MICHEL, R.L., R.S. KEIR. and A. SCHROEDER (1985): Chemical Oceanography during the 1985 Wilkes Land Expedition. Antarctic Journal of the United States, **20**, 105–106.

POISSON, A. and C.T.A. CHEN (1987): Why is there little anthropogenic CO_2 in the Antarctic bottom water? Deep-Sea Res., **34**, 7, 1255–1275.

TRUMBORE, S.E, S.S. JACOBS and W.M. SMETHIE, Jr (1991): Chlorofluorocarbon evidence for rapid ventilation of the Ross Sea, Deep-Sea Res., **38**, 845–870.

WEISS R.F., H.G. OSTLUND and H. CRAIG (1979): Geochemical studies of the Weddell Sea. Deep Sea Res., **26**, 1093–1120.

ロス海アデーレ岬沖における過剰 CO_2 透入の徴候

Chen - Tung Arthur CHEN

要旨：南極底層水（AABW）は一般にウェッデル海で形成されると考えられており，人為起源の CO_2 をわずかに含んでいる。ウェッデル海に比べ，ロス海は過剰 CO_2 の沈降の場としての役割は小さいと考えられるが，GEOSECS, IGY および R/V Polar Sea のデータのより詳細な解析により，ロス海北西かどのアデーレ岬沖において，過剰の CO_2 がより深い層へ透入している事実が明かとなった。

La mer 32: 173-185, 1994
Société franco-japonaise d'océanographie, Tokyo

Three Dimensional Structure of Tidal Currents in Tokyo Bay, Japan*

Xinyu GUO** and Tetsuo YANAGI**

Abstract: Tides and tidal currents in Tokyo Bay are calculated by using a three dimensional numerical model, where vertical eddy viscosity coefficient is computed by the Prandtl's mixing length theory. The results well reproduce the two-dimensional structure of tides and tidal currents in Tokyo Bay, Japan. On the basis of these results, we calculate the vertical tidal current whose amplitude is smaller than 10^{-3}cm/s in the most places of Tokyo Bay. At the mouth of Tokyo Bay, where water depth varies rapidly, the amplitude of vertical tidal current attains to the order of 10^{-2}cm/s. The tidal stresses calculated in two ways, e.g. two dimensional and three dimensional methods, have no differences in principle in most places of Tokyo Bay.

1. Introduction

It is well known that the currents play an important role in the material transport processes and the tidal currents consist of the major parts of the movements of water in coastal seas. Because the tidal currents have some potential effects to the primary production, the structure of tidal currents, especially its three dimensional structure is worth to study.

The tides and tidal currents in Tokyo Bay have been studied by YAMADA (1971), UNOKI *et al.* (1980) and NAGASHIMA and OKADA (1984) based on the observed data. YANAGI and SHIMIZU (1993) calculated the two dimensional tidal currents as a part of the research on the sedimentation processes in Tokyo Bay.

It can be said that we have known the general characters of tides and tidal currents in Tokyo Bay. But as for the vertical tidal currents we have neither observed data nor calculated results about its order or the place where the vertical tidal current is large. And for the research of material transport processes, we need a basic three dimensional current field. For these purposes, we calculate the three-dimensional structure of tides and tidal currents in Tokyo Bay in this paper.

2. Model

2.1 Formulation

Based on the fact that tidal waves are gravitaional long-waves (by nature), the first order linear equations is:

$$\frac{\partial u}{\partial t} - fv = -g\frac{\partial \zeta}{\partial x} + \frac{\partial}{\partial z}\left(\nu \frac{\partial u}{\partial z}\right), \tag{2-1-1}$$

$$\frac{\partial v}{\partial t} + fu = -g\frac{\partial \zeta}{\partial y} + \frac{\partial}{\partial z}\left(\nu \frac{\partial v}{\partial z}\right), \tag{2-1-2}$$

$$\frac{\partial \zeta}{\partial t} + \frac{\partial}{\partial x}\int_{-h}^{0} u dz + \frac{\partial}{\partial y}\int_{-h}^{0} v dz = 0, \tag{2-1-3}$$

where the continuity equation (2-1-3) has been integrated from the sea bed to the sea surface.

The boundry conditions are:

$$z = -0: \frac{\partial u}{\partial z} = \frac{\partial v}{\partial z} = 0, \tag{2-1-4}$$

$$z = -\mathrm{h}: \ u = v = w = 0, \tag{2-1-5}$$

along the shore boundary C_1:

$$\cos\alpha_x \int_{-h}^{0} u dz + \cos\alpha_y \int_{-h}^{0} v dz = 0, \tag{2-1-6}$$

along the open boundary C_2:

$$\zeta = S. \tag{2-1-7}$$

In the above, x, y, z constitute a Cartesian coordinate system at the right-hand side, the plane x, y coinsides with the undisturbed sea surface, and z is positive upward; t denotes the time; u, v denote the components of tidal currents in x,

* Recieved July 7, 1994
** Department of Civil and Ocean Engineering, Ehime University, Matsuyama 790, Japan

y directions, respectively, and w represents the vertical component; ζ is the elevation of the tide measured from the undisturbed sea surface; f is the Coriolis parameter ($=8.469\times10^{-5}\text{sec}^{-1}$); ν is the coefficient of vertical eddy viscosity; g is the gravitational acceleration($=980\text{cm/sec}^2$); S denotes the tidal elevation along the open boundary; h is the water depthe; $\cos\alpha_x$, $\cos\alpha_y$ denote the direction-cosines normal to the boundary.

Before calculation, we have to make a turbulence closure model to decide the value of ν. The simplest one is to take up the vertical eddy viscosity coefficients as a constant (YANAGI *et al.*, 1983; FANG and ICHIYE, 1983) or a variable which can vary in the vertical direction according to a given function (WANG , 1989; 1992) or vary in horizontal direction by given different values at different horizontal positions (YANAGI and IGAWA, 1993). But such ways include too many factors of mankind and usually fail to give a correct vertical profile of the tidal currents near the sea bed (FANG and ICHIYE, 1983). If we use the high level turbulence closure models such as the first order model or second order model of turbulence described by KOUTITAS (1987), we must solve another one or two different equations of the turbulent kinetic energy or the rate of dissipation of the turblulent kinetic energy besides the above equations. Considering the boundary layer character of the coastal water (YANG, 1992) and reasonable time consumption in computer, we would like to choose the zero order turbulent model, that is the Prandtl's mixing length theory as our turbulence closure model. It will be shown that in our numerical schemes the Prandtl's mixing length theory will not cost much calculating time than the model where the vertical eddy viscosity coefficient is a constant and this model really improve the accuracy of calculated results. The another reason why we choose the Prandtl's mixing length theory is that two papers (FANG and ICHIYE, 1983; YANG, 1992) show that the mixing length theory suits to the study of tides and tidal currents.

Using the same denotations as the above equations, we have

$$\nu=\nu_0+l^2\left[\left(\frac{\partial u}{\partial z}\right)^2+\left(\frac{\partial v}{\partial z}\right)^2\right]^{1/2} \quad (2\text{-}1\text{-}8)$$

the mixing length l is

$$l=\kappa_0(z+h+z_0)\left[1-\frac{z+h}{(1+s)h}\right] \quad (2\text{-}1\text{-}9)$$

Where κ_0 is the Karman constant approximately equal to 0.4, and z_0 is the sea bed roughness length, s is a parameter introduced by FANG and ICHIYE (1983) which express the roughness of sea surface. ν_0 is a small number ($=2.0\text{cm}^2/\text{sec}$) which prevent the vertical eddy viscosity coefficient from equaling to zero.

2.2 Procedure

The above equations with the constant vertical eddy viscosity coefficient had been solved by means of the splitting velocity method (SUN, 1992) which was applied to tidal problem in Bohai Sea (WANG, 1989) or the East China Sea (WANG, 1992). In their calculations, the authors mainly follow the line of Hansen's boundary-value problem which need many observed data along the coatal line. Usually this is very difficult. By the thought that a correct tidal currents field could produce a correct tidal elevation, we would like to follow the idea of hydrodynamics numerical methods. Along this line, YANG (1992) has calculated the tide in Bohai Sea. In our paper, we made some improvements over his works and calcutated the tides in Tokyo Bay.

Here, we want to use the A.D.I method (LEENDERTSE *et al.*, 1973), which had been proved as an effective and corrective method in coastal numerical calculations, to treat the time-depending differential terms in the above equation. In the first half time step, we have:

$$\frac{u^{n+1/2}-u^n}{0.5\Delta t}-fv^{n+1/2}=-g\left(\frac{\partial\zeta}{\partial x}\right)^{n+1/2}+\frac{\partial}{\partial z}\left(\nu\frac{\partial u^{n+1/2}}{\partial z}\right), \quad (2\text{-}2\text{-}1)$$

$$\frac{v^{n+1/2}-v^n}{0.5\Delta t}-fu^n=-g\left(\frac{\partial\zeta}{\partial y}\right)^{n}+\frac{\partial}{\partial z}\left(\nu\frac{\partial v^{n+1/2}}{\partial z}\right), \quad (2\text{-}2\text{-}2)$$

$$\frac{\zeta^{n+1/2}-\zeta^{n}}{0.5\,\Delta t}+\frac{\partial}{\partial x}\int_{-h}^{0}u^{n+1/2}dz+\frac{\partial}{\partial y}\int_{-h}^{0}v^{n+1/2}dz=0, \qquad (2\text{-}2\text{-}3)$$

In the second half time step, we have:

$$\frac{u^{n+1}-u^{n+1/2}}{0.5\Delta t}-fv^{n+1/2}=-g\left(\frac{\partial\zeta}{\partial x}\right)^{n+1/2}+\frac{\partial}{\partial z}\left(\nu\frac{\partial u^{n+1}}{\partial z}\right), \qquad (2\text{-}2\text{-}4)$$

$$\frac{v^{n+1}-v^{n+1/2}}{0.5\Delta t}-fu^{n+1}=-g\left(\frac{\partial\zeta}{\partial y}\right)^{n+1}+\frac{\partial}{\partial z}\left(\nu\frac{\partial v^{n+1}}{\partial z}\right), \qquad (2\text{-}2\text{-}5)$$

$$\frac{\zeta^{n+1}-\zeta^{n+1/2}}{0.5\Delta t}+\frac{\partial}{\partial x}\int_{-h}^{0}u^{n+1}dz+\frac{\partial}{\partial y}\int_{-h}^{0}v^{n+1}dz=0, \qquad (2\text{-}2\text{-}6)$$

By this way, in each time step we only need to solve a triangle matrix which can be easily done by the Thomas algorithm (ROACHE, 1976).

Other than the finite-difference of the space-depending terms directly, we would like to split the horizontal velocities in advance as follows:

in the first half time step,

$$u^{n+1/2}=g\left(\frac{\partial\zeta}{\partial x}\right)^{n+1/2}Pe^{n+1/2}+Pv^{n+1/2}, \qquad (2\text{-}2\text{-}7)$$

$$v^{n+1/2}=g\left(\frac{\partial\zeta}{\partial y}\right)^{n}Ge^{n+1/2}+Gv^{n+1/2}; \qquad (2\text{-}2\text{-}8)$$

in the second half time step,

$$u^{n+1}=g\left(\frac{\partial\zeta}{\partial y}\right)^{n+1/2}Pe^{n+1}+Pv^{n+1}, \qquad (2\text{-}2\text{-}9)$$

$$v^{n+1}=g\left(\frac{\partial\zeta}{\partial y}\right)^{n+1}Ge^{n+1}+Gv^{n+1}. \qquad (2\text{-}2\text{-}10)$$

By this way, we separate the velocity into two parts, in which one is connected to the gradient of tidal elevation and another one is connected to other force such as the Coriolis force. This method had been successfully used in many aspects of coastal calculations such as storm surge, tide and circulations (SUN, 1992) and were called as the velocity splitting method in China.

Here Pe, Pv, Ge, Gv represent the vertical profile functions of the tidal currents respectively and superscripts n, $n+1/2$, $n+1$ represent different time levels. Substitute (2-2-7) and (2-2-8)into the momentum equations (2-2-1) and (2-2-2)in the first half time step or substitute (2-2-9)and (2-2-10) into the momentum equations(2-2-4) and (2-2-5) in the second half time step, we can get a series of one dimensional differential equations about the vertical profile functions Pe, Pv, Ge, Gv as follows:

$$\frac{\partial}{\partial z}\left(\nu\frac{\partial F}{\partial z}\right)-\frac{2}{\Delta t}F=\mathrm{B}, \qquad (2\text{-}2\text{-}11)$$

$$z=0:\ \frac{\partial F}{\partial z}=0,$$

$$z=-h:\ F=0,$$

where as $\mathrm{F}=Pe^{n+1/2}$, $Ge^{n+1/2}$, Pe^{n+1}, or Ge^{n+1}, $\mathrm{B}=1$;

as $F=Pv^{n+1/2}$, $\mathrm{B}=-fv^{n+1/2}-\frac{2}{\Delta t}u^{n}$;

as $F=Gv^{n+1/2}$, $\mathrm{B}=fu^{n}-\frac{2}{\Delta t}v^{n}$;

as $F=Pv^{n+1}$, $\mathrm{B}=-fv^{n+1/2}-\frac{2}{\Delta t}u^{n+1/2}$;

as $F=Gv^{n+1}$, $\mathrm{B}=fu^{n+1}-\frac{2}{\Delta t}v^{n+1/2}$.

This equation is just a one-dimensional differential equation which can be solved by many methods (SUN, 1992). If we have some interests about the profile of tidal currents near the sea bed, we can use the logarithm coordinate transfer in the vertical direction such as FANG and ICHIYE (1983). Here, we just use the general methods to solve these equations in which we replace the unknown vertical eddy viscosity coefficient by using the upper time level's value. If we take the vertical eddy viscosity coefficient as a constant, we will need not calculate it and even can get the analytical solotuin about Pe and Ge. In fact, apart from the calculation of the vertical eddy viscosity coefficient in each time step, there is no difference between the Prandtl's mixing length theory and constant vertical eddy viscosity coefficient model in our numerical model.

As for the water elevations, we can substitute (2-2-7) and (2-2-8) into the continuity equations (2-2-3) in the first half time step or substitute (2-2-9) and (2-2-10) into the continuity equations (2-2-6) in the second half time step

and get a two dimensional differential equation only about the water elevations as follow:

in the first half time step,

$$A_{i-1,j}\zeta_{i-1,j} + B_{i,j}\zeta_{i,j} + C_{i+1,j}\zeta_{i+1,j} = T_{i,j} \quad (2\text{–}2\text{–}12);$$

in the second half time step,

$$D_{i,j-1}\zeta_{i,j-1} + E_{i,j}\zeta_{i,j} + F_{i,j+1}\zeta_{i,j+1} = S_{i,j} \quad (2\text{–}2\text{–}13);$$

where the coefficients of these algorithm equations are the integrated values of Pe, Ge, Pv and Gv from the sea bed to the sea surface. By the Thomas Algorithm, we can solve these algorithm equations just on the lines parallel to X-axis in the firt half time step and on the lines parallel to Y-axis in the second half time step.

The process in which we solve the equations is that at first, we solve $Ge^{n+1/2}$, $Gv^{n+1/2}$ and we can get the value of $v^{n+1/2}$, according to (2–2–8). After this step, we solve the $Pe^{n+1/2}$, $Pv^{n+1/2}$, and substitute these values into the tidal elevation equation (2–2–12) to get the values of $\zeta^{n+1/2}$. Then we can get the value of $u^{n+1/2}$ according to (2–2–7). At the second half time step, we make some changes on the order of the solving processes and almost repeat the same procedure as that at the first half time step.

By this way, it can be known that instead of solving a three dimensional tidal problem, we may solve a two dimensional finite-difference equation and a series of one dimensional differential equation at each horizontal point. And also, if we need, we can get a detail vertical profiles of the tidal currents without too much increase of calculating time.

3. Results

The size of horizontal mesh is 1km in X-direction and Y-direction and we divide the water depth into 10 layers. The time step is 45 seconds which is 2.8 times longer than Courant-Friedrichs-Lewy condition. The sea bed roughness length z_0 is taken as 0.04 cm according to MATSUMOTO (1983) and SOULSBY (1983). The parameter of s is taken as 0.1 according to FANG and ICHIYE (1983). The whole time of calculation is four tidal periods.

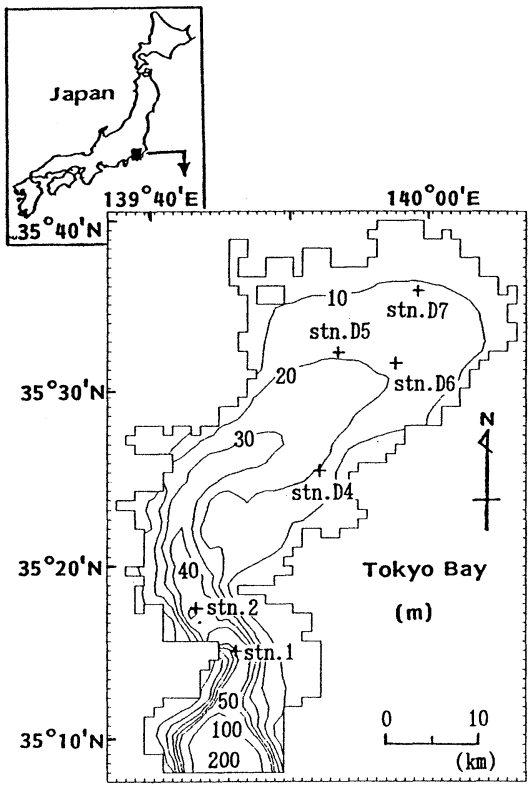

Fig. 1. Water depth in Tokyo Bay.

Figure 1 is the contour line of water depth of Tokyo Bay which is produced by the water depth data used in calculation.

The observed and calculated co-range and co-tidal charts of M_2 and K_1 are drawn in Figs. 2 and 3, respectively. As for the M_2 tide, the calculated amplitudes agree to the observation very well but the phases have some difference with the observation. This may be brought by the no slip condition at the sea bed which lead to a large velocity gradient near the sea bed in the vertical direction and then lead to a large sea bed friction. From Fig. 3, it can be seen clearly that the calculated phases of K_1 tide are nearly the same as the observed ones, but in the head of the bay the calculated amplitudes are smaller than the observed ones. We guess that the less increase of the tidal elevation may be brought by the large dissipation of the kinetic energy caused by the large vertical eddy viscosity coefficient.

The M_2 tidal current ellipses in Tokyo Bay

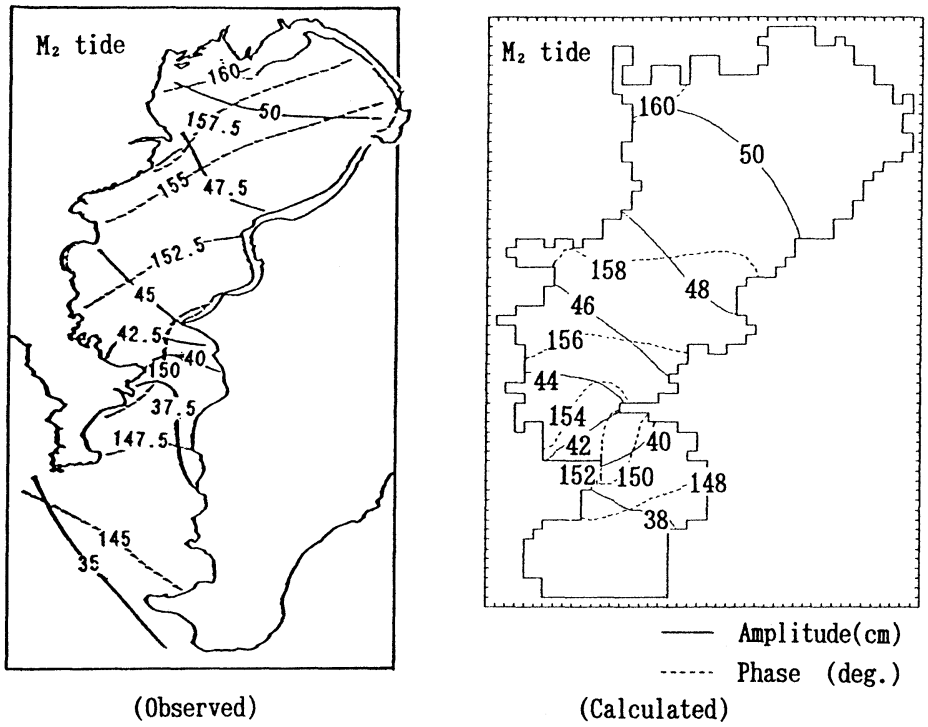

Fig. 2. Observed and calculated co-range and co-tidal chart of M_2 tide.

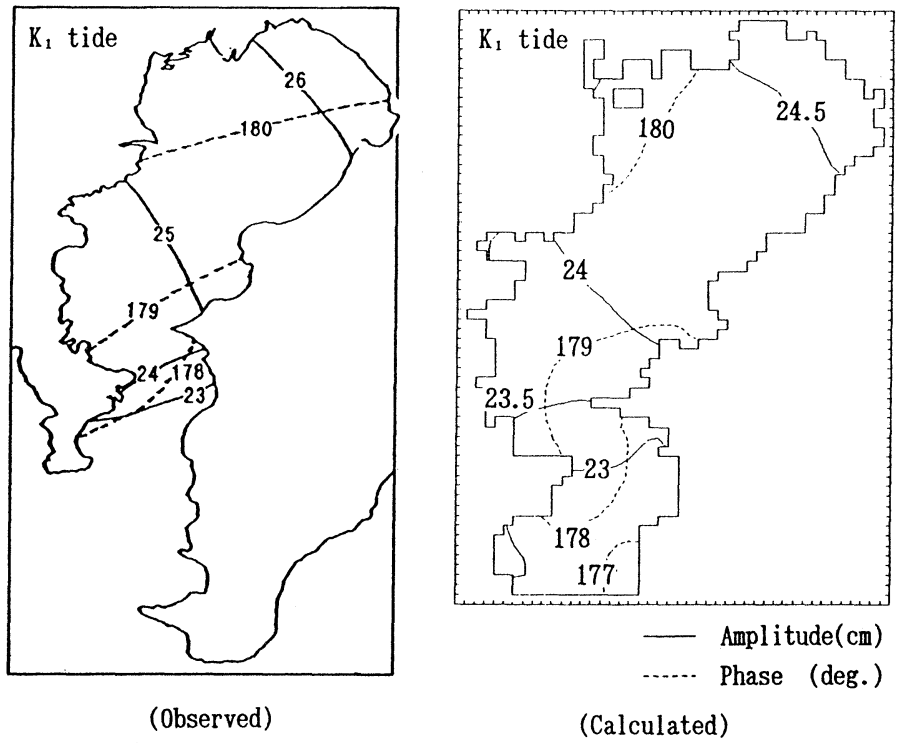

Fig. 3. Observed and calculated co-range and co-tidal chart of K_1 tide.

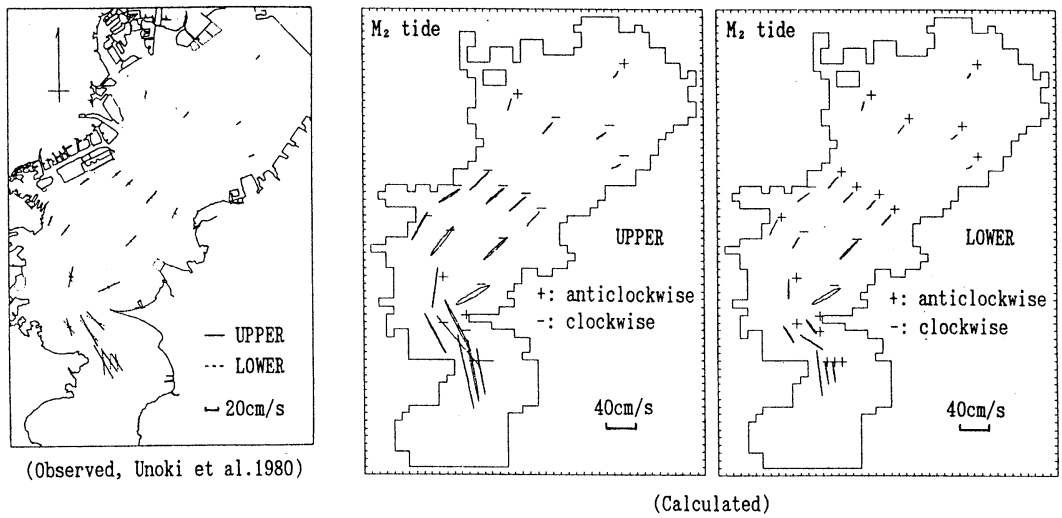

Fig. 4. Horizontal distribution of observed and calculated M_2 tidal current ellipses.

have been drawn by UNOKI *et al.* (1980). Here we reprint their chart of tidal current ellipses in winter season, and draw the calculated M_2 tidal current ellipses at the same points in Fig.4 where "upper" represents the results at the depth of 3 meters below the sea surface and "lower"represents the results at the 5 meters over the sea bed. By this way we can know that the calculated horizontal distribution of M_2 tidal current ellipses are similar to the observed results. Noticing the characters of the rotation direction of M_2 tidal current ellipses, we can find easily that the rotation direction varies from clockwise in the upper layer to the anticlockwise in the lower layer or keeps anticlockwise from the upper layer to the lower layer in the most part of Tokyo Bay. This character is the same as the conclusion of NAGASHIMA and OKADA (1984).

Figure 5 is the vertical distribution on M_2 tidal current ellipses at the points shown in Fig. 1. The left ones is the observed results (reprinted from the book of *Tokyo Bay*, ed. by OGURA, 1993) and the right ones is the calculated results. From this figure we can see that apart from the rotation direction of the tidal currents, the calculated tidal currents are nearly the same as the observed ones. In fact, we can not know the rotation direction of the observed tidal currents from the observed tidal currents ellipses, so we can not say anything about this point.

The amplitude and phase of calculated M_2 and K_1 tidal currents at the depth of 10 meters are shown in Fig. 6 which show that the amplitude of M_2 tidal currents is 30–40 cm/s at the mouth of Tokyo Bay, 15 cm/s in the central part of the bay and 5–10 cm/s in the head of the bay. This result is the same as the observed ones (UNOKI *et al.*, 1980). From Fig. 6, we can also know that the tidal currents along the west coast are stronger than those along the east coast of Tokyo Bay. This phenomenon had been found by YAMADA (1970). The phase distribution of M_2 and K_1 tidal currents show that the shallower the water depth is, the earlier the turn of tidal current is.

After the above comparisions, it can be said that we have well reproduced the tides and tidal currents in Tokyo Bay by a three dimensional scheme.

The vertical component of tidal currents have been thought to have some potential effects on the primary production in the coastal sea. It is valueable for us to calculate the vertical component of tidal currents in Tokyo Bay. The formula used in the calculation of w is

$$w|_z = -\int_{-h}^{z} \frac{\partial u}{\partial x}\, dz' - \int_{-h}^{z} \frac{\partial v}{\partial y}\, dz' \qquad (3\text{-}1)$$

Figure 7 is the calculated amplitude of the

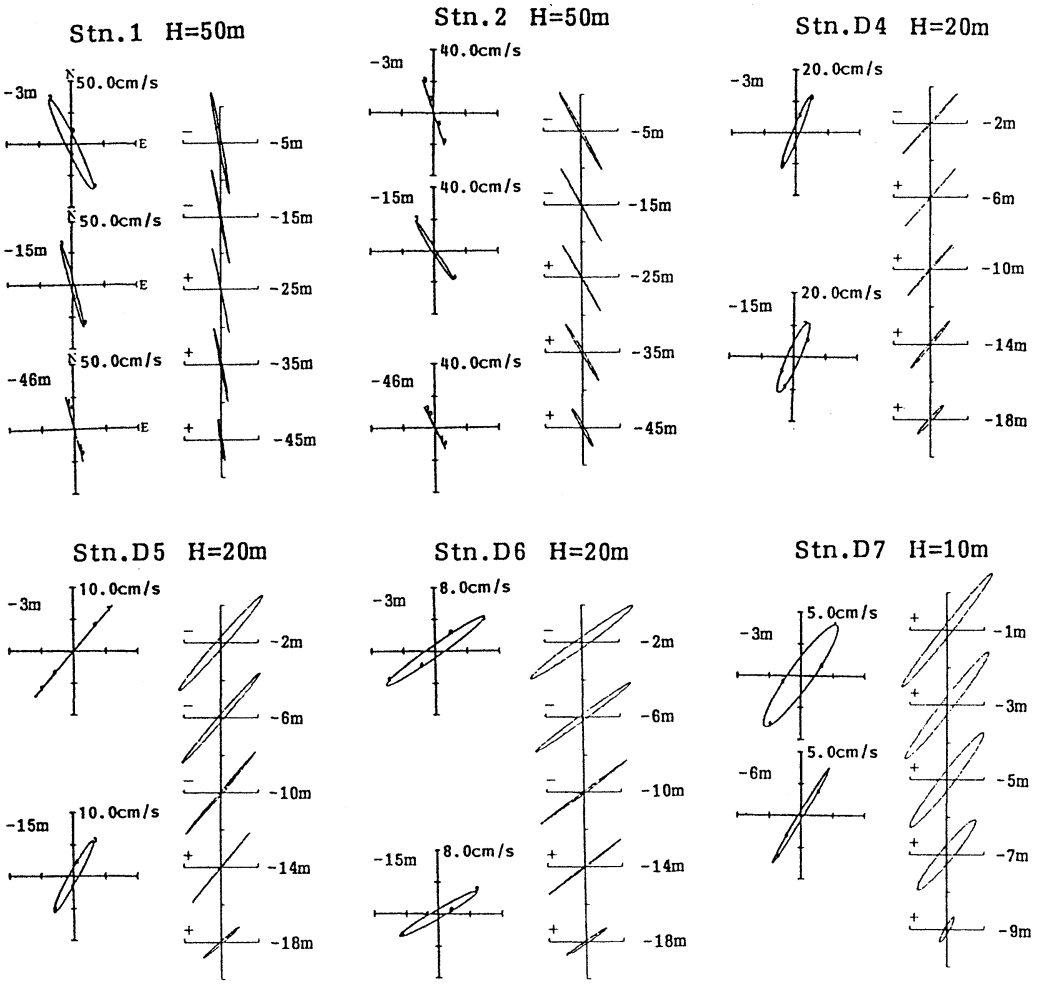

Fig. 5. Vertical distribution of observed (left) and calculated (right) tidal current ellipses at 6 points shown in Fig.1

vertical tidal currents. From this figure, we can know that the order of vertical tidal current in most of Tokyo Bay is smaller than 10^{-2}cm/s. In the region such as the mouth of the bay where the water depth varies rapidly, the vertical tidal current can get the order of 10^{-2}cm/s. If we divide the speed of horizontal tidal currents to that of vertical tidal current, we can know the ratio is about 10^3. This order is the same as the aspect ratio of the horizontal length scale of Tokyo Bay, 60km, to the characteristic depth of Tokyo Bay, 20 m, which is usually used to estimate the order of the vertical tidal currents.

4. Discussion

It is a difficult point to decide the values of the vertical eddy viscosity coefficient in the numerical calculation of coastal oceanography. In our calculation, we take the vertical eddy viscosity coefficient as a constant (50 cm^2/s) at first and get the co-range and co-tidal chart of M_2 tide as shown in Fig. 8 which could be said having the same distributing tendency as the observed ones. But as trying other constants such as 10 cm^2/s or 100 cm^2/s, we got some little different results from Fig.8. This suggests that we have to choose a high level turbulence closure model such as the Prandtl's mixing length theory to enclose our turbulent model.

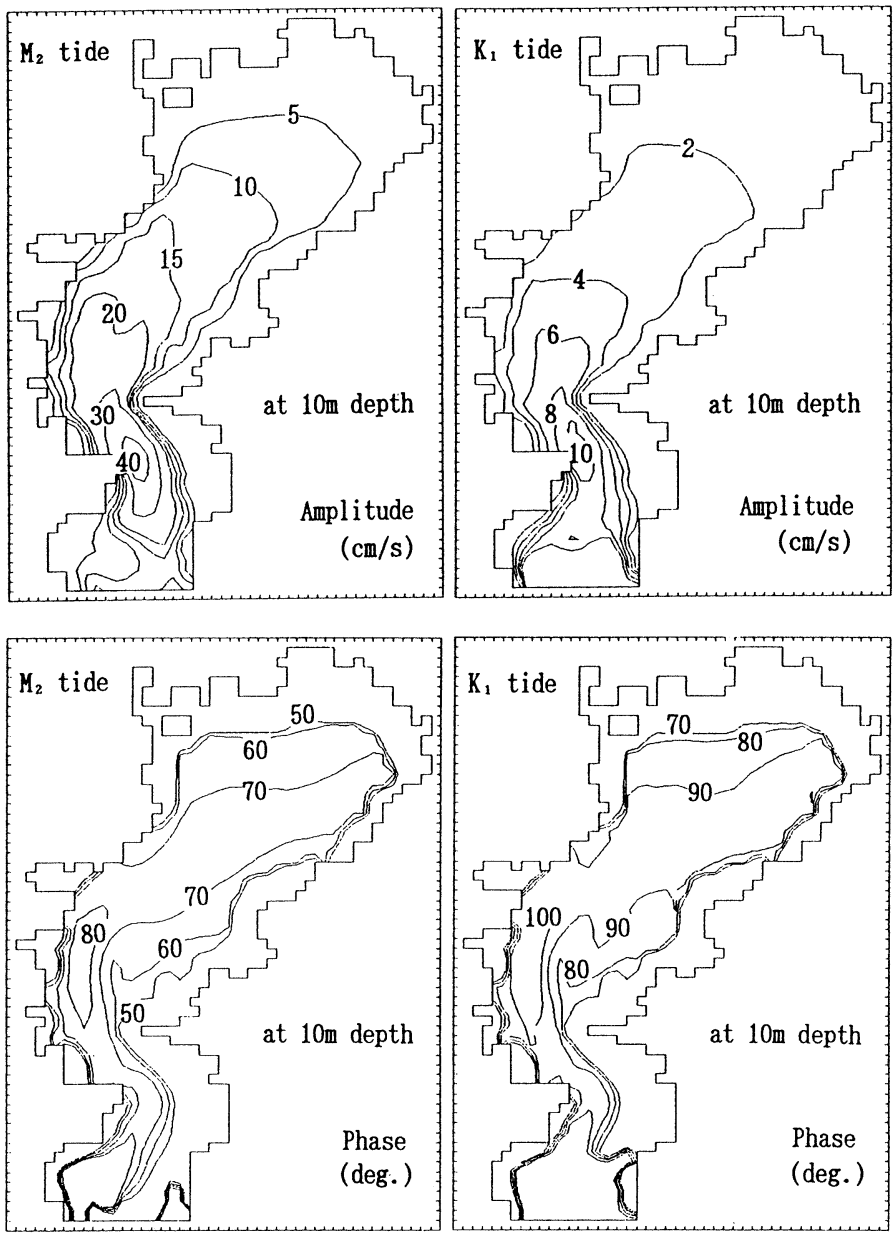

Fig. 6. Horizontal distribution of the amplitude and phase of horizontal M_2 and K_1 tidal currents at the depth of 10 meters.

Here we show the horizontal distribution of calculated $<\upsilon>$ at the depth of 10 meters in Fig.9 and the vertical distribution of calculated $<\nu>$ for M_2 tide at one point with the depth of 29 meters in Fig. 10 whose horizontal position is expressed by "+" in Fig. 9. Here $<\ >$ expressed the average over one tidal period. On the fact that we have well reproduced the tides and tidal currents in Tokyo Bay, we think that the value of $<\upsilon>$ calculated by the Prandtl's mixing length theory can be accepted although these values are larger than the general concept. In fact the order of 10 cm/s has been used for many times (WANG, 1989, 1992) and the result of

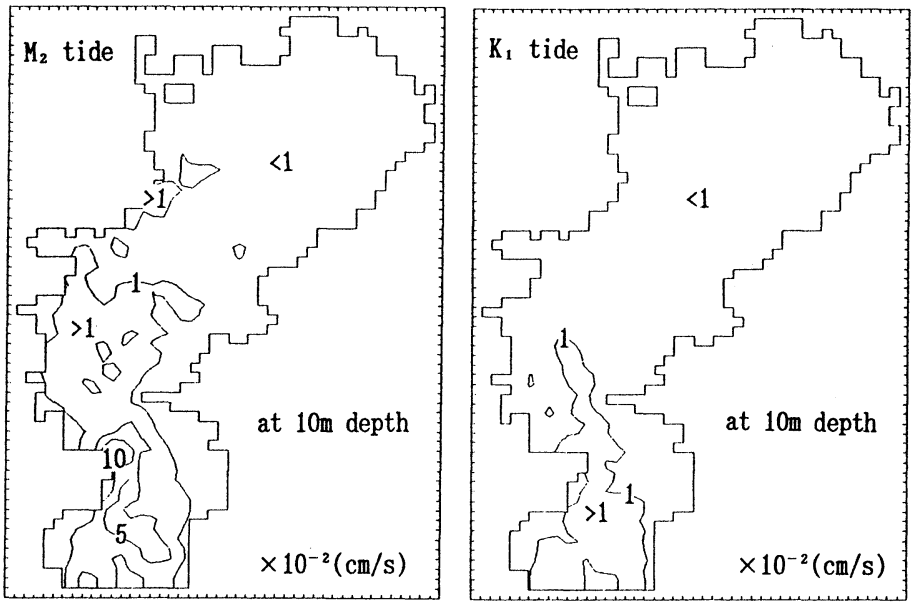

Fig. 7. Horizontal distribution of the amplitude of M_2 and K_1 vertical tidal currents at the depth of 10 meters.

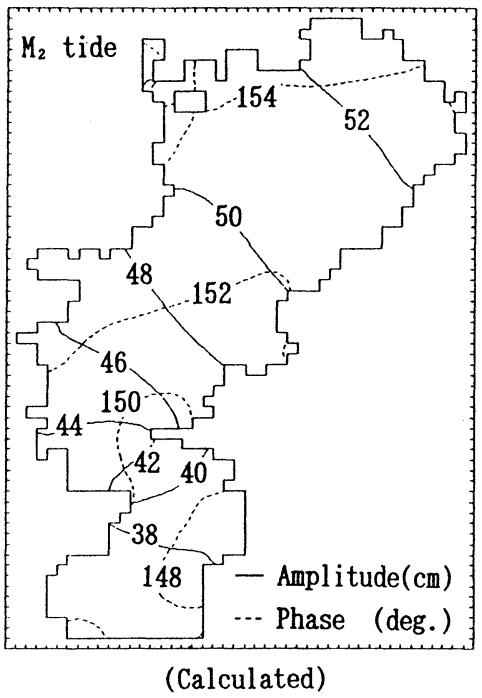

Fig. 8. Calculated co-range and co-tidal of M_2 tide as $\nu=50\text{cm}^2/\text{s}$.

FANG and ICHIYE (1983) has also been this order. From Fig. 9, we can see that at the mouth of bay where the tidal currents and water depth vary rapidly the value of $<v>$ is large. From Fig.10, we can see that below the middle layer of the whole water depth, the $<v>$ take its maximal value and the distribution curve from the sea bed to the sea surface approach a parabola which is similar to the experimental result reported by SUMI (1991). In fact, this form is also usually used in three dimensional coastal ocean models (NIHOUL, 1977; TEE, 1979). From this chart, we can also see that because the number of mesh points in vertical deirection is just 10, there is a little anomalous near the sea bed.

It is well known that the tide-induced residual current, which has important effects on the material transports processes in the coastal sea, is produced by the nonlinear effects of the tidal current. The tidal stress has been accepted as a force which have the same effects to the sea water as the wind or the buoyancy (NIHOUL and RONDAY, 1975; YANAGI, 1989). In a two dimensional tidal model, the tidal stress is calculated by:

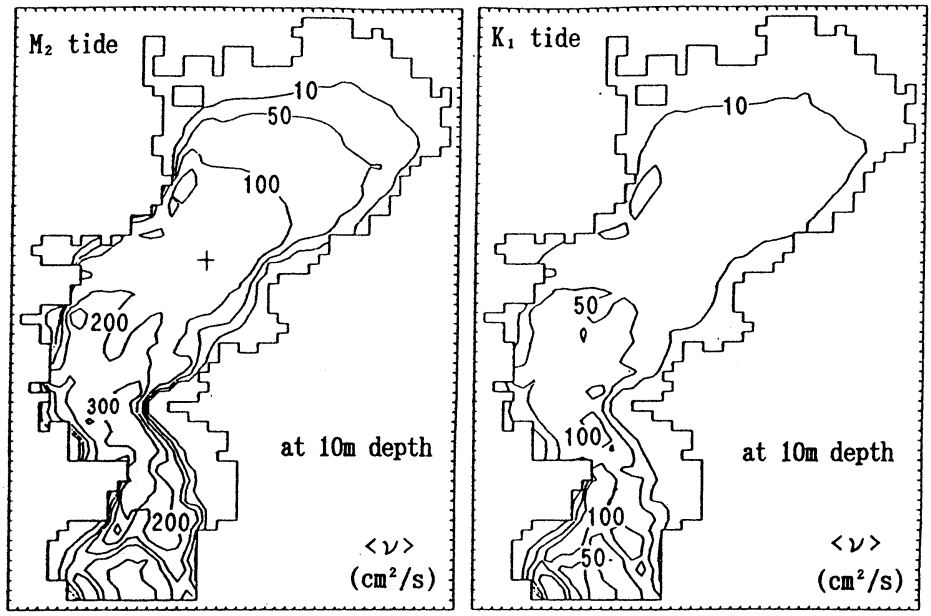

Fig. 9. Calculated horizontal distribution of $<v>$ at the depth of 10 meters.

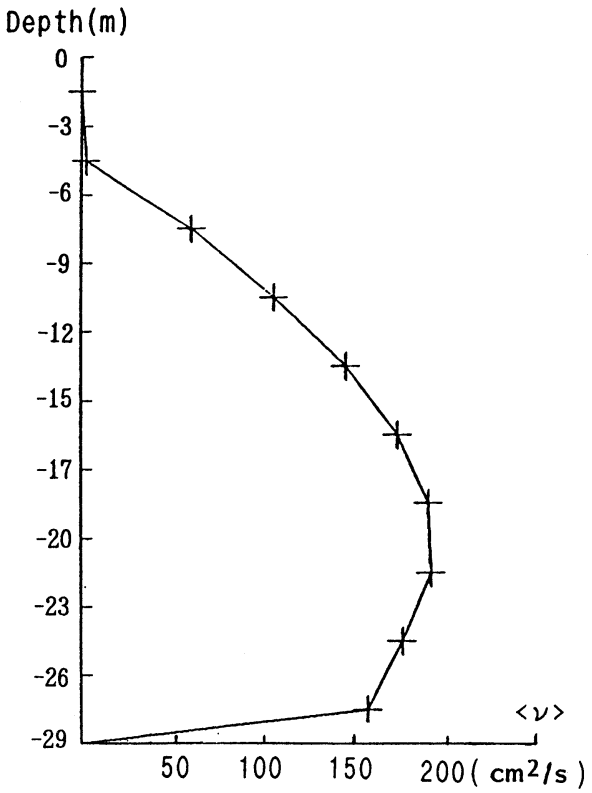

Fig. 10. Vertical distribution of $<v>$ for M_2 tide at the central part of Tokyo Bay calculated by Prandtl's mixing length theory.

$$S_x = \left\langle \tilde{u}\frac{\partial \tilde{u}}{\partial x} + \tilde{v}\frac{\partial \tilde{u}}{\partial y} \right\rangle \quad (4\text{-}1)$$

$$S_y = \left\langle \tilde{u}\frac{\partial \tilde{v}}{\partial x} + \tilde{v}\frac{\partial \tilde{v}}{\partial y} \right\rangle \quad (4\text{-}2)$$

where $\tilde{u}$, $\tilde{v}$ represent the water depth averaged velocity, $< >$ represent the average over one-tidal cycle. In a three dimensional tidal model, the tidal stress is

$$S_x = \left\langle u\frac{\partial u}{\partial x} + v\frac{\partial u}{\partial y} + w\frac{\partial u}{\partial z} \right\rangle \quad (4\text{-}3)$$

$$S_y = \left\langle u\frac{\partial v}{\partial x} + v\frac{\partial v}{\partial y} + w\frac{\partial v}{\partial z} \right\rangle \quad (4\text{-}4)$$

As these two ways are usually used in the calculation of tidal stress, we would like to check the difference between these two ways. Figure 11 is the results we get by these two ways in which "2-D" represents the results calculated by formula (4-1) and (4-2), "3-D" represents the results at the depth of 10 meters calculated by formula (4-3) and(4-4), "3-D'" represents the results at the same depth calculated by the first two terms in formula (4-3) and (4-4). From these results we can know that the difference between 2-D and 3-D models is very small in most parts of Tokyo Bay. The contribution coming

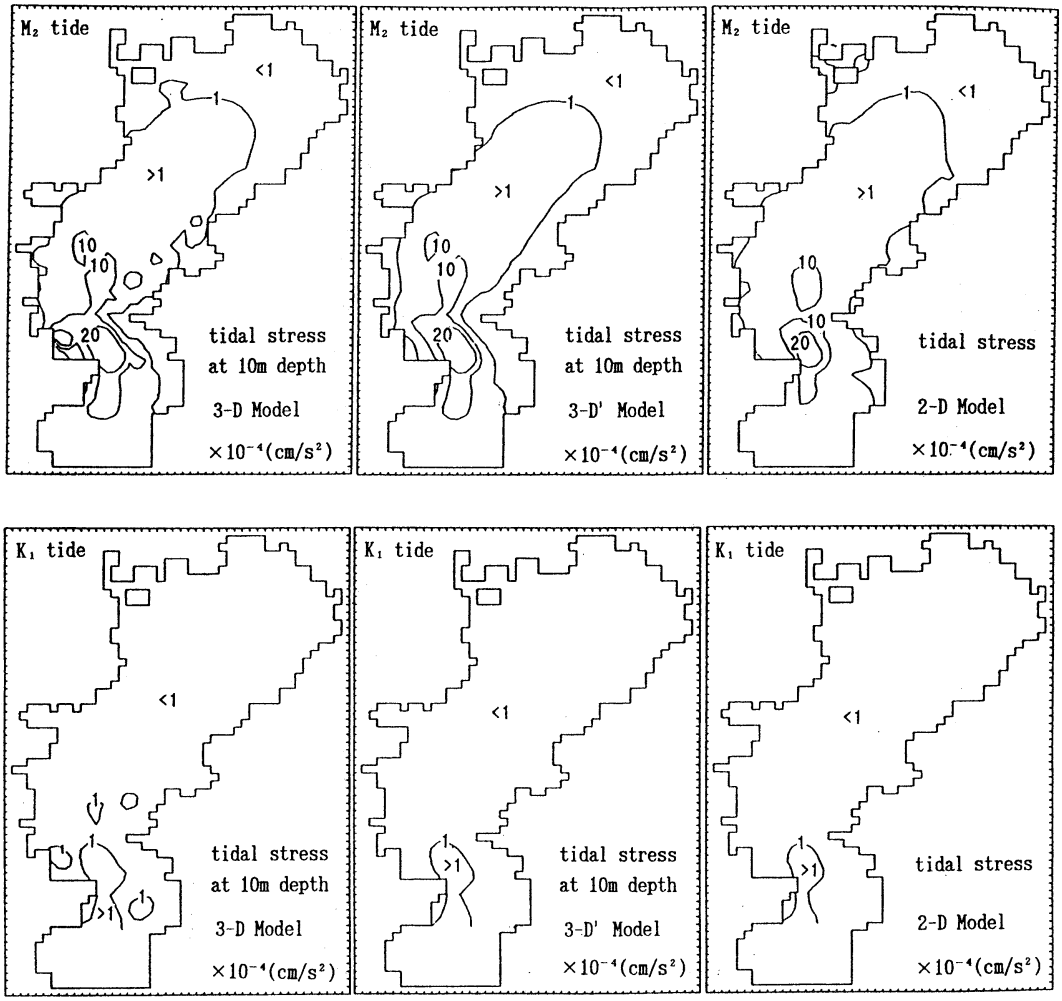

Fig. 11. Tidal stress produced by M_2 and K_1 tidal currents.

from the last term of formula (4-3) and (4-4) is also small in most parts of Tokyo Bay. By comparing to the tidal stress in Osaka Bay (YANAGI and TAKAHASHI, 1995), we can also know that the tidal stress in Tokyo Bay is smaller than that in Osaka Bay by one or two orders. On the other hand, it is clear that we can ignore the contribution of K_1 tidal currents when we calculate the tide-induced residual currents in Tokyo Bay.

5. Conclusion

(1) The tides and tidal currents in Tokyo Bay calculated by a three dimensional model well reproduce the observed ones. The vertical eddy viscosity coefficient has a great influence on the accuracy of calculated results.

(2) The vertical tidal current is smaller than 10^{-2}cm/s in most parts of Tokyo Bay. In the places such as the mouth of Tokyo Bay, where the water depth varies rapidly, the vertical tidal current can attain to the order of 10^{-2}cm/s.

(3) The tidal stress calculated by two dimensional model and three dimensional model have no difference in principle in most parts of Tokyo Bay. The tidal stress caused by M_2 tide in Tokyo Bay suggests that the tide-induced residual current is large near the bay mouth but small in most parts of Tokyo Bay. The tide-induced residual current caused by K_1 tide can be ignored in Tokyo Bay.

Acknowledgements

The authors greatly thank Drs. H. TAKEOKA and Y. ISODA for the useful discussions during this study. Thanks are also due to Prof. S. FENG and Dr. Z. YANG for their helps. The calculation was carried out on a FACOM M770 of Ehime University.

Refferences

Coastal Oceanography Research Committee, the Oceanographical Society of Japan (ed.) (1985): Coastal Oceanography of Japanese Islands. Tokai Univ. Press, Tokyo, 1106pp.

FANG, G. and T. ICHIYE (1983): On the vertical structure of tidal currents in a homogeneous sea. Geophys. J. Roy. Astr. Soc., **73**, 65–82.

FENG, S.(1977): A three dimensional nonlinear model of tides. Scientia Sinica, **20**, 436–446.

KOUTITAS, C. (1987): Three dimensional models of coastal circulation: An engineering viewpoint. *In*, Three Dimensional Coastal Ocean Models (Coastal and Estuarine Sciences 4), p.107–124, HEAPS, N.S.(ed.), American Geophysical Union, Washington.

LEENDERTSE, J.J., R.C. ALEXANDER and S.K. LIU (1973): A three dimensional model for estuaries and coastal seas, Vol. 1, Principle of computation. The Rand Corporation, R-1477-OWRR, 57pp.

MATSUMOTO, E. (1983): Sediment environments in Tokyo Bay. Geochemics, **17**, 27-32(in Japanese).

NAGASHIMA, H. and K. OKADA (1984): The tidal currents in Tokyo Bay-its vertical distribution. Abstract in the spring meeting of the Oceanographical Society of Japan, 118–119 (in Japanese).

NIHOUL, J.C.J. and R.C. RONDAY (1975): The influence of the tidal stress on the residual circulation. Tellus, **27**, 484–489.

NIHOUL, J.C.J. (1977): Three-dimensional model of tides and storm surges in a shallow well-mixed continetal sea. Dyn. Atmos. Ocean, **2**, 29–47.

OGURA, N.(ed.)(1993): Tokyo Bay, Koseisha Koseikaku, Tokyo, 193pp.

ROACHE, P.J. (1976): Computational Fluid Dynamics, Hermosa, Albuquerque, 446pp.

SOULSBY, R.L. (1983): The bottom boundary layer of shelf seas. *In*, Physical Oceanography of Coastal and Shelf Seas, p.189-266, JOHNS, B.(ed.), Elsevier, Amsterdam.

SUMI, K. (1991): The turbulent structure in the bottom boundary layer on the shallow sea. 38th Proceedings on the Ocean Engineering, 176–180 (in Japanese).

SUN, W. (1992): A numerical method in three dimensional shallow sea hydrodynamics-the velocity splitting method. *In*: Numerical Calculation in Physical Oceanography, p.100–195, FENG, S. and W. SUN (ed.), Henan Scientific Press, Luoyang, China(in Chinese).

TEE, K.T. (1979): The structure of three-dimensional tide-generating currents, Part I : Oscillating currents. J. Phys. Oceanogr. **9**, 930–944.

UNOKI, S., M. OKAZAKIand H. NAGASHIMA (1983): The circulation and hydrographic conditions in Tokyo Bay. Tech. Rep. No.4, Inst. of Phys. and Chem. Res., Japan, 262pp.(in Japanese).

WANG, H. (1989): Numerical calculation of the wind-driven, thermocline and tide-induced Lagrangian residual current in Bohai sea. MS. thesis, Ocean Univ. of Qigdao Press, Qindao, China, 52pp. (in Chinese).

WANG, H. (1992): On the research of shelf circulation and transport processes. Ph. D. thesis, Ocean Univ. of Qindao Press, Qindao, China, 300pp. (in Chinese).

YAMADA, T. (1971): The tidal current in Tokyo Bay. Report of hydrographic Department, Japan, **91**, 85–90 (in Japanese).

YANAGI, T., M. Nishii and H. Higuchi (1983): The vertical structure of tidal ellipse. 30th proceeding on the Ocean Engineering, 495-499 (in Japanese).

YANAGI, T. (1989): Coastal Oceanography. Koseisha-Koseikaku, Tokyo, 154pp.(in Japanese).

YANAGI, T. and M. SHIMIZU (1993): Sedimentation processes in Tokyo Bay, Japan. La mer, **31**, 91-101.

YANAGI, T. and S. IGAWA (1993): Diagnostic numerical model of residual flow in the coastal sea-an example of adaption to Suo-Nada and Iyo-Nada. Bull. Coast. Oceanogr., **30**, 12–19(in Japanese).

YANAGI, T. and S. TAKAHASHI (in press): Variability of the residual flow in Osaka Bay, Japan. Memoir of Dept. Engineering, Ehime Univ.

YANG, Z. (1992): On the theoretical and numerical models of shallow water circulation and mass transport processes. Ph. D. thesis, Ocean Univ. of Qindao Press, Qindao, China, 150pp.(in Chinese).

東京湾の潮流の3次元構造

郭 新宇　柳 哲雄

要旨：三次元数値モデルを使って，東京湾の潮汐と潮流を計算した。鉛直渦動粘性係数はPrandtl's混合距離論によって求めた。計算の結果は東京湾の潮汐と潮流の水平二次元構造をよく再現した。これらの結果をもとに潮流の鉛直成分を計算した。東京湾の大部分の所では潮流の鉛直成分の振幅は10^{-2}cm/sより小さいが，湾口のような水深の変化が激しい所では10^{-2}cm/sを越えることがある。三次元モデルと二次元モデルにより計算した潮汐応力を比べると，東京湾の大部分の所では両者に本質的な差がないということが分かる。

La mer 32: 187–194, 1994
Société franco-japonaise d'océanographie, Tokyo

Studies on the Accuracy of Counting Seedlings Fry by Image Processing Techniques*

Sadami YADA**, Koichi HIGUCHI** and Takatomo KOIKE**

Abstract: To count fry by an image processing system, a counting system comprising first and second belt conveyors, and a device to prevent multiplication of fry was fabricated, thereby the effects of the optimum circumferential speed difference between the first and the second conveyor belts, the threshold selection method for image analyses, lighting direction and illumination intensity upon counting accuracy were investigated. 1) Threshold selections of fry pictures at threshold values of 40 and 50 are recommended rather than the discriminant analytical method. 2) Lighting from below the conveyor belt are suitable in order to obtain stable video pictures. 3) To achieve an efficient and accurate fry count, it is suitable to maintain the circumferential speed difference between the first and second conveyor belts in the range from −5 cm/s to 25 cm/s. 4) If the circumferential speed of the second conveyor belt is set at 20 cm/s, it is estimated that 24,000 fry per unit time per one processing line can be counted by the image processing thchnique.

1. Introduction

Mechanization of manual fish-counting processes used when seedlings fry is shipped has been strongly desired. Conventionally, the method of counting fry, when in a large number, is to approximate the number through assumptions on the mean unit weight or volume of fish. This, however, involves remarkable counting errors (CHEN, 1992).

In some cases of high-grade fish species, unjustifiably large discrepancies in fish count have caused lawsuits by both buyers and sellers, because of the large economic impact involved. A fry counting system is proposed in studies on counting systems of fry. However, this system has multiple drawbacks including the low counting ability per unit time (YADA *et al*, 1993). Moreover, bubbles generated from fish bodies at low pressures, minute bubbles attaching to gills, and a variety of other bubbles generated at vents in the system and in low-pressure areas are detecred by sensors, giving a false count that is larger than the real count. To solve the problem of such large counting errors, precision techniques are indispensable (CHEN *et al.*, 1993). Nothing the background and the problems above, a fish counting system using image-processing thchniques designed to enhance counting accuracy and efficiency, as well as to prevent duplicated fish counts was test fabricated, and the counting accuracy was evaluated.

* Received July 11, 1994
** Laboratory of Fishing Technology and Engineering, Tokyo University of Fisheries, Konan 4-5-7, Minato-ku, Tokyo, 108 Japan

2. Experimental Method

1) *Experimental equipment*

Figure 1 shows experimental equipment comprising a vibrating unit that transfers fishes fed onto the first conveyor by vibratory motion, the second belt-conveyor that separates multiple fish in mass, and a video camera (SONY CCD-TR705) that takes photos of fishes laying on the conveyor.

An unseparated mass of fish precludes accurate fish counting. To solve this problem, different circumferential speeds are given to the first belt conveyor and the second belt conveyor; i.e., the second belt conveyor runs faster than the first conveyor to break the mass of fish into individual fish.

As shown in the figure, photos are taken from above the second belt conveyor with two fluorescent lamps (FL20) provided in the space between the upper and lower belts serving as the light source to radiate beams from below fishes.

The second conveyor belt is made of transilon

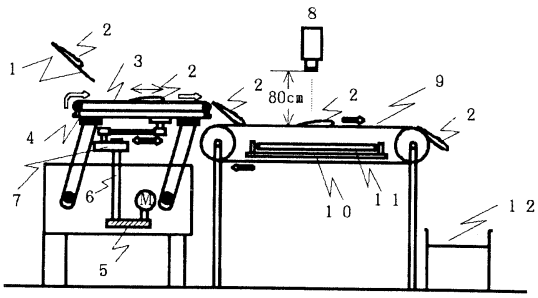

Fig. 1. Outline of the experimental equipment
1: shoot, 2: fish, 3: the first belt conveyer, 4: vibratory plate, 5: belt, 6: shaft, 7: crank, 8: video camera, 9: the second belt conveyer, 10: stand furnished fluorescent light, 11: fluorescent light (20 W×2, length 57.5cm, intervals 13.5cm, illuminance on the belt conveyer 1,100*lx*), 12: water tank, M: motor

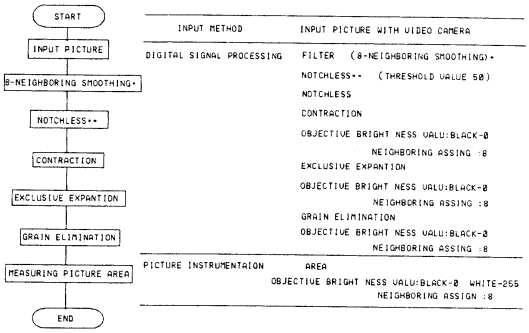

Fig. 2. A flowchart showing the picture area measuring procedure using the image processing technique with particulars
* The pixel at the centre and the eight adjacent pixels are used as the processing object.
** The threshold selection method prodeces a picture by designating brightness values at brightness zero and brightness 255 without any intermediate brightness. Concretely, when black is designated at brightness zero, those with threshold values of 50 or less are converted into black, and those there-above are converted into white.

(E2/i UO/UO-NA FDA, white), which has a high transmission factor. Two transparent acrylic partitions (height: 2.3 cm, width: 38.5 cm, thickness: 0.1 cm) are provided 30 cm apart, and the image between the partitions was analyzed.

2) *Image analysis method*

The partition-to-partition picture of the second belt conveyor is inputted to an image analyzer (PIAS, model PIAS Ⅲ), analyzed to count the number of fish, and, by intermittent cycled operations, the sum of the fish count of each image was determined to yield the total number of fish. The performance of an analyzer is an important consideration for image processing, but the art of photographing images adapted well to counting fry in seedlings is more important. The test image analyzer is capable of inputting moving images, but in view of possible deterioration of analyzing accuracy when high-speed motion pictures are inputted, studies were done on the relationship between the circumferential speed of the second conveyor belt and analytical accuracy.

Subsequently, each area of the photographed images taken from the side and back of fish with the intensity of illumination changed was subjected to threshold selections by the image analyzer, and the relationship between the luminous intensities when photographed with beams in both normal and reverse directions and the reduction in image areas was investigated. Figure 2 is an image analysis flowchart. Pictures taken were subjected to threshold selections and left to contract after being smoothened on eight sides for the approximation.

Subsequently, picture areas were measured after removing noise formed after exclusive enhancement by the mass of minute pixels (hereafter referred to as "particles"). The term "smoothening on eight sides for approximation" means to remove image noise from the eight pixels on the periphery of a pixel, "contraction" means to reduce the boundary of a picture by one pixel, and "exclusive enhancement" means to enhance without overlapping adjacent pictures. The term "removing particles" is a generic term indicating the deletion of unnecessary date that cause errors (TAMURA, 1985).

3) *Transferring fish by vibration*

To measure the travelling speed of fish conveyed by vibration motion, the video camera was set 80 cm immediately above the second belt conveyor. One fish placed on the second vibrating conveyor belt was photographed at the video

camera shutter speed of 1/100 second, and the travelling speed was determined by image processing.

The coefficient of friction between fish and the conveyor belt was measured by pulling a fish placed on the non-moving first conveyor belt using the method reported by HIGASHIKAWA *et al.*, (1993).

4) *Fish counting method and experimental procedure*

Twelve carp fry with a length ranging from 6 cm to 8 cm were fed from a water-filled vessel to the first belt conveyor through a chute. The circumferential speeds of the first belt conveyor were set at 5 cm/s to 40 cm/s at regular intervals of 5 cm/s, while the circumferential speeds of the second belt conveyor were set at 10 cm/s to 20 cm/s, and the effects of conveyor vibrations upon analytical accuracy were investigated.

Figure 3 is a frowchart showing the fish counting method. According to degree of reduction of picture area after image processing, the picture can be classified into three categories; i.e., the group of the pictures taken from behind the fish, which have relatively small picture areas (hereafter called the "back picture area"), the group taken from the side, which have intermediate picture areas (hereafter called the "side picture area"), and the group taken on a mass of fish in close contact, which have relatively large picture areas (hereafter called the "multiple picture area"). The picture areas after image processing are considered to represent the number of fry with greater accuracy if the numbers of fry in each category are summed. To determine the sectional paramenters of each picture area in the three sections, the back picture area and the side picture area of sample fry are measured in advance with a planimeter, whereby sectional parameters P_1 and P_2 were determined according to the frequency distribution of the picture areas after image processing each picture relative to the class value.

Similarly, parameter P_3, which discriminates the side picture area and the multiple picture areas, was determined according to the frequency distribution of the side picture area and the multiple picture area.

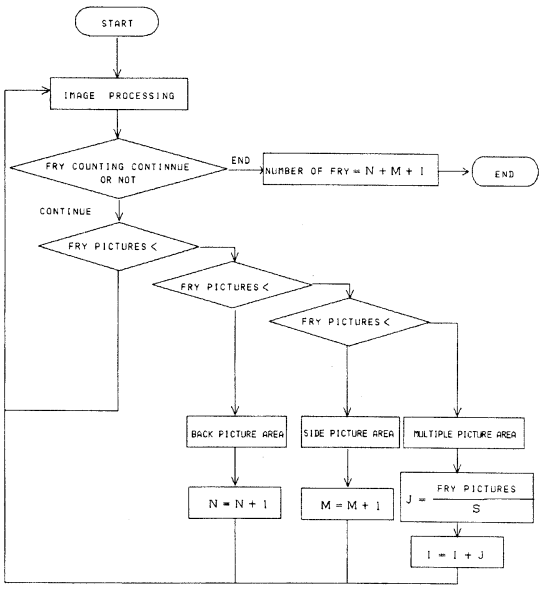

Fig. 3. A flowchart showing the fry counting procedure

Notes:

N: Number of fry after processing fry pictures taken from behind by the threshold selection method

M: Number of fry after processing fry pictures taken from the side by the threshold selection method

I: Number of fry in contact

P_1: Parameter representing the back picture area of sample fry measured with a planimeter

P_2: Parameter representing the side picture area of sample fry measured with a planimeter

P_3: Parameter representing the multiple picture area of sample fry measured with a planimeter

S: Calculated parameter of the back picture area and the side picture area of sample fry measured with a planimeter

Parameter S is a mean value of the back picture areas and the side picture areas. Because there are possibilities of counting picture noise, for example, which is a minute area comparing the back picture area, can be counted as one piece of fry, any area smaller than parameter P_1 was neglected as picture noise.

In summary, areas equal to or greater than parameter P_1 and less than P_2 were classified

into the back picture area, areas equal to or greater than P_2 and less than P_3 were classified into the side picture area, and areas equal to or greater than P_3, which were assumed to be duplications of multiple fry, were classified into the multiple picture area. As a result, the respective unit numbers of fry classified into the back picture area and the side picture area were the fry count, the values obtained by dividing the multiple picture areas by section parameter P were also counted as fry number, and the aggregate number of fry was taken as the total fry count. Analytical accuracy is shown by the ratio of the number of fry counted by image processing to the actual fry count.

3. Experimental Results and Discussion

1) *Luminous intensity when pictures are taken and image processing accuracy*

Figure 4(a) shows the luminous intensity of the overhead light and the analytical accuracy of fry images after image processing, converted in to areas. Analytical accuracy on the ordinate is expressed in terms of the ratio of the side picture area determined by the image processing equipment and planimeter to the back picture area.

When lighting is provided from an overhead light source with a intensity of illumination of not less than 1,600 *lx* immediately above the belt conveyor, the area measured with a planimeter reduced to less than approximately 50 persent, due to intense reflection from the fry. Table 1 shows factors that cause variations of picture areas after image processing when lighting is provided from above or below the belt conveyor. For image a analyses with a high accuracy, clear-cut outlines after processing are essential, but lighting is provided from above, variation factors become larger at illumination intensities of 280, 1,100 and 1,950 *lx*, with dispersed analytical accuracy, and no images with clear-cut outlines can be obtained.

Figure 4(b) shows the relationship between the illumination intensity immediately above the conveyor belt when lighing is provided from below the conveyor belt and the analytical accuracy available with the image analyzer. The discriminant analytical method proved that the analytical accuracy of fry back images was high

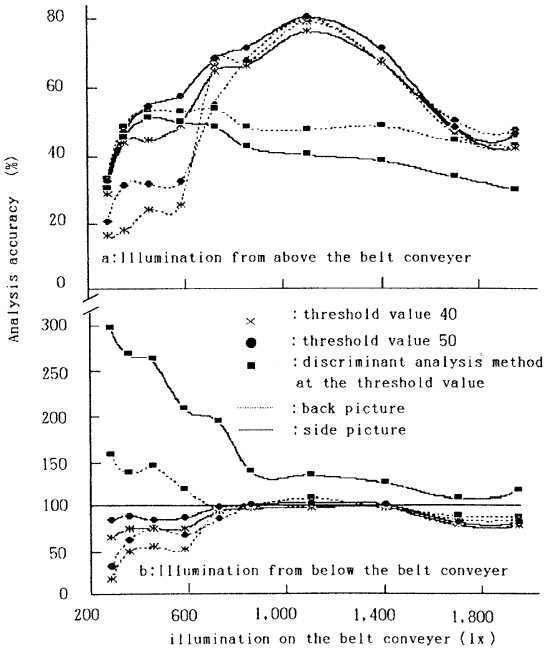

Fig. 4. Illumination intensity when taking video pictures and analytical accuracy
Analytical accuracy (%) = (B/A) × 100
where
A: Area of video picture of fry measured with a planimeter
B: Area of video picture of fry after image processing by the threshold selection method

at the illumination intensities of 850 *lx* to 1,400 *lx*, but that of fry side images dropped at the illumination intensities of 280 *lx* to 1,950 *lx*. The analytical accuracy of fry back and fry side images at the threshold values of 40 and 50 was 100 persent at the illumination intensities of 280 to 1,950 *lx*, decreased slightly at the illumination intensity of 1,600 *lx* and above. When analytical accuracy is evaluated in terms of factors causing variations of image areas after image processing, the factors were small when lighting was provided from below the conveyor belt with pictures taken from above at a high illumination intensity; i.e., 1,100 and 1,950 *lx* comparing with the low illumination intensity of 280 *lx*, where analytical accuracy was high. However, uniform images of fry could not be obtained at the illumination intensity of 900 *lx* or below, and if threshold selections were made at the threshold values of 40 and 50, the picture areas

Table 1. Variation coefficient (%) of picture area after image processing back picture

Directionof lighting	Direction at taking video pictures	Method of notchless	Illumination intensity(*lx*) 280	1,100	1,950
Lighting from above the belt conveyer	Side picture	Notchless 40	8.9	7.0	10.4
		〃 50	8.7	6.9	10.7
		Discriminant analysis method at the threshold value	15.3	7.7	11.6
	Back picture	Notchless 40	8.1	3.2	13.5
		〃 50	9.3	5.4	13.7
		Discriminant analysis method at the threshold value	11.2	8.7	15.8
Lighting from below the belt conveyer	Side picture	Notchless 40	4.9	1.0	0.5
		〃 50	4.9	1.4	0.4
		Discriminant analysis method at the threshold value	9.6	3.0	4.0
	Back picture	Notchless 40	3.1	1.9	0.8
		〃 50	3.3	2.7	1.0
		Discriminant analysis method at the threshold value	7.2	6.6	2.2

Note: The tabulated data were obtained by processing the back picture areas and the side picture areas of fry (still pictures at illumination intensities: 280, 1,100 and 1,950 *lx*) by the discriminant analysis method at the threshold values of 40 and 50.

obtained were smaller than those measured with a planimeter.

The picture areas determined by the discriminant analysis method were larger than those determined by the threshold selection method at threshold values of 40 and 50. Because the best threshold values are automatically set on the basis of a density histogram of pictures by the discriminant analysis method, the geometrical structure of pictures is not considered, and they do not necessarily agree with human vision (AUTSU,1980). For these reasons, threshold values in the discriminant analysis method were set lower than those of the threshold selection method at threshold values of 40 and 50. As a result, measured picture areas of fry were considered to become slightly lager. Furthermore, the discriminant analysis method failed to produce fry pictures after threshold selecrion, loosing the original geometric identity of the fry, and this method is considered to be unsuitable for the purposes of this experiment. It is inferred from the discussion above that lighting should be provided from below the conveyor belt, the intensity of illumination should be set at 1,100 *lx* to 1,400 *lx* to obtain stable fry pictures, and the threshold selection method at threshold values of 40 and 50 is better than the discriminant analysis method.

2) *Circumferential spped of belt conveyor and analytical accuracy of fry pictures*

Figure 5 shows the relationship between the circumferential speed of the conveyor belt and analytical accuracy. A high analytical accuracy of 98 to 99.5% is available at circumferential speeds of 20 cm/s or below, but the accuracy was low at speeds of 30 cm/s or more. The causes of this are assumed to be that fry pictures taken are displaced in the travelling direction of the fry at a high conveyor belt speed, as a result, the outlines of fry are subjected to threshold selections in minute particles with a resultant reduction of the number of pixels; these particles are deleted, the outlines of fry pictures become vague, and the picture areas after image

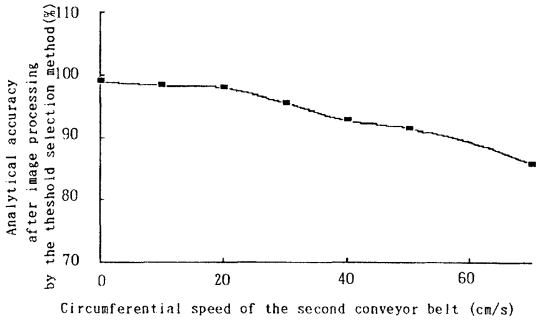

Fig. 5. Circumferential speed of the second conveyor belt and analytical accuracy
Analytical accuracy (%) = (B/A) × 100
where
A: Area of video picture of fry measured with a planimeter
B: Area of video picture of fry after image processing by the threshold selection method

processing decrease.

At a circumferential speed of 20 cm/s or below, the analytical accuracy does not decrease due to the generation of the phenomena mentioned. This proves that the circumferential speed of the second conveyor belt of 20 cm/s or below is suitable in the absence of the aforementioned phenomena.

3) *Behaviour of fry on the vibrating conveyor belt*

It is assumed here that fry lay on a conveyor belt that undergoes sinusoidal vibratory motions as shown in Fig. 6, and the coordinate system of the conveyor belt is denoted by X_1, Y_1, the coodinate system of fry, X_2, Y_2, the circumferential speed of the conveyor belt, V_1, and the travelling speed of fry, V_2.

According to TANIGUCHI *et al.*,(1962), it is considered that fry laying on a flat conveyor belt undergo the following modes of behaviour A, B and C.

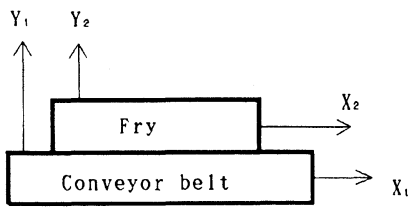

Fig. 6. Co-ordinate axis of conveyor belt and fry

Namely, the conveyor belt moves faster than the travelling fry in behaviour A, and the travelling speed of fry is expressed by the following equation:

$$V_A = \frac{\mu g}{\omega}\theta + \alpha\omega \qquad (1)$$

where,

V_A: travelling speed of fry in behaviour A
μ : coefficient of friction between fry and conveyor belt
g : gravitational acceleration
ω : angular velocity of crank
θ : rotating angle of crank
α : amplitude of crank

Travelling fry in behaviour B move faster than the conveyor belt, and the travelling speed of the fry is expressed by the following equation:

$$V_B = \frac{\mu g}{\omega}\theta + \alpha\omega \qquad (2)$$

where,

V_B: travelling speed of fry in behaviour B

Travelling fry behaviour C move at the same speed as the conveyor belt, where fry undergoes vibratory motrions as an integral part of the conveyor and are not transferred. The travelling speed of fry in this case is expressed by the following equation:

$$V_C = \alpha\omega\cos\theta \qquad (3)$$

where,

V_C : travelling speed of fry in behaviour C

Variations of these three modes of behaviour are determined by the accelerations of the fry and the conveyor belt. When the amplitude is extremely small, the frictional force of the conveyor belt acting upon the fry is larger than the inertial force. As a result, fry undergo vibratory motions as an integral part of the conveyor belt at all times, and therefore the fry are not transferred.

When type A behaviour and type B behaviour appear in one period with type C behaviour appearing between them, fry are not transferred as they slip. When types A, B and C behaviour appear in a normal sequence within one period, the fry are transferred.

Theoretical travelling speed of fry V_{ave} in this case is expressed by the following equation:

$$V_{ave}=\frac{\mu g}{16}\pi - \frac{\alpha\omega^2}{2\pi}\{1+\sin(\cos^{-1}\frac{\mu g}{2\alpha\omega^2}\pi+\pi)\} \quad (4)$$

Figure 7 shows the theoretical travelling speed of fry V_{ave} when the acceleration of the conveyor belt is changed and at the travelling speeds measured by a video camera.

The acceleration of fry caused by the first belt conveyor when the transfer of fry is started is 7.1 cm/s^2 or thereabouts, at which the theoretical value agrees well with the measured value. However, the measured values of travelling speed are slightly larger than the theoretical values within the acceleration range of apporoximately 7.1 cm/s^2 to 18 cm/s^2 involving disagreements, but they agree in the higher acceleration range than above. These disagreements featuring the trend of a gradual increase are considered to have been caused by mechanical resistance, viscosity, inertial force, and loss of kinetic energy due to collisions among fry, all of which were difficult to measure and were neglected in introducing the theoretical equations.

This, therefore, means that the travelling speed of fry will not increase even if they are subjected to acceleration at 18 cm/s^2 or greater.

4) *Avoiding multiplication of fry on the conveyor belt*

The variations of picture areas of fry due to close contact and multiplication of fry causes a degradation of analytical accuracy, and hence must be eliminated. Figure 8(a) shows the relationship between the speed difference between the first and the second conveyor belts and the analytical accuracy. The circumferential speed defference between these conveyor belts was obtained by deducting the circumferential speed of the second conveyor belt from that of the first conveyor belt. The negative sign on the abscissa shows that the circumferential speed of the second conveyor belt is greater than that of the first conveyor belt. If the first conveyor belt is vibrated when the circumferential speed of the second conveyor belt is at 10 cm/s, the analytical accuracy was 100% for the speed differential range of 10 cm/s to 30 cm/s between these belts, but is dispersed and degraded when the first conveyor belt is not vibrated.

If the first conveyor belt was not vibrated, even when the circumferential speed of the second conveyor belt was 20 cm/s, analytical accuracy was unstable and dispersed as shown in Figure 8(b). When, however, the first conveyor belt was vibrated, the analytical accuracy registered 100% for the circumferential speed deifference range from −5 cm/s to 20 cm/s.

On the basis of the results above, it was concluded that rapid and accurate fry counts by the image processing technique are available if the circumferential speed of the second conveyor belt is set at 20 cm/s, the first conveyor belt is forced to vibrate, and the circumferential speed difference between these conveyor belts is maintained at from −5 cm/s to 20 cm/s. In commercial applications, it is necessary to do these

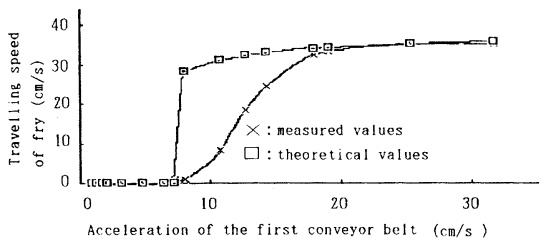

Fig. 7. Acceleration of the first conveyor belt and travelling speed of fry
Note: The coefficient of friction between fry and the conveyor belt was assumed to be 0.2.

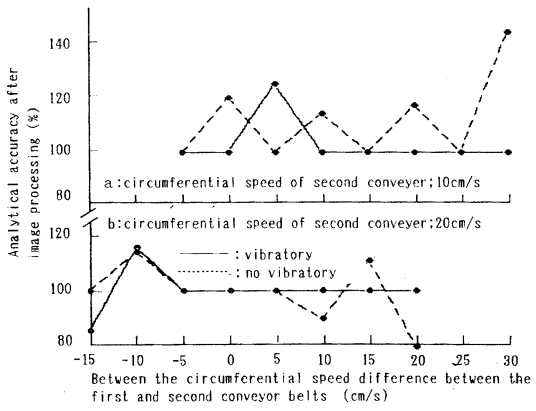

Fig. 8. Relationship between the circumferential speed difference between the first and second conveyor belts and analytical accuracy

operations on a real-time basis.

If the circumferential speed of the second conveyor belt is set at 20 cm/s, it is estimated that 24,000 fry per unit time per one processing line, or 120,000 fry per unit time per five processing lines can be counted by the image processing technique.

4. Conclusion

To count fry by an image processing system, a counting system comprising first and second belt conveyors, and a device to prevent multiplication of fry was fabricated, thereby the effects of the optimum circumferential speed difference between the first and the second conveyor belts, the threshold selection method for image analyses,lighting direction and illumination intensity upon counting accuracy were investigated. The results of the investigation are summarized below:

1) Threshold selections of fry pictures at threshold values of 40 and 50 are recommended rather than the discriminant analytical method.

2) To obtain stable video pictures, lighting from below the conveyor belt and an illumination intensity of 1,100 *lx* to 1,400 *lx* immediately above the conveyor belt are suitable.

3) Excited vibration of the first conveyor belt is effective for preventing multiplication of fry, but the travelling speed of fry neither increases nor decreases at acceleration of 18 cm/s^2 or above.

4) To achieve an efficient and accurate fry count, it is suitable to set the circumferential speed of the second conveyor belt at 20 cm/s, and maintain the circumferential speed difference between the first and the second conveyor belts in the range from −5 cm/s to 25 cm/s or thereabouts.

Acknowledgment

We wish to thank graduate students of department of fishery mechanical engineering, Tokyo University of Fisheries for their assistance in experimenting

References

CHEN, H. (1992): Studies on the conveying and counting system for seedlings fry sucked. Thesis for a degree of master (Tokyo university of Fisheries), 4–7.

YADA, S., H. CHEN, H. SAKAI and H. AKIZAWA (1993): Studies on the counting system for seedlings fry sucked by the vacuum pump. Fisheries Engineering, **30**(2), 93–99.

CHEN, H., S. YADA and H. SAKAI (1993): Effect of bubbles on the count accuracy of seedlings fry sucked with vacuum pump. Fisheries Engineering, **30**(2), 100–101.

HIGASHIKAWA, N., H. YADA, H. SAKAI and H. AKIZAWA (1993): Study on the automatic arrangement system of catched fresh fish for packaging. Fisheries Engineering, **30**(1), 9–14.

OTSU, N. (1980): Automatic threshold selection method based on discriminant and least squares criteria. ICE Trans, **1**(4) J63-D, 349–356.

TAMURA, H. (1985): Introduction to picture processing with computer compiled. Japan industrial technology center, Souken, Tokyo, 66-68.

TANIGUCHI, O., M. SAKATA, Y. SUZUKI and Y. OSANAI (1962): Studies on vibratory feeder. Transaction of the JSME, **18**, 485–491.

画像解析による種苗幼魚の計数精度に関する研究

矢田貞美・樋口宏一・小池孝知

要旨：画像解析装置による種苗幼魚の尾数計数を目的として，魚体の重複防止装置における2本のベルトコンベヤの組合せ方法，材質，構造及び適正周速度，魚体画像の2値化方法，照明方法と適正照度について究明した。

La mer 32: 195–207, 1994
Société franco-japonaise d'océanographie, Tokyo

Distribution of Diatom Assemblages in and around a Warm Core Ring in the North Pacific Polar Frontal Zone*

Kuo Ping CHIANG**†, Akira TANIGUCHI** and Satoshi KATO**

Abstract: Distribution of diatom assemblages in the North Pacific Polar Frontal Zone east of northern Japan in late spring was investigated in relation to distribution of water types. By principal component analyses, nine diatom assemblages and five water types were defined. Patterns of distribution of the diatom assemblages and the water types were not always consistent with each other, probably because of more conservative nature of the diatom assemblages than physico-chemical properties of the water types. The most widely distributed diatom assemblage, which is named as the Background Assemblage, was mainly composed of neritic cosmopolitan species and was observed to be small in population density. Production of the diatom assemblages is likely to be enhanced in the surface layer when water types other than a background mixed water intrude and then the new assembalges are formed there.

1. Introduction

The Kuroshio flows along the south coast of Japan archipelago and turns around 36° N into the Kuroshio Extension flowing eastward. The latter forms the southern border of the North Pacific Polar Frontal Zone, which demarcates the frontal zone from the subtropical waters in south. When the Kuroshio Extension has an extensive meander to north, a warm core ring is sometimes pinched off and shifts to further north. On the other hand, the Oyashio is usually flows in far north and demarcates the frontal zone from the subarctic water in north by forming the Oyashio Front. In addition to these two currents a less prevailing Tsugaru Warm Current intrudes from the Japan Sea through the Tsugaru Straits into the western edge of the frontal zone and flows southward along the east coast of Sanriku District. Consequently, oceanographic conditions in the western part of the Polar Frontal Zone are very complicated due to the interaction of several different water masses such as warm and cold core rings and streamers, coastal Tsugaru warm water, and neritic water which are scattered over a so-called mixed water (*e.g.* KAWAI, 1972; KAWAI and SAITOH, 1986: NAGATA *et al.*, 1992). The last water mass, which is the final mixture of all the water masses listed just above, occupies widely and then forms a background water mass of the frontal zone. It has been pointed out that identification of these water masses by a conventional T-S analysis is difficult (HANAWA and MITSUDERA, 1987).

A low productive diatom assemblage which is composed mainly of neritic cosmopolitan species is almost homogeneously distributed in the mixed water and named the Background Assemblage in the Polar Frontal Zone (CHIANG and TANIGUCHI, 1993). This assemblage is likely to be formed by winter convection of water which selects a few tolerant species to winter conditions. It has been suggested that some other productive assemblages are formed during warm seasons on this Background Assemblage particularly at the Kuroshio Front and coastal front and in a cold ring (*e.g.* MARUMO and AMANO, 1956; MARUMO, 1967; YAMAMOTO *et al.*, 1981, 1988). Therefore, the distribution of diatom assemblages in warm seasons can indicate the origin of very slightly different water masses that can not be identified by the T-S analysis.

In this paper, we try to identify water masses of different origins in detail by principal

* Received July 20, 1994
** Laboratory of Biological Oceanography, Faculty of Agriculture, Tohoku University, Sendai, Miyagi 981, Japan
† Present address: Department of Fishery Science, National Taiwan Ocean University, Keelung 20224, Taiwan, R.O.C.

component analyses of diatom assemblages in the western Polar Frontal Zone. Possible enhancement of diatom productivity in the localities where different waters intrude into the background mixed water mass is suggested.

2. Materials and methods

Samples were collected on the Cruise KT-90-7 of R/V "Tansei Maru" of the Ocean Research Institute of the University of Tokyo (Fig. 1). The cruise was divided into two legs. Leg 1 was for samplings at Sts. C20–C22 arranged on a longitudinal section crossing a warm core ring and St. C18 as a reference station in the Kuroshio Extension. Leg 1 was carried out during the period from 29 May to 2 June 1990. Leg 2 was for samplings at Sts. C30–C35 on a section crossing the edge of the same warm core ring, and Sts. C40 and C59 as references in cold mixed water and the Oyashio. Leg 2 was done in 3-10 June 1990. The section through Sts. C19–C22 and a supplemental St. C40 is named Line A and that through Sts. C30–C35 is Line B below.

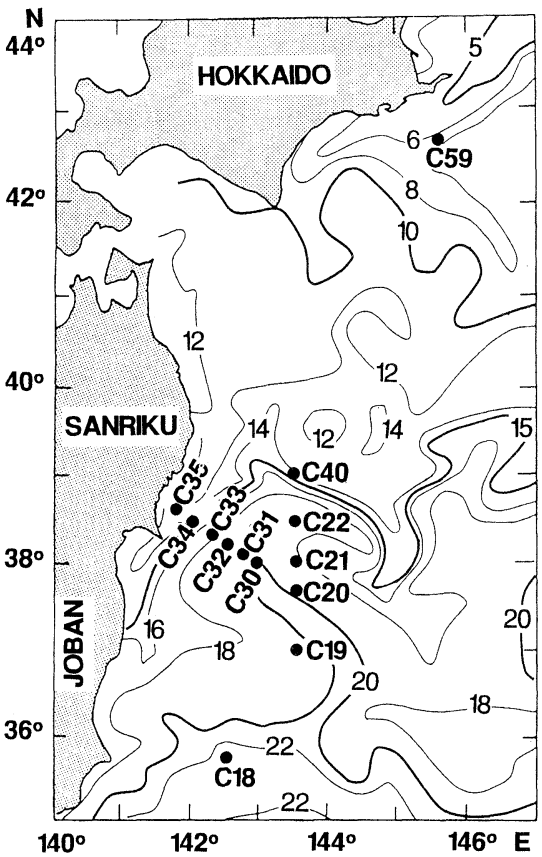

Fig. 1. Sampling stations occupied on the Cruise KT-90-7 to the western North Pacific Polar Frontal Zone during the period from 29 May to 10 June, 1990. Isotherms at the sea surface are adapted from the Japan Fisheries Information Service Center (1990)

Water samples were collected from 8–12 depths in the surface layer down to 75 m on Line A and down to 200 m on Line B. Methods of microscopic examination of diatom assemblages and chemical analyses of the nutrients such as dissolved silica, phosphate, nitrite, nitrate and ammonia were given in CHIANG and TANIGUCHI (1993).

To see relationships between diatom assmblages and water types in distribution, principal component analyses (PCAs) and cluster analyses (PIELOU, 1984) were done by using the oceanographic data set on temperature, salinity and five nutrients (PCA-OD) (Table 1) and the diatom data set. The latter was processed in the following two ways to reduce number of parameters reaching 160 species in total. At first, diatom species identified were grouped into 14 types according to their distributional characteristics (DC) reported in literature (KOKUBO, 1960, MARUMO *et al.*, 1966, YAMAJI, 1984) (Table 2). In the second way 24 common and dominant species (DS) which occurred in more than 50 % of samples were selected (Table 3). In the following sections, we describe the first as PCA-DC and the second as PCA-DS.

Position of the first principal component PC1 on X-axis and that of the second principal component PC2 on Y-axis in scatter diagrams of PC2 on PC1 were used to identify clusters of components by an average clustering method (Euclidean distance=0.6).

3. Results

3.1. *Water Types*

Line A: Data on the surface temperature over the sea areas around Japan gathered during the period from 1 to 5 June were compiled by the Japan Fisheries Information Service Center (Fig. 1). It gives general configuration of water masses at the surface around the day of the present sampling; the Kuroshio Extension which flowed eastward along the 22°C isotherm, a

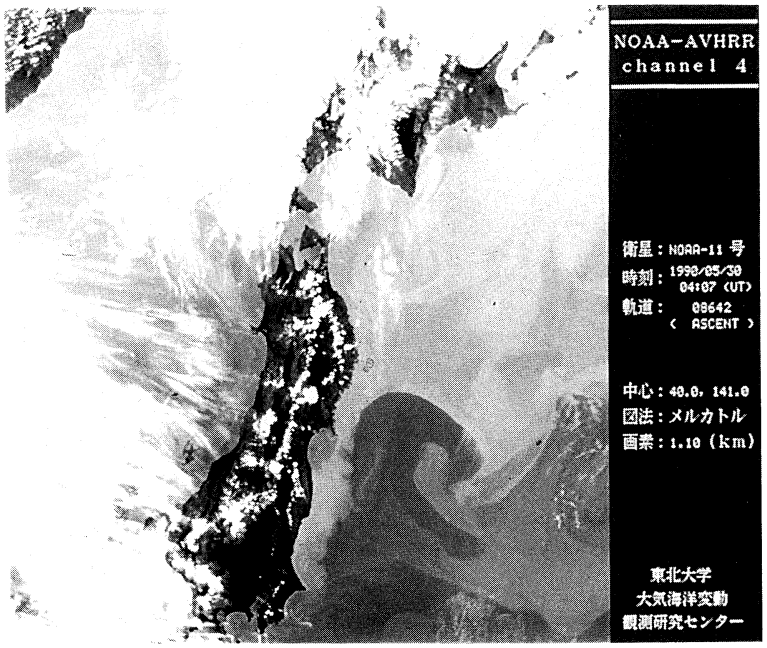

Fig. 2. An image of the warm streamer shot to the warm core ring around St. C22 (*cf.* Fig. 1) from the other ring in the east (NOAA-AVHRR Channel 4)

warm core ring which centered around 38°30′ N, 143°30′ E, and a narrow coastal flow or the Tsugaru Warm Current which flows southward along the isotherms of 12–14°C. Although a warm streamer seems to extrude from the Kuroshio Extension and form a mushroom-shaped warm water body in this figure, satellite imagery (NOAA AVHRR) taken on 30 May indicates that the streamer ran out of the other warm core ring in the east (Fig. 2), which is indicated by a 20°C isotherm on the right end of Fig. 1. The streamer was taken into the south-western edge (around St. C31) of the warm core ring which occupied the area around Sts. C20–22 (see blow).

Thermal structure in the longitudinal vertical section along Line A illustrates the lens-shaped warm core between 100 m and 400 m depths (Fig. 3). Therefore, we could identify position of the sampling stations in relation to the warm core ring: St. C19 was in south and St. C40 were in north of the ring, Sts. C20 and C22 were at the edge and St. C21 was at the center of the ring. Details of hydrographic structure in the surface layer of these stations, where the plankton samples were collected are given in Figs. 4 and 5. High temperature and high salinity water

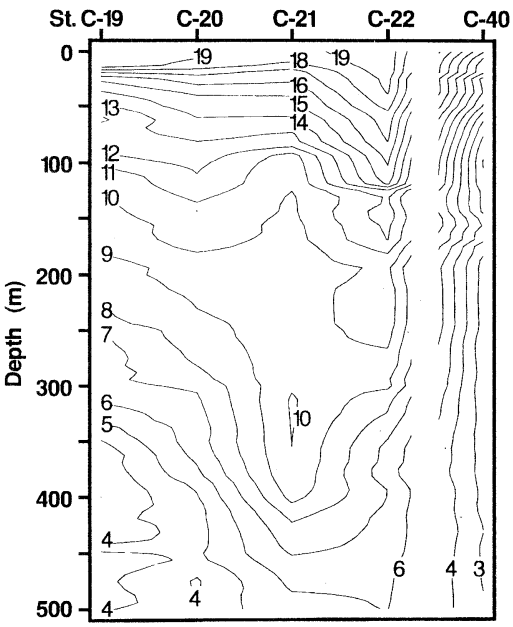

Fig. 3. Distribution of temperature (℃) in vertical section along the longitudinal Line A(143°30′ E) crossing the warm core ring. Data were obtained by CTD casts down to 1000 m. Since Sts. C19–C22 and St. C40 were occupied on different legs of the same cruise, a space is set between Sts. C22 and C40.

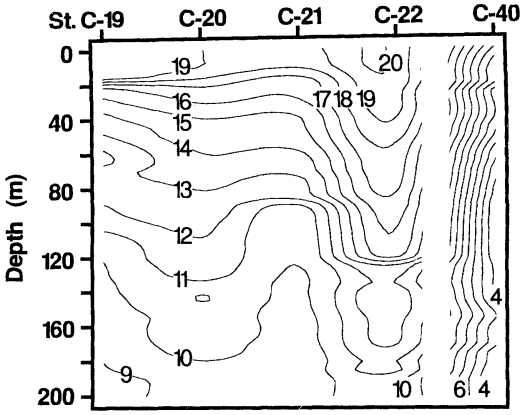

Fig. 4. Detail of temperature (℃) section in 0-200 m layer on Line A. Since Sts. C19–C22 and St. C40 were occupied on different legs of the same cruise, a space is set between Sts. C22 and C40.

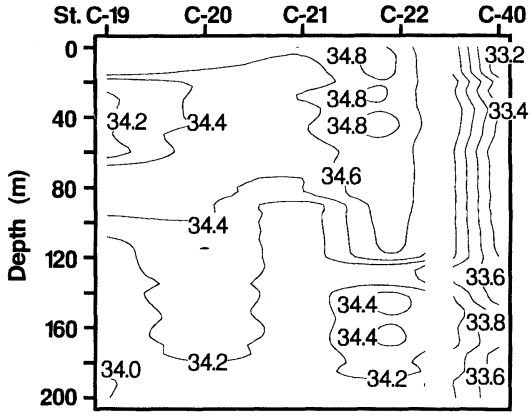

Fig. 5. Salinity (psu) section in 0-200 m layer on Line A. Since Sts. C19–C22 and St. C40 were occupied on different legs of the same cruise, a space is set between Sts. C22 and C40.

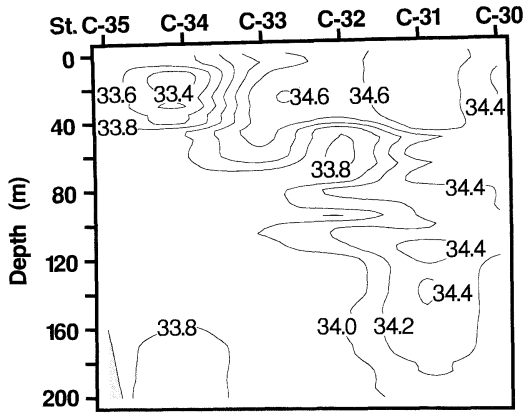

Fig. 6. Temperature(℃) section in 0–200 m layer on Line B crossing western edge of the warm core ring. Data were obtained by CTD casts down to 1000 m.

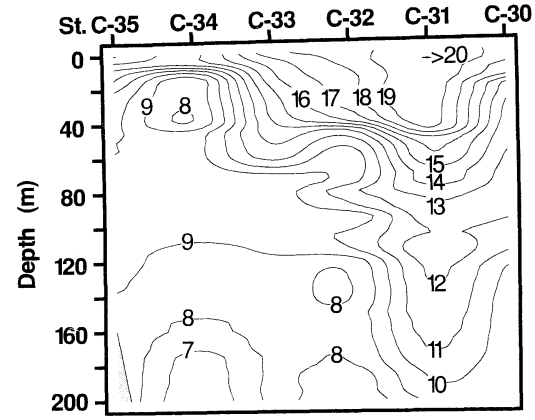

Fig. 7. Salinity (psu) section in 0-200 m layer on Line B.

(>19°C, >34.7 psu) originated from the warm streamer was observed in 0–20 m at Sts. C19 and C20 and in 0–40 m at St. C22. Low salinity subsurface water observed between 20 m and 60 m at St. C19 might be derived from the coastal water off Joban District (*cf.* Fig. 1).

Line B: In the vertical sections of temperature and salinity along Line B (Figs. 6 and 7), low temperature and low salinity coastal water originated from the Tsugaru Warm Current can be seen in the layer between 10 m and 50 m at St. C34, while the same current is illustrated at St. C35 in Fig. 1. In this vertical section, St. C30 was judged to be at the western edge of the ring because edge of the lens-shaped core was detected by the CTD casts (CHIANG, 1993). This is partly illustrated by 10℃ isotherm in Fig.6. St. C31 was judged to be in the warm streamer, which intruded into the surface 40 m at St. C31. Consequently, thermocline and halocline were bent upward to the surface at Sts. C33 and C34 and downward to the subsurface at St. C31.

By the method of T-S analysis described by HANAWA and MITSUDERA (1987), following three water systems were defined. First, high temperature and high salinity water (10–20°C, >34.2 psu) occupied most part of the top 200 m water columns in and south of the warm core

ring was recognized as derived from the Kuroshio Current. HANAWA and MITSUDERA (1987) named this type of water the Kuroshio Water System. Second was high temperature and intermediate salinity water (5–20°C, 33.7–34.2 psu) which was observed in west of the ring. This type was named the Tsugaru Warm Current Water System by HANAWA and MITSUDERA (1987). Third was low temperature and low salinity water (0–7°C, 33.0–33.7 psu) named as the Coastal Oyashio Water System (HANAWA and MITSUDERA, 1987). This type was observed in north of the ring (St. C40) indicating the influence of the Oyashio Current. In this paper, however, water types were defined by the principal component analysis using oceanographic data including not only temperature and salinity but also five nutrients (PCA-OD) (Table 1). PC1 explains 47.31% of total variance and positively correlates with dissolved silica and nitrate but negatively with temperature. PC2 accounts for 15.15% of the variance and positively correlates with salinity and nitrite.

In a scatter diagram of PC2 on PC1 eight clusters were identified (Fig. 10), which are given in column OD of Tables 4 and 5. Then, five water types could be recognized (*cf.* Figs. 13 and 14). The first was high temperature surface water (Cluster A) occupied the surface layer in and south of the warm core ring (Sts.C19–C22,C30–C33) as well as in the Kuroshio Extension (St. C18). This is named here the Surface Water Type. The second which occupied the surface layers in west (Sts. C34–C35) and north (St. C40) of the ring is named the Coastal Water Type

Table 1. Oceanographic data used as variables for the PCA-OD and their eigenvectors of PC1 and PC2. Percentage of variance explained is indicated below each of PC1 and PC2.

Variables	PC1 47.31%	PC2 15.15%
Temperature	−0.499	0.242
Salinity	−0.385	0.511
Dissolved Silica	0.450	0.111
Phosphate	0.326	0.023
Nitrate	0.483	0.154
Nitrite	0.182	0.743
Ammonia	0.166	0.302

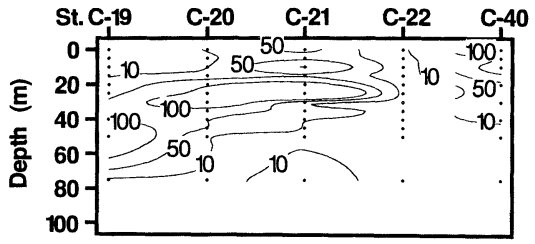

Fig. 8. Distribution in cell number of total diatom populations (10^3 cells l^{-1}) in vertical section along Line A.

(Clusters B and E). This seems to be originated from the northern coastal area off Sanriku District. Similar water type was also found in subsurface at St. C19 (Cluster B), which is likely to be originated from the Joban coastal area instead of the Sanriku coastal area (Fig. 1) and named the Joban Coastal Water Type. The fourth was the Mid-layer Water Type (Clusters C, D and F) widely occupying subsurface layer in almost entire area. The fifth was the Oyashio Water Type (Clusters G and H) which was found in subsurface at Sts. C40 and C59.

3.2. *Diatom Assemblages*

On Line A, the maximum abundance of diatoms in vertical distribution was found in subsurface layer except at St. C40 where the maximum was found at the surface (Fig. 8). It should be noted that the subsurface maximum around 50 m at St. C19 was coincident with position of the Joban Coastal Water Type described

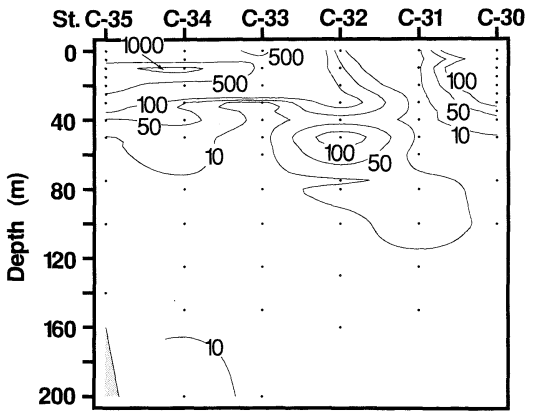

Fig. 9. Distribution in cell number of total diatom populations (10^3 cells l^{-1}) in vertical section along Line B.

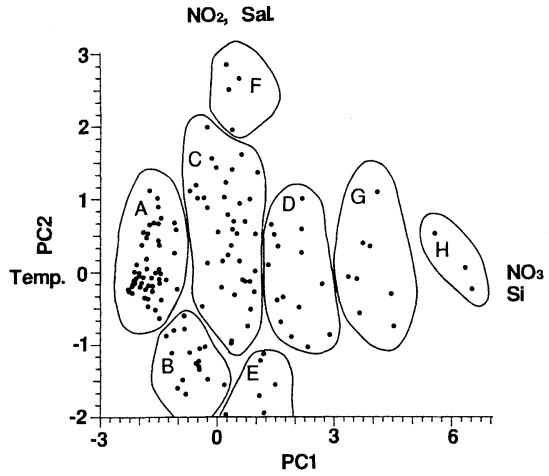

Fig. 10. Scatter diagram of PC2 on PC1 of the principal component analysis using oceanographic data (PCA-OD) (*cf.* Table 1). Envelops denote eight clusters identified by an average cluster analysis.

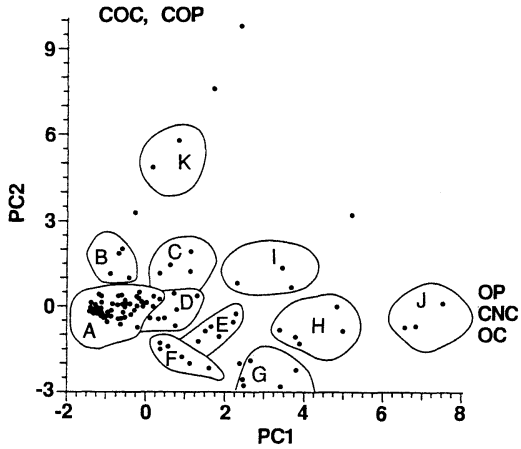

Fig. 11. Scatter diagram based on 14 groups of diatoms which were grouped by their distributional characteristics (PCA-DC) (*cf.* Table 2). Envelops denote 11 clusters identified by cluster analysis. Five points out of envelops A-K are marked # in Tables 5 and 6.

above. On the other hand, abundance of diatoms was low at St. C22 and in the warm streamer in the surface layer shallower than 20 m at Sts. C19–C20.

On Line B, the maximum abundance was generally found in the top 20 m except Sts. C31 and C32, where diatom became abundant in 50–100 m layer (Fig. 9). In the surface layer at St. C31 occupied by the warm streamer, diatom stock was low as observed at Sts. C19 and C20.

In the principal component analysis based on groups of diatom species classified by the distri-

Table 2. Fourteen types of diatoms grouped by their distributional characteristics used as variables for the PCA-DC and their eigenvectors of PC1 and PC2. Percentage of variance explained is indicated below each of PC1 and PC2.

Diatom group/Variable	PC1 28.43%	PC2 18.04%
Cold oceanic centric diatoms (COC)	0.074	0.572
Cold neritic centric diatoms (CNC)	0.452	0.158
Warm oceanic centric diatoms (WOC)	0.306	−0.235
Warm neritic centric diatoms (WNC)	0.154	0.311
Oceanic cosmopolitan centric diatoms (OCC)	0.268	−0.267
Neritic cosmopolitan centric diatoms (NCC)	0.321	0.035
Other centric diatoms (OC)	0.430	−0.057
Cold oceanic pennate diatoms (COP)	0.040	0.570
Cold neritic pennate diatoms (CNP)	0.000	0.000
Warm oceanic pennate diatoms (WOP)	0.057	−0.076
Warm neritic pennate diatoms (WNP)	0.249	−0.266
Oceanic cosmopolitan pennate diatoms (OCP)	0.000	0.000
Neritic cosmopolitan pennate diatoms (NCP)	0.193	0.127
Other pennate diatoms (OP)	0.457	0.042

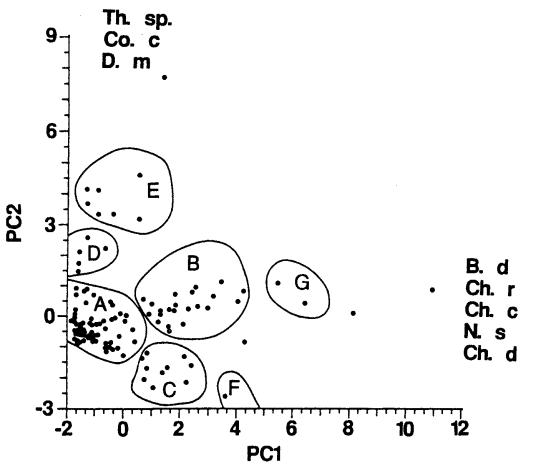

Fig. 12. Scatter diagram based on 13 dominant and common daitom species which occurred in more than 50 % of samples (PCA-DS)(*cf.* Table 3). Envelops denote seven clusters identified by cluster analysis. Six points out of envelops A-K are marked # in Tables 5 and 6, two of which are far out of this diagram.

bution nature (PCA-DC), the first (PC1) and second principal components (PC2) account for 46.47% of total variance (Table 2). PC1 positively correlates with three groups of cold neritic centric diatoms, other centric diatoms and other pennate diatoms, and PC2 with two groups of cold oceanic centric diatoms and cold oceanic pennate diatoms. In principal component analysis based on dominant diatom species (PCA-DS), PC1 and PC2 account for 36.16% of the variance. PC1 is influenced by *Bacteriastrum delicatulum, Chaetoceros compressum, C. didymum, C. radicans* and *Nitzschia seriata*, and PC2 by *Corethron criophilum, Denticulopsis marina* and *Thalassiosira* sp. (Table 3). Figs. 11 and 12 illustrate scatters of PC2s on PC1s in PCA-DC and PCA-DS, respectively, and eleven and seven clusters were identified. These results are summarized in the columns of DC and DS in Tables 4 and 5. Compiling these results nine diatom assemblages were finally defined as below (also *cf.* Table 6).

(1) Kuroshio Extension Assemblage: This assemblage was defined by the combinations of Cluster A in PCA-DC and Cluster C or Cluster F in PCA-DS. These combinations can be expressed in A-C and A-F and found only in the surface

Table 3. Twenty-four dominant diatom species, which occurred in more than 50% of samples, used as variables for the PCA-DS and their eigenvectors of PC1 and PC2. Percentage of variance explained is indicated below each of PC1 and PC2.

Variables	PC1 23.00%	PC2 13.16%
Asterionella glacialis	0.191	−0.070
Bacteriastrum delicatulum	0.377	−0.022
Chaetoceros compressum	0.326	0.045
Chaetoceros decipiens	0.134	0.014
Chaetoceros didymum	0.323	−0.101
Chaetoceros peruvianum	0.160	0.069
Chaetoceros radicans	0.330	0.157
Corethron criophilum	0.031	0.481
Denticulopsis marina	−0.017	0.470
Leptocylindrus danicus	0.070	−0.125
Navicula distans	0.134	0.056
Navicula membranacea	0.170	−0.082
Navicula sp.	−0.022	−0.041
Nitzschia closterium	0.232	0.096
Nitzschia longissima	0.277	0.008
Nitzschia seriata	0.324	−0.057
Nitzschia sp.	−0.001	0.361
Rhizosolenia alata	0.191	0.108
Rhizosolenia bergonii	0.124	−0.154
Rhizosolenia fragilissima	0.247	−0.004
Rhizosolenia stolterfothii	0.154	−0.187
Pseudoeunotia doliolus	0.124	0.031
Thalassionema nitzschioides	0.119	−0.144
Thalassiosira sp.	0.042	0.488

layer between 0 m and 35 m at St. C18 (Table 4). Dominant species in this assemblage were *C. compressum, Hemiaulus sinensis, Leptocylindrus danicus, N. seriata* and *Thalassionema nitzschioides*, which have been reported as warm neritic or neritic cosmopolitan species. Population density of this assemblage ($3\times10^4-1.2\times10^5$ cells l^{-1}) was not large comparing to the other assemblages in this season.

(2) Joban Coastal Assemblage: This assemblage was defined by Clusters D, E, F, G, H in PCA-DC, all of which appeared in the fourth quadrant of scatter diagram (Fig. 11), and Clusters B and G in PCA-DS (Tables 4 and 5). Isolated Cluster # in PCA-DS found at 10 m at St. C21, which is different from Clusters B and

G but very similar to them, appeared in the first quadrant of Fig. 12. Therefore, this cluster was also categorized in this assemblage. This assemblage was found in the subsurface layer (20–50 m) at St. C19 below the warm streamer and in the surface and subsurface layer of the warm core ring, *i.e.* 20–45 m St. C20, 0–35 m at St. C21 and 0–35 m at St. C30. Dominant species were *Chaetoceros compressum, C. peruvianum, C. radicans, N. seriata* and *Pseudoeunotia doliolus*. Peak-forming species, whose peak (or one of peaks) in distribution occurred in the distributional range of this assemblage, were *C. compressum, C. peruvianum, C. radicans, P. doliolus, B. delicaturum* and *Rhizosolenia fragilissima*. These species indicate the relatively warm water preference of this assemblage, while a few cold neritic species were mixed with. Population density was intermediate being $4\times10^4-4.8\times10^5$ cells l^{-1}.

(3) Coastal Front Assemblage: This assemblage was clearly defined by combinations of clusters of G-# and H-# and also by D-B, E-E and F-A. The latter three were considered to be derived from A-A and similar to H-# in the scatter diagrams. This assemblage was intermediate in population density ($1\times10^5-6\times10^5$ cells l^{-1}) and found only in frontal zone between the warm core ring and the coastal water (Sts. C32 and C33) (Table 5). Dominant species were *B. delicatulum, C. compressum, C. peruvianum, C. radicans* and *N. seriata*, and the peak-forming species were *Asterionella gracialis, B. delicatulum, C. compressum, C. didymum, C. peruvianum* and *P. doliolus*. This species composition seems to be similar to the Joban Coastal Assemblage, but the neritic nature is much stronger.

(4) Tsugaru Warm Current Assemblage: This assemblage was defined by Cluster I and its closely allied Cluster # in PCA-DC and by Clusters B, C and F in PCA-DS. This assemblage was found in 5–20 m at St. C34 where the Tsugaru Warm Current flowed from north. The maximum diatom abundance throughout this investigation was observed in this assemblage (10 m at St. C34). The dominant species were *C. compressum, C. frichei, C. radicans, L. danicus* and *N. seriata*, and the peak-forming species were *C. frichei, R. fragilissima, R. stolterfothii, Skeletonema costatum* and *T. nitzschioides*. These species indicate the neritic nature of this assemblage. Population density was $2\times10^5-1.1\times10^6$ cells l^{-1}.

(5) Southern Sanriku Coastal Assemblage: The assemblage defined by C-C was found in 0–25 m at St. C35 which was the nearest station to the coast. However, neritic nature as well as population density ($3\times10^5-9\times10^5$ cells l^{-1}) of this assemblage was smaller than those of the Tsugaru Warm Current Assemblage. The dominant species were *C. compressum, C. curvisetum, C. frichei, L. danicus* and *N. seriata*, and the peak-forming species were *C. curvisetum, C. decipiens* and *L. danicus*.

(6) Northern Mixed Assemblage 1: The assemblage defined by D-B and I-B occurred in 0-10 m at St. C40 which was located in north of the warm core ring. The dominant species were *C. curvisetum, C. radicans, L. danicus, N. closterium* and *N. seriata*, and the peak-forming species were *A. gracialis, B. delicatulum, C. compressum, C. curvisetum, C. decipiens, C. frichei, C. radicans, L. danicus* and *T. nitzschioides*. This species composition indicates that this assemblage was formed by mixing of cold-water species such as *C. decipiens* into the Background Assemblage, which is described later. Population density was intermediate, being $1.1\times10^5-3\times10^5$ cells l^{-1}.

(7) Northern Mixed Assemblage 2: This assemblage defined by A-D and A-E occurred in 20-40 m at St. C40 or just below the Northern Mixed Assemblage 1. Therefore, population density was one order of magnitude lower than the Assemblage 1, being $1.2\times10^4-4\times10^4$ cells l^{-1}. The dominant species were *C. curvisetum, D. marina, L. danicus, N. closterium* and *N. seriata*. The peak-forming species was not found in this assemblage.

(8) Oyashio Assemblage: This assemblage was defined by combinations of Clusters #, K and B in PCA-DC and of Cluster #, D and E in PCA-DS. This was found at 0–50 m and 100–150 m at St. C59 and dominated by *Chaetoceros concavicorne, C. curvisetum, C. radicans, D. marina* and *Thalassiosira nordenskioldii*. Since St. C59 was isolated in north of the Polar Frontal Zone, the peak-forming species were not judged. Nevertheless, cold-water nature of this

Table 4. Distribution of the clusters separated by three PCAs based on oceanographic data (OD), and abundances of distributional groups (DC) and dominant species (DS) as variables for Leg 1 of the Cruise KT-90-7.

ST& Dep.	OD	DC	DS	ST& Dep.	OD	DC	DS	ST& Dep.	OD	DC	DS	ST& Dep.	OD	DC	DS	ST& Dep.	OD	DC	DS	ST& Dep.	OD	DC	DS
C18-0	A	A	C	C19-0	A	A	A	C20-0	A	A	A	C21-0	A	D	B	C22-0	A	A	A	C40-0	E	I	B
5	A	A	C	5	A	A	A	5	A	A	A	5	A	D	B	5	A	A	A	5	B	D	B
10	A	A	C	10	A	A	A	10	A	A	A	10	A	E	#	10	A	A	A	10	B	D	B
15	A	A	F	15	A	A	A	15	A	A	A	15	A	D	B	15	*	A	A	20	E	A	D
20	A	A	C	20	B	F	A	20	A	E	B	20	C	E	B	20	A	A	A	30	D	A	E
25	A	A	F	25	B	F	A	25	*	E	B	25	A	H	B	25	A	A	A	40	G	A	D
30	A	A	C	35	C	*	*	30	A	G	B	30	C	F	A	30	A	A	A	50	E	A	A
35	A	A	C	40	B	G	B	35	*	G	B	35	F	D	A	35	A	A	A	75	D	A	A
40	A	A	A	50	B	H	B	40	C	F	A	40	F	A	A	40	A	A	A	100	G	A	A
45	A	A	A	75	C	A	A	45	F	F	A	45	C	A	A	45	A	A	A	125	D	A	A
50	A	A	A					50	F	A	A	50	C	A	A	50	A	A	A	150	G	A	A
								75	F	A	A	75	C	A	D	75	A	A	A	200	G	A	A

*: Samples were not collected from the layers.
#: The community is different from all others.

Table 5. The same as Table 4 but for Leg 2.

ST& Dep.	OD	DC	DS	ST& Dep.	OD	DC	DS	ST& Dep.	OD	DC	DS	ST& Dep.	OD	DC	DS	ST& Dep.	OD	DC	DS	ST& Dep.	OD	DC	DS	ST& Dep.	OD	DC	DS
C30-0	A	J	G	C31-0	A	A	A	C32-0	A	A	A	C33-0	A	J	#	C34-0	B	A	A	C35-0	B	C	C	C59-0	E	#	E
5	A	E	B	10	A	A	A	10	A	A	A	10	A	J	#	5	B	I	C	5	B	A	A	5	E	*	*
10	A	H	G	20	A	A	A	20	A	A	A	20	C	H	#	10	B	#	F	10	B	C	C	10	E	#	E
15	C	H	B	30	A	A	A	30	A	D	B	30	C	A	A	20	B	I	B	15	B	C	A	15	E	K	#
20	C	G	B	40	A	A	A	40	C	A	A	40	C	A	A	30	D	A	A	20	B	C	C	20	G	#	E
25	D	G	B	50	B	A	A	50	C	E	E	50	C	A	A	40	C	A	A	25	B	B	A	30	D	K	#
30	C	G	B	60	C	A	A	75	D	F	A	60	C	A	A	50	C	A	A	30	B	A	A	40	G	B	E
35	C	F	A	80	C	A	A	80	C	A	A	80	C	A	A	80	B	A	A	40	B	A	A	50	G	B	E
40	C	A	A	100	C	A	A	100	D	A	A	100	C	A	A	100	C	A	A	50	C	A	A	75	G	A	A
50	C	A	A	125	C	A	A	130	D	A	A	125	C	A	A	125	C	A	A	75	C	A	A	100	H	A	D
75	C	A	A	150	D	A	A	160	D	A	A	150	C	A	A	150	C	A	A	100	C	A	A	150	H	B	D
100	B	A	A	200	D	*	*	200	D	A	A	200	D	A	A	200	D	A	A	140	C	A	A	200	H	A	A

*: Samples were not collected from the layers.
#: The community is different from all others.

assemblage is clearly indicated by these dominant species, while a few warm neritic species were mixed. Population density was intermediate being $2\times10^4-8\times10^5$ cells l^{-1}.

(9) Background Assemblage: This assemblage was defined by A-A. Neritic cosmopolitans *C. compressum, N. closterium, S. seriata, T. nitzschioides*, and a cold neritic *C. radicans* were major components of this assemblage. Important is that this assemblage was smallest in population density but most widely distributed over the sampling area. The density rarely exceeded 1×10^4 cells l^{-1} with a few exceptions in the surface layer at St. C34. This assemblage is considered to be produced and distributed homogeneously in water column by winter convection

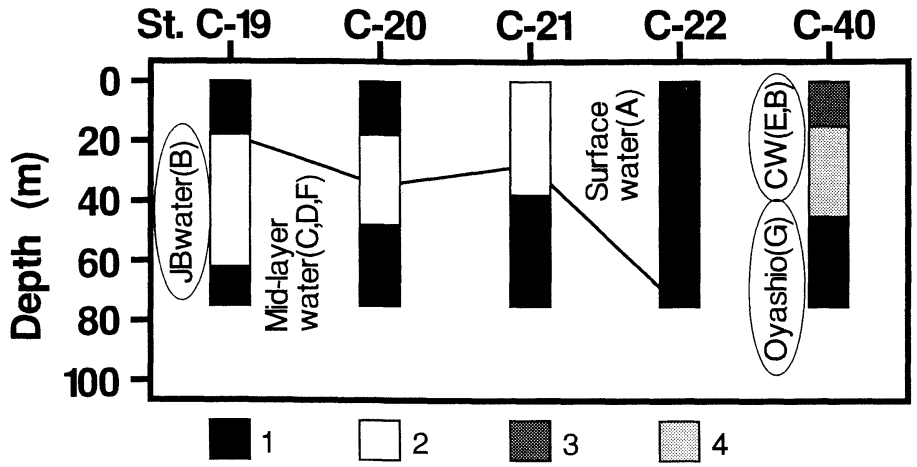

Fig. 13. Distributions of water types and diatom assemblages defined by PCAs in vertical section along Line A (*cf.* Table 6). 1: Background Assemblage, 2: Joban Coastal Assemblage, 3: Northern Mixed Assemblage 1, 4: Northern Mixed Assemblage 2.

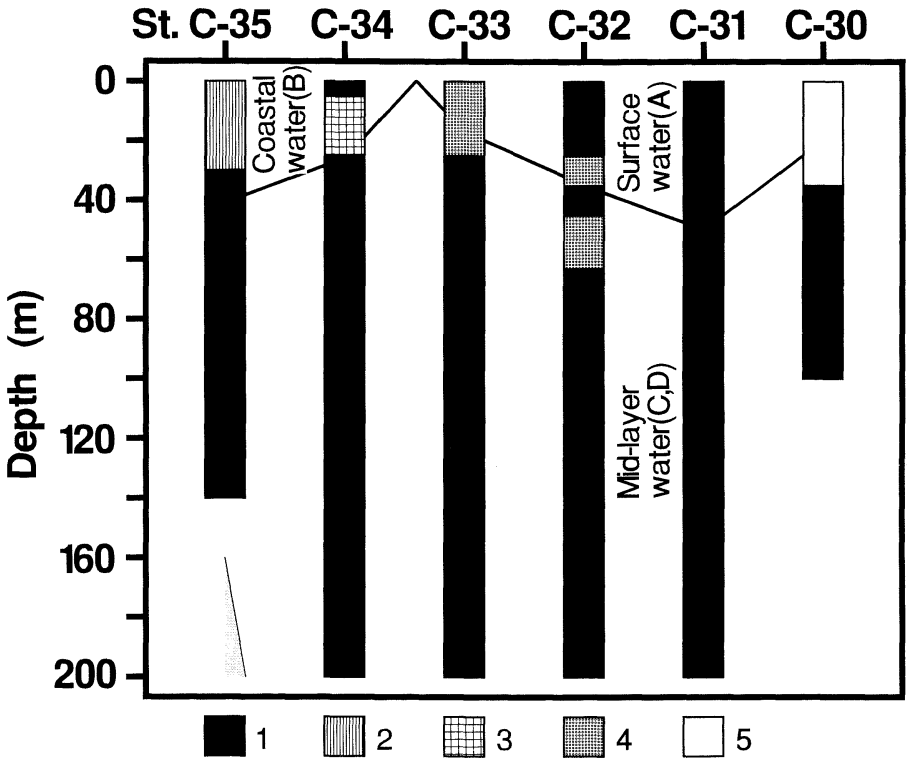

Fig. 14. Distributions of water types and diatom assemblages defined by PCAs in vertical section along Line B (*cf.* Table 6). 1: Background Assemblage, 2: Southern Sanriku Coastal Assemblage, 3: Tsugaru Warm Current Assemblage, 4: Coastal Front Assemblage, 5: Joban Coastal Assemblage

down to the permanent halocline in the entire Polar Frontal Zone (CHIANG and TANIGUCHI, 1993).

4. Discussion

PCA-OD yielded double layered structure of water column in vertical sections along Lines A and B where the shallow Surface Water Type covers the thick Mid-layer Water Type except the southernmost (St. C19) and northernmost stations (St. C40) outside of the warm core ring. At the latter two stations the Joban Coastal Water Type, the Coastal Water Type and the Oyashio Water Type were identified separately from the prevailing two water types in the surface and mid-layers. This result gives rather simple picture of hydrographic feature in this area as if foreign water masses other than the Surface and Mid-layer Water Types intrude only at both edges of Line A (Sts. C19 and C40) (Figs. 13 and 14).

Distribution of the nine diatom assemblages defined above indicates configuration of water types of different natures much more precisely. The Kuroshio Extension Assemblage which was composed of warm neritic species existed only in the top 35 m at St. C18. This indicates that the Kuroshio Extension water carrying neritic species entrained by the Kuroshio during its flow along southeast coast of western to central Japan (YAMAMOTO *et al.*, 1988) did not extend to the other stations. Although the warm streamer is illustrated as if ran out from the Kuroshio Extension in Fig. 1, no direct influence of the Extension water was observed in the diatom assemblages at the surface at Sts. C19, C20, C31 and C32 in and near the streamer.

At the latter stations the Background Assemblage was found, below which the Joban Coastal Assemblage containing a few cold neritic species was found (Figs. 13 and 14). Coexistence of the cold neritic species indicates that the Joban Coastal Assemblage came from the Joban coastal region north of the Kuroshio Extension. The Joban Coastal Assemblage was found as intruded subsurface layer (20–70 m) at St. C19 and uplifted to the surface at Sts. C21 and C30. Low-salinity water (<34.5 psu) found at Sts. C19 and C21 seems to indicate partly this course (Fig. 5) but PCA-OD as well as conventional T-S analysis could not reveal this. Such a discrepancy is thought to be produced by different natures between the physico-chemical property of water and the plankton assemblage. The former (temperature, salinity and five nutrients) changes gradually and continuously by mixing of water types. However, individual plankters continue to exist after their populations are mixed. This conservative nature vests plankton assemblage with practical value as the tracer of changing and mixing water types (FRYXELL *et al.*, 1984; KACZMARSKA *et al.*, 1986). PCAs can identify those assemblage different from neighboring assemblages being composed of similar species.

At St. C59 in the northern extreme of the study area the Oyashio Assemblage was found. Since this assemblage contained a few warm water species, it can be understood that influence of the warm water had extended to east of Hokkaido in this season. The Oyashio Assemblage was likely to be modified into the Northern Mixed Assemblages 1 and 2 by further mixing with warm water at St. C40, which indicated by relative position of respective clusters in Figs. 11 and 12. Degree of the mixing of warm water was lesser in subsurface (Assemblage 2) than in the surface (Assemblage 1) as expected. On the other hand, typical Oyashio Assemblage was not found even below the Assemblage 2 where the Oyashio Water System was identified by T-S analysis; the Background Assemblage was found there. This fact demonstrates that the Background Assemblage which had been formed in winter through entire water column in the Oyashio and the mixed water regions (CHIANG and TANIGUCHI, 1993) was kept unchanged below the euphotic zone. This is the possible reason why the Background Assemblage was pervading the deeper part of water columns over the entire area (Figs. 13 and 14).

In the Coastal Water Type at Sts. C34 and C35 which was identified by PCA-OD, two different diatom assemblages, *i.e.* the Tsugaru Warm Current Assemblage and Southern Sanriku Coastal Assemblage, were found. The Tsugaru Warm Current is known as a narrow coastal flow in the surface layer which is hardly distinguished from the Sanriku coastal water system by conventional T-S analysis (*cf.* KAWAI, 1972; HA-

NAWA and MITSUDERA, 1987). The present PCA-OD could not distinguish these two waters too, but the PCA-DC and PCA-DS detect the distinction between them. Revelation of the Coastal Front Assemblage at Sts. C32 and C33 is an another example showing high ability of diatom assemblage to distinguish slightly different water types. Two-layered structure of this assemblage at St. C32 (Fig. 14) strongly indicates the complexity in fine scale of local mixing process of converging waters at frontal region.

The facts described above demonstrate that the distribution pattern of diatom assemblages was not always consistent with that of the water types, usually being more complex. The Background Assemblage pervaded the entire section, on which seven other assemblages were distributed in different way from the distribution of water types (Figs. 13 and 14). In other words, PCA-DC and PCA-DS can trace distribution of different waters more precisely than PCA-OD and conventional T-S analysis as well.

It should be noted again that the Background Assemblage was smallest in population density among assemblage found in this season except the Nothern Mixed Assemblage 2 which was at the same level or exceeded very slightly the Background Assemblage in the density. Since the Northern Mixed Assemblage 2 occurred in subsurface layer at St. C40, low underwater light intensity may be primarily responsible for its lower population density. The same can undoubtedly be the case for the Background Assemblage distributed in subsurface layer over entire area. However, although the Background Assemblage was also found commonly in the surface layer (Figs. 13 and 14), its size was small. This is most likely to indicate that the diatom production is not high in the background water type occupying large part of the North Pacific Polar Front (*cf.* TANIGUCHI, 1981). The production is enhanced in the surface layer where the other water types such as warm streamer and coastal water as well as the Oyashio water intrude, where, in turn, new assemblage are formed.

Acknowledgment

We are grateful to Drs. A. OKATA, K. MORI and Y. ENDO of the Tohoku University for their constructive comments on this work. Kind guidance in PCA given by Dr. Y. ENDO was particularly appreciated. We also thank Dr. H. KAWAMURA of the same university for his kind permission for us to use satellite imagery filed in the Center for Atmospheric and Oceanic Science.

Reference

CHIANG, K.P. (1993): Studies on Oceanographic Structure and Distribution of Phytoplankton Assemblages in the Sea Area off Eastern Hokkaido and Tohoku Districts, Japan. Ph. D. Thesis, Tohoku University, Sendai, 260 pp. (In Japanese with English abstract)

CHIANG, K.P. and A. TANIGUCHI (1993): Formation of diatom assemblage distributed widely in the North Pacific Polar Frontal Zone. Bull. Jap. Soc. Fish. Oceanogr., **57**, 307–318.

FRYXELL, G.A., R.W. GOULD, Jr., E.R. BALMORI and E.C. THERIOT (1985): Gulf Stream warm core rings: phytoplankton in two fall rings of different ages. J. Plankton Res., **7**, 339–364.

HANAWA, K. and H. MITSUDERA (1987): Variation of water system distribution in the Sanriku coastal area. J. Oceanogr. Soc. Japan, **42**, 435–446.

JAPAN FISHERIES INFORMATION SERVICE CENTER (1990): Prompt Report of Fisheries Oceanographical Conditions, No. 1119, 2 pp. (In Japanese)

KACZMARSKA, I., G.A. FRYXELL and T.P. WATKINS (1986): Effect of two Gulf Stream warm-core rings on distribution patterns of the diatom genus *Nitzschia*. Deep-Sea Res., **33**, 1843–1868.

KAWAI, H. (1972): Hydrography of the Kuroshio and Oyashio, pp. 129–309. *In* Kaiyo-kagaku Kiso Koza, 2 MASUZAWA, J. (ed.) Tokai Univ. Press., Tokyo (in Japanese).

KAWAI, H. and S. SAITOH (1986): Secondary fronts, warm tongues and warm streamers of the Kuroshio Extension system. Deep-Sea Res., **33**, 1487–1507.

KOKUBO, S. (1960): Planktonic Diatoms. Koseisha Koseikaku, Tokyo, 330 pp. (in Japanese).

MARUMO, R. (1967): General features of diatom communities in the North Pacific in summer. Inform. Bull. Planktol. Japan, Commem. No. Dr. Y. MATSUE , 115–122.

MARUMO, R. and M. AMANO (1956):Planktological and hydrographical conditions in the Yakumizu water east of Miyako in May 1955. J. Oceanogr. Soc. Japan, **12**, 53–58. (in Japanese with English abstract)

MARUMO, R., H. TAKANO and Y. KAWARADA (1966): Illustrations of the Marine Plankton of Japan, Vol. 1. Soyoshya, Tokyo, 69 pp. (in Japanese).

NAGATA, Y., K. OHTANI and M. KASHIWAI (1992): Subarctic Gyre in the North Pacific Ocean. Umi no Kenkyu, **1**, 75–103. (in Japanese with English abstract)

PIELOU, E.C. (1984): The Interpretation of Ecological Data. John Wiley, New York, 263 pp.

TANIGUCHI, A. (1981): Plankton productivities in the Pacific Subarctic Boundary Zone: food condition of the pelagic fishes. Res. Inst. Nor. Pac. Fish. Hokkaido Univ., Spec. Vol., 23–35. (in Japanese with English abstract)

YAMAJI, I. (1984): Illustration of the Marine Plankton of Japan (3rd edn.), Hoikusha, Osaka, 537 pp. (in Japanese)

YAMAMOTO, T., A. TANIGUCHI and S. NISHIZAWA (1981): Microplankton distribution at an oceanic front formed in the Sanriku Water off northeast Japan. Bull. Plankton Soc. Japan, **28**, 111–120.

YAMAMOTO, T., S. NISHIZAWA and A. TANIGUCHI (1988): Formation and retention mechanisms of phytoplankton peak abundance in the Kuroshio Front. J. Plankton Res., **10**, 1113–1130.

北太平洋極前線海域の暖水塊およびその周辺における珪藻群集の分布

蒋　国平・谷口　旭・加藤　聡

要旨：北太平洋極前線海域における晩春の珪藻群集の分布を，水型の分布との関連で調査した。主成分分析法により，珪藻は9群集，また水型は5水型に分けられた。両者の分布は常に一致するとは限らなかったが，それは海水の物理化学的性格よりも珪藻群集の方が保存的なためであると考えられる。この海域の背景をなすように最も広く分布する群集を背景群集と名付けたが，その主要構成種は沿岸性コスモポリタン種であり，群集密度は低かった。広く背景をなす極前線の混合水の表層に異水型が流入したときに，珪藻群集の生産が促進され，異なった種組成の珪藻群集が新しく形成されるらしいことがわかった。

La mer 32: 209–213, 1994
Société franco-japonaise d'océanographie, Tokyo

資　料

雨台風による高潮について*

中　村　重　久**

On Storm Surge at Typhoon with Packed Heavy Rain*

Shigehisa NAKAMURA**

Abstract: Storm surge caused by typhoon with packed heavy rain is studied using the sea level records on the coast of the Japanese Islands in 1993. One case of typhoon 9311 brought a heavy rain in the urban area of Tokyo, which induced storm surge in the eastern Japan mainly by barometric effect. The other case is that of typhoon 9313 which caused a heavy rain as a trigger of land slides in Kagoshima, Kyushu. No hazardous storm surge was observed at typhoon 9313 in the coastal zones. There are left many problems to be solved at evaluationg storm surge quantitatively.

1. 緒　言

太平洋北西部でも，日本列島は台風高潮による被害が顕著である．しかし，来襲した台風のすべてが被害をもたらすというわけではない．稲作農業に慈雨をもたらすものもある。

ここでは，とくに雨台風といわれる分類に属する台風が，日本列島に来襲したときにどのような高潮があらわれるかについて述べたい。

2. 台風高潮研究の概要

現在，台風についての研究は気象庁において推進されており，これにともなう高潮予報の問題もとりあげられている。理論解析による研究は，1930年代（たとえばNOMITSU, 1934）に多数みられた。高潮の数値計算は，HANSEN(1956)によってはじめて実用的なものとなった。中村(1990)は，日本列島周辺の台風高潮パターンについて検討した。さらに，台風高潮の陸棚沿岸域における特性も検討している（中村, 1991; 1992)。ただ，これまでの研究では，台風の気圧や強風の効果に注目されていた。ここでは，いわゆる雨台風の場合の台風高潮の例を述べる。

*1994年7月20日受理　Received July 20, 1994
**京都大学防災研究所附属白浜海気象観測所
〒649-22　和歌山県西牟婁郡白浜町堅田畑崎
Shirahama Oceanographic Observatory, Disaster Prevention Research Institute, Kyoto University, Katada-Hatasaki, Shirahama, Wakayama 649-22 Japan

3. 雨台風の最近の例

台風には，強風の影響が顕著な風台風や，豪雨の影響が顕著な雨台風など，いろいろの特徴をもったものがある。とくに，雨台風の最近の例としては，1993年の台風11号および13号をあげることができる。

（1）台風9311号の例

台風は，Fig. 1に示すように1993年8月26日夕刻には八丈島へ進路を向け，27日朝には八丈島東南海上を20 km/時の速さで北上（台風中心気圧 970 hPa），千葉県九十九里浜付近に上陸の後，北上し，28日夕刻には釧路北方で熱帯低気圧となった。この台風のため，27日には首都圏は豪雨となり，広域にわたって浸水状態となった。

（2）台風9313号の例（cf. Fig. 1）

台風は，西日本の各地を襲い，九州から四国，中国地方を縦断した後日本海に抜け，1993年9月4日21時までに温帯低気圧になった。この台風が直撃した鹿児島県では，川辺郡川辺町小野の鉄砲水や，日置郡金峰町大坂の山崩れなど，豪雨が原因で被害が生じた。被害は全国32府県に及び，政府は22省庁による災害対策関係省庁連絡会議を招集した。

このように，雨台風の例では沿岸域での海岸災害についてはとくに情報がないようである。しかし，それでも台風9313号では，日本海において波の高さが4〜6mになった（たとえば，新聞記事など）ことは事実である。

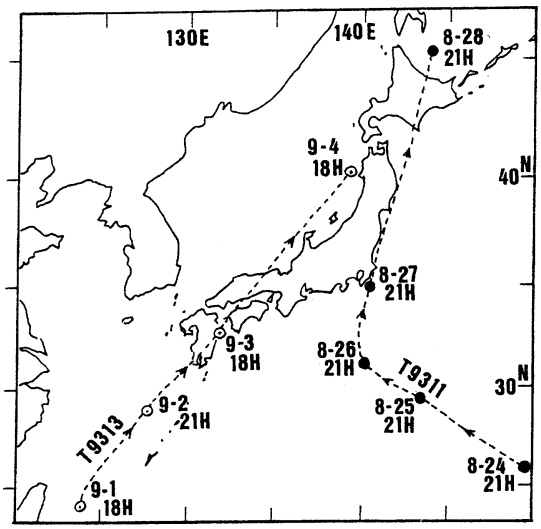

Fig. 1. Tracks of typhoon 9311 and 9313.
1) As for typhoon 9311, during period of 21h on 24 August to 28 August 1993.
2) As for typhoon 9313, during period of 18h on 1 September to 4 September 1993.

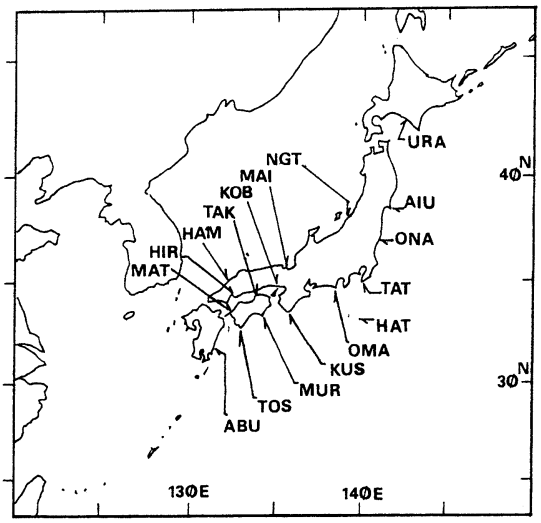

Fig. 2. Location map of the tide stations.
Notations are ABU for Aburatsu, TOS for Tosa-shimizu, MUR for Muroto－misaki, KUS for Kushimoto, OMA for Omaezaki, HAT for Hachijyo-jima, TAT for Tateyama, ONA for Onahama, AIU for Ayukawa, URA for Urakawa, NGT for Niigata, MAI for Maizuru, KOB for Kobe, TAK for Takamatsu, HAM for HAMADA, HIR for Hiroshima and MAT for Matsuyama.

4. 検潮記録

前述の雨台風2例の経路はFig. 1に示し，この台風による高潮の検討のために用いた記録は，気象庁所管の検潮所のもの（Fig. 2）を利用した。

5. 首都圏に浸水を起した台風の例

台風9311号は，首都圏に豪雨と浸水とをもたらしたが，沿岸域では高潮を起した（cf. Fig.3）。八丈島（土底港）では，台風北上にもとない気圧の効果（破線）が最大となる前後で，高潮の特徴を表す潮位変動があらわれている。この図では，推算潮位（主として天文潮の効果）を除いているので，実線で示した高潮は気圧低下の効果，風の吹き寄せ効果，周辺地形の効果などを含む非線型効果をすべてが重なっているものとみられる。

本州太平洋沿岸での台風9311号による高潮は，Fig. 3のようになる。図中の矢印は，最低気圧を記録した時刻である。気圧低下の効果を静的気圧で換算できるものとして，その効果を除いた潮位偏差が得られることになる。

このFig. 3をみると，台風は三陸沿岸沖を北上しているとき，高潮は気圧低下の効果ではほとんど説明できそうである。しかも高潮はそれほど顕著なものではない。検潮記録にあらわれた潮位変動の一部は，検潮儀の設置状況を十分考慮しなくては理解できそうには思えない。

6. 鹿児島県に災害を起した台風の例

台風9313号は，鹿児島県に豪雨と山崩れによる被害をもたらしただけではなく，32府県にわたって被害をもたらした。この場合についても，前の例のように天文潮を除いた高潮を図示した。これがFig. 4である。

このFig. 4をみると，豊後水道海域周辺の油津，土佐清水，松山では気圧が最低になる前に，すでに高潮のピークがみとめられる。これは，風向を考慮にいれると，風の吹き寄せ効果によるものと言える。瀬戸内海の広島，高松，神戸では，気圧が最低となった後に高潮のピークが出る。これも，台風通過後西寄りの風が強くなることによるものであろう。さらに日本海沿岸では，浜田で神戸によく似た高潮ピークのあらわれ方が認められる。それに，台風接近前から約20cmの振幅の半日周期程度の潮位変動が持続している。しかし舞鶴では，気圧が最低となった後，約6時間後に負の高潮があらわれている。浜田のような半日周期程度の潮位変動は舞鶴では認められない。また新潟では，台風の接近とともに負の高潮が顕著となり，気圧が最低となった後（台風通過後）は，潮位はまもなく台風の影響のあらわれる前の状態に戻っ

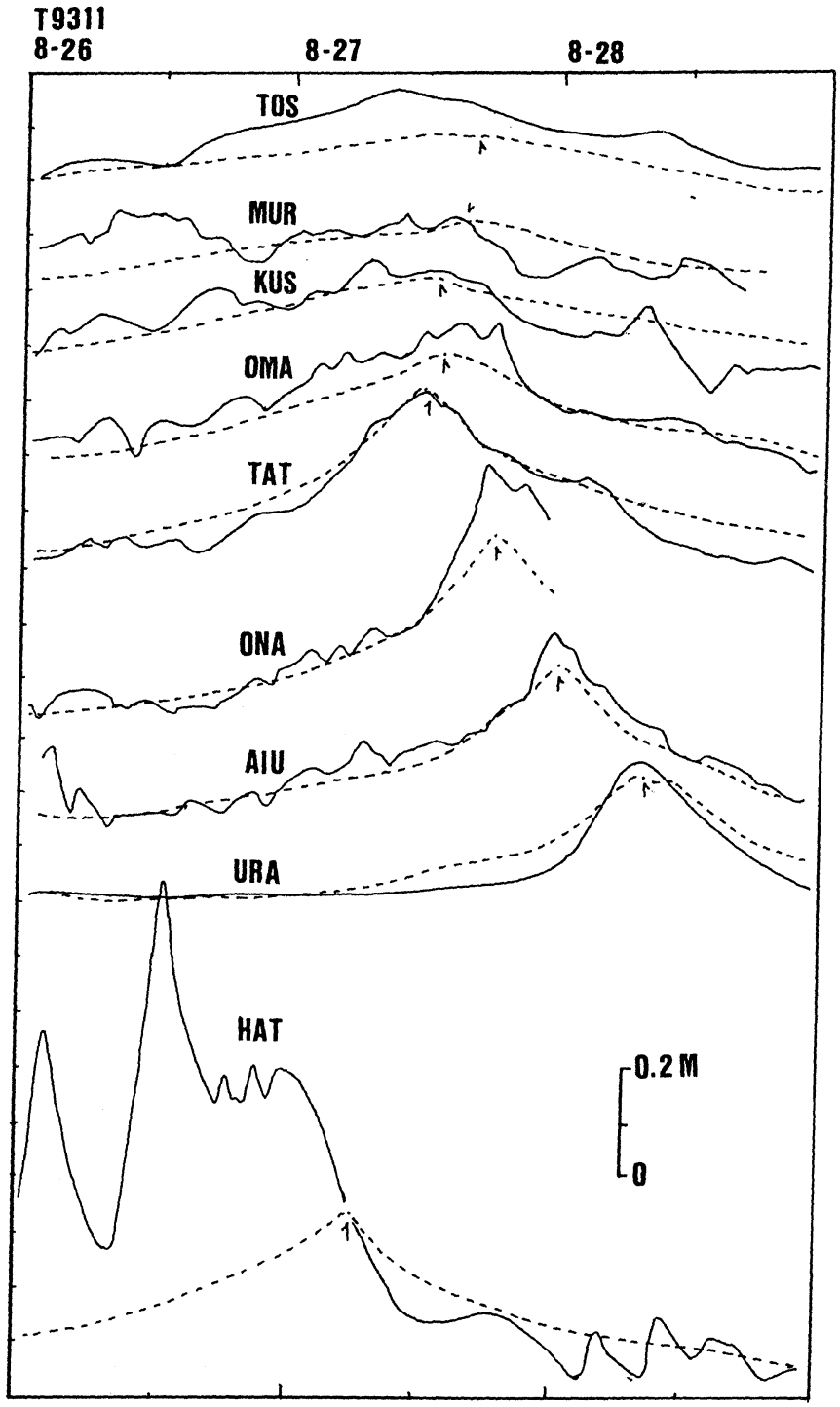

Fig. 3. Meteorological anomaly (solid line) of the sea level and the inversed barometric variations (broken line) with arrow indicated the time of the minimum pressure of the atmosphere, for typhoon 9311.

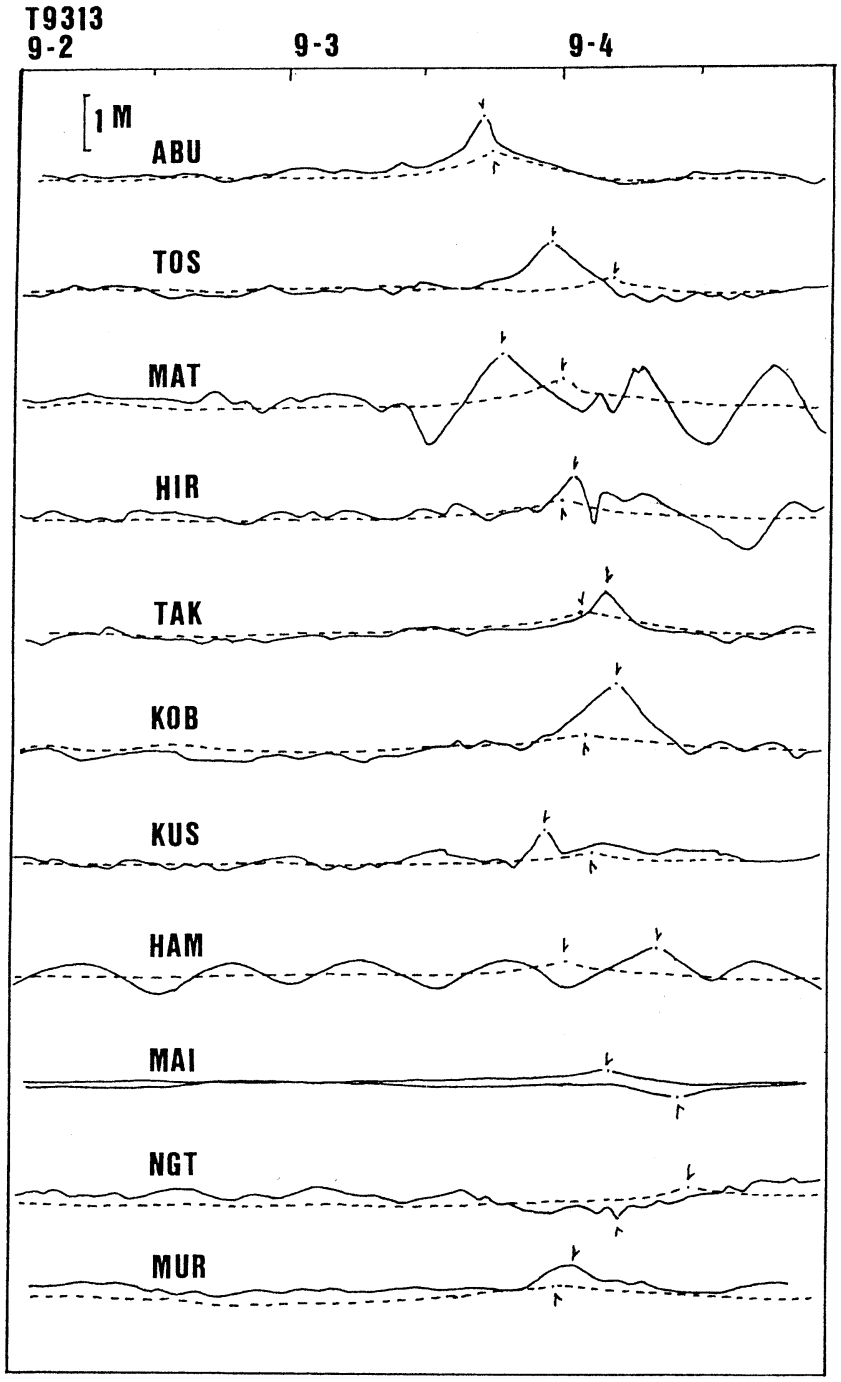

Fig. 4. Meteorological anomaly (solid line) of the sea level and the inversed barometric variations (chain line) with arrow indicated the time of the minimum pressure of the atmosphere and the maximum of the sea level, for typhoon 9313.

ている。これに加えて，室戸岬，串本，神戸の高潮をみると，紀伊水道から，台風の影響で生じた潮位変動が大阪湾に侵入し，神戸の高潮を大きくしているものと解釈される。いづれにしても，台風を中心として形成された風の場の効果と台風の進行速度の効果とが有効に作用しているものとみてよいであろう（たとえば　中村，1992）。

ここで，Fig. 4 の高潮（実線）から気圧低下の効果（破線）を除くと，海と風の効果や地形など非線型効果が得られると考えられる。

7. 考　察

雨台風による高潮について，以上のように検討を加えたが，ここで対象とした台風9311および9313号の例では，台風高潮が甚大な災害の原因とはなっていないこと，そして高潮は，気圧低下の効果あるいは風の効果によって定性的に理解できそうなことを指摘した。

ところで，これまでの研究例をみると，理論的研究としてのNOMITSU (1934) の論文では，気圧低下の効果のみが考慮されている。HANSEN (1956) は，海上の気象条件を考慮して，気圧と風とをあわせて数値モデルを構成している。それ以後，台風高潮の数値モデルは改良を重ねられて現在に至っているが，日本では東京湾，伊勢湾，瀬戸内海東部，瀬戸内海西部，有明海に限って，数値モデルが利用されている。中村 (1991; 1992) は，陸棚沿岸域における台風高潮について論じているが，本文の例は，また別の見地からあらためて検討する必要があるものと考えられる。とくに台風の経路に沿って，大気と海洋との間でのエネルギー授受や水収支がどのようになっているかを十分考慮すべきであろう（たとえば，中村，1988）。

さて，本文中では風の効果という言葉を無造作に用いた。理論的根拠を明らかにさせるためには，たとえば，GILL and SCHUMANN (1974) のような手法で力学的な評価をしなくてはならない。しかし理論的モデルでは，現実に複雑な地形条件下での台風の挙動や台風高潮の定量的評価には大きな困難がある。現時点においては，定性的評価を，ひとつの目安とするべきであろう。残された問題点はまだ多数あるが，その解決には今後の検討をまたなくてはならない。

謝　辞

本研究をすすめるにあたって，気象庁ならびに海上保安庁の関係諸官の御好意を得て，気象資料および検潮記録などの利用をすることができた。ここに記して，心から感謝の意を表す。

文　献

GILL, A. E. and E. H. SCHUMANN (1974): The genration of long shelf waves by the wind. J. Phys. Oceanogr., **4**, 83–90.

HANSEN, W. (1956): Theorie zur Errechnung des Wasserstands und der stroemungen in Randmeeren nebst Anwendungen. Tellus, **8**, 287–300.

中村重久 (1988)：近畿圏沿岸の高潮災害の要因としての黒潮について．京都大学防災研究所年報，No.31 B-2，753–773.

中村重久 (1990)：日本列島周辺の台風高潮のパターン２例．La mer, **28**, 58–62

中村重久 (1991)：陸棚沿岸における台風高潮について．京都大学防災研究所年報，No.34B-2，471–492.

中村重久 (1992)：陸棚沿岸域における台風高潮について．京都大学防災研究所年報，No.35B-2, 215–230.

NOMITSU, T. (1934): Coast effect upon the ocean current and the sea level. II. Changing state, Mem. Coll. Sei. Univ.Kyoto, Ser. A, **17**, 249–280.

La mer 32: 215–221, 1994
Société franco-japonaise d'océanographie, Tokyo

学 会 記 事

1. 1994年5月13日（金） 東京水産大学において平成6年度評議員会が開かれた。

主要な議事は下記のとおり。

1）平成6，7年度評議員選挙結果報告　資料に基づいて報告が行われた。

2）平成6，7年度会長選挙結果報告　資料に基づいて報告が行われた。

3）平成6，7年度副会長，幹事，監事の選出

下記のとおり選出した。

副会長	高木和徳　岡市友利
幹事（庶務）	須藤英雄，有元貴文
（会計）	森永　勤，岸野元彰
（編集）	佐藤博雄　落合正宏
（研究発表）	関　文威，小池勲夫
（渉外）	佐伯和昭，隆島史夫
監事	久保田穣，辻田時美
編集委員会委員長	山口征矢

なお，会長から佐藤博雄，落合正宏，佐伯和昭各幹事，および久保田穣監事の4名を評議員に追加することが提案され，承認された。

4）平成5年度事業報告

5）平成6年度学会賞受賞候補者選考経過報告

6）平成5年度収支決算報告および監査報告

7）平成6年度事業計画案審議

原案どおり承認した。

8）平成6年度予算案審議

原案どおり承認した。

9）平成6年度学会賞受賞候補者推薦委員会委員選出

下記のとおり選出した。

青木三郎，今脇資郎，落合正宏，鎌谷明善，岸野元彰，小池勲夫，高野健三，竹松　伸，谷口　旭，中村重久，松生　洽，村野正昭，門谷　茂，柳　哲雄，山口征矢

10）その他

① 学会誌の原著論文等については，奇数ページ起こしとすることにしたので，現在無料掲載となっている7印刷ページを偶数に改める必要がある。6ページまで無料という方向で編集委員会で投稿規定の見直しを行うこととした。

② 平成6年度の予備費に余裕があれば，学会賞のメダルを10個程度まとめて製作する。

③ 1995年の日仏学術シンポジウムについては，フランス側からテーマ等についての問い合わせがきている。

④ 文部省から，平成6年度科学研究費補助金「研究成果公開促進費」に係わる「研究成果公開発表（B）」（社会人・青少年を対象に，当該学問分野の最新の研究動向等を普及啓蒙するために開催するシンポジウムや学術講演会の開催経費の一部を助成する事業）の募集がきている。今年度は準備不足で応募は困難であるが，明年度からはこの制度を積極的に利用できるよう準備することとした。

2. 1994年5月30日（月） 日仏会館会議室において平成6年度日仏海洋学会学術研究発表会が開催された。

発表題目と発表者は下記のとおり。

午前（10：00〜12：00）

座長　森永　勤（東水大）

1．北極海（バレンツ・カラ海）の水塊特性
……和田　明（東海大海洋）

2．日本海10m 深表層水の水温－塩分度数分布
……須藤英雄（東水大）

3．海嶺上の内部波の構造
……○北出裕二郎・松山優治・千手智晴・石丸　隆（東水大）

座長　佐藤博雄（東水大）

4．鶴見川河口域における懸濁態有機物の挙動
……○落合正宏・清水裕一（都立大理）

5．東京湾における植物プランクトンの最大光合成活性の年変動とその要因
……石田興三・○山口征矢（埼玉大教養）

6．アサリ摂餌粒子の量・大きさ
…○荒川久幸・矢尾板俊秀・森永　勤（東水大）

午後（13：00－14：20）

座長　山口征矢（東水大）

7．冬季，アラビア湾（海鷹丸55次航海）における動物プランクトンの生物量と生産量
……○野村英明・森　潔・石丸　隆・村野正昭（東水大）

8．*Gnathia* sp.（等脚類）の組織形態と生活史

……○本間義治・石見喜一（新潟大理）・
千葉　晃（日本歯科大新潟）・
布村　昇（富山市科学文化センター）

9．飼育下に於ける小型歯鯨類の個体間行動
……○山田　裕（東水大）・毛利国明・
三橋孝夫（サンシャイン国際水族館）

10．アラビア湾における原油流出に関する研究－潮間帯堆積物中の漂着風化油の鉛直分布－
……○佐藤博雄・辻本　良・田畑彰久（東水大）

3．1994年5月30日（月）　日仏会館会議室において第35回（平成6年度）総会が開催された。議事の概要は下記のとおり。

議長：有賀会長

1）平成5年度事業報告

a）庶務

会員移動状況

	5年4月	入会	退会	6年4月
名誉会員	3	－	－	3
正会員	300	9	9	300
学生会員	2	1	0	3
賛助会員	22	1	4	9

活動状況

評議員会　1回(5/27)
幹事会　3回(5/27, 8/31, 1/28)
総会　1回（5/31　日仏会館）
学会誌の発行　31巻2号～32巻1号
学会賞授与　岸野元彰（理化学研究所）（5/31　日仏会館）
平成6，7年度評議員，会長選挙
日本学術会議第16期会員選出にかかる学術研究団体の登録，会員の候補者および推薦人（予備者を含む）の届出（第4部　水産学研究連絡委員会）
会員の候補者　有賀祐勝　　推薦人　須藤英雄
推薦人予備者　山口征矢
日仏会館学者交換事業（日仏会館）候補者の推薦
八木宏樹
講演会の共催・協賛
日本学術会議シンポジウム「海の生態系と生物資源－環境との調和をめざして」（8/27日本学術会議）（共催）
日本学術会議主催アジア学術会議（11/15－18　東京）（後援）
理化学研究所第16回科学講演会（10/22仙台）（協賛）
フランクフルト・ブックフェアー'93「学協会誌」展示会への学会誌の出展(10/6-11)

b）編集

La mer 30/3（第6回JECSS シンポジウム・プロシーディングズ），30/4，31/1（前年度分合計334頁）
31/2－32/1の4号を平成5年度文部省科学研究費補助金研究成果公開促進費の補助を得て刊行
英文　原著13（12）編 124（124）頁
その他計134（134）頁
和文　原著8（10）編 53（76）頁
その他計128（122）頁
（　）内は計画頁数

c）平成6，7年度役員，評議員選出結果報告

佐藤博雄，落合正宏，佐伯和昭各幹事および久保田穣監事の4名を評議員に追加する。

2）平成5年度収支決算報告および監査報告

収　入

前年度繰越金	160,226
正会員会費	1,070,000
学生会員会費	12,000
賛助会員会費	200,000
学会誌売上金	1,195,800
広告料	150,000
著書負担印刷費	1,083,427
雑収入	302,837
寄付金収入	0
国庫	1,140,000
計	5,314,380

支　出

学会誌等印刷費	3,934,179
送料・通信費	326,000
事務費	707,693
交通費	23,760
会議費	26,638
学会賞経費	71,704
雑費	27,391
次年度繰越金	297,015
計	5,314,380

3）平成5年度事業計画案審議

評議員会1回，総会1回，学術研究発表会1回，

幹事会4回
シンポジウムおよび講演会の開催
学会誌の発行（4号）
平成6年度学会賞授賞および平成7年度年度学会賞受賞候補者推薦
日仏会館学者交換事業による会員のフランス派遣（八木宏樹会員）
日本学術会議第16期研究連絡委員会委員候補者の推薦
第7回日仏学術シンポジウム（1995年日本）参加の準備
その他

4）平成6年度収支予算案審議

平成6年度収支予算

収 入

前年度繰越金	297,015
正会員会費	1,800,000
学生会員会費	40,000
賛助会員会費	200,000
学会誌売上金	345,000
広告料	200,000
著書負担印刷費	600,000
雑収入	50,000
寄付金収入	1
国庫	1,140,000
計	4,674,016

支 出

学会誌等印刷費	2,450,000
送料・通信費	250,000
事務費	700,000
交通費	20,000
会議費	15,000
学会賞経費	75,000
雑費	10,000
予備費	1,152,016
計	4,672,016

5）その他

4. 平成6年度日仏海洋学会賞

受賞者：門谷 茂（香川大学）

受賞課題：浅海域の生物起源粒子の生成・崩壊課程に関する化学的研究

推薦理由：海水の濁りはその中に含まれる微細な粒子によるが，その構成は主として動・植物プランクトンなどの微生物，それに由来するデトライタスと呼ばれる破屑物からなっており，一般的に懸濁物といわれている。最近ではこの懸濁物中の比較的沈降しやすい粒子は沈降粒子として，沈降物捕集器で集められ，その形態や化学分析結果からいわゆる懸濁物と区分されるようになった。海水中にはこのような微細な粒子以外に比較的大きな粒子が浮遊しているのが認められ，浅海域ではヌタなどと呼ばれている。また，比較的深い海ではマリンスノーと呼ばれる大きな粒子の存在も知られている。しかし，このような大型の浮遊性粒子の海洋生態学的重要性は，指摘されながらも採集時に壊れ易いなどの理由で研究はほとんど進んでいなかった。

この浮遊性大型粒子（以下，NUTA と称する）が，粘着性を有することに注目して，網のなかにガラスウールを入れ，NUTA をガラスウールに付着させて捕集する方法を考案して，これによって採集されたものを「NUTA」として，海水中の他の微細粒子との科学的性質の違いおよびその存在量などを調べ，それにより NUTA の海洋生態的役割について考究した。

NUTA は懸濁粒子にくらべて POC/ATP，C/Chl. *a* 比が大きいことや，成分濃度の違いなどから，NUTA には生きている植物プランクトンはほとんど含まれていないことを明らかにした。アミノ酸組成のクラスター分析の結果および植物色素の組成から，NUTA は懸濁粒子よりも沈降粒子に近いことが示されている。NUTA が懸濁粒子全体に対してどの位含まれるかは極めて興味があるところで，特に瀬戸内海のような浅海域では，環境保全と共に動物プランクトンや稚魚の飼料としての役割からみて検討すべき重要な点であった。この点については，スキューバサンプリングを行い，小型密閉型の採水器で NUTA を破壊しないように採水して，その評価を行った。その結果によれば表層から10m の水柱当たりで全懸濁粒子中の30～40%を占めること，1日当り NUTA の現存量の10～20%が沈降していることを見積もった。本研究ではまた，NUTA を構成するアミノ酸の必須アミノ酸は70～80にあり，飼料として十分栄養学的意味を有することおよび分解実験によれば NUTA からかなりの栄養塩類が溶出し，NUTA がバクテリアその他の微小生物の活動の場を与えていることにより，NUTA が栄養塩類の循環に重要な働きをしている

ことを示した。

これらの結果は，現在量の推定にまだ多少検討の余地を残すものの，海洋生態学的に極めて重要な知見を提供したものということができる。

本研究では，「NUTA は植物プランクトン等が枯死してデトライタス化した粒子群がお互いに絡みあって大型化した巨視的粒子であり，空隙率が大きいために沈降速度は遅い粒子群」であると定義した。海洋の懸濁物はこれまで懸濁粒子と沈降粒子の二つの群として研究されてきたが，これに浮遊性巨視的粒子としてのNUTA を分画し，その化学的性質が前二者と異なっており，海水中の第三番目の粒子群として位置付けを明らかにしたとの意義は大きい。さらにNUTA が飼料として，又栄養塩の再生，循環に大きな働きをしているとの指摘も重要な考えである。

本委員会は門谷　茂博士の研究を高く評価し，本学会賞を受賞するにふさわしい候補者としてここに推薦する。

学会賞受賞候補者推薦委員会
委員長　柳　　哲雄

主　要　論　文

1. Flux of Nitrogen compounds in coastal marine sediment and pore water (Funka Bay, Hokkaido), Chemical Geology, **30**, 35-45, (1980) (with Maita Y. and Fukase S.)

2. Early diagenesis of amino acids in Okhotsk Sea sediments, Deep-Sea Research, **29**, 485-498, (1982) (with Maita Y. and Ishii J.)

3. Possible occurrence of diatom cell wall-derived amino acids in Okhotsk Sea sediments, Geochemical Journal, **16**, 259-262, (1982) (with Maita Y. and Fukase S.)

4. Amino acid variations in marine particles during sinking and sedimentation in Harima Nada, the Seto Inland Sea, Japan, Marine and Estuarine Geochmistry, 15-27, (1985) (with Okaichi T.)

5. 播磨灘堆積物中の有機炭素・窒素，全リンおよびフェオフィチンの水平分布，La mer, **25**, 67-72, (1987) (多田邦尚，岡市友利と共著)

6. Purine and pyrimidine bases in marine particles in the Seto Inland Sea, Japan, Marine Chemistry, **25**, 359-371, (1988) (with Tada K. and Okaichi T.)

7. Changes in cell chemical composition during the life cycle of *Scrippsiella trochoidea* (Dinophyceae), Journal of Phycology, **26**, 299-306, (1990) (with Lirdwitayaprasit T., Okaichi T., Ochi T. and Anderson D.M.)

8. The nature and distribution of large amorphous particles (NUTA) in Osaka Bay, Japan, Geochemical Journal, **24**, 197-206, (1990) (with Mishima Y. and Okaichi T.)

9. 巨視的浮遊性大型粒子 (NUTA)，採取装置の開発と懸濁粒子・沈降粒子との関係　La mer, **28**, 123-130, (1990) (三島康史，岡市友利と共著)

10. Scavenging processes of marine particles in Osaka Bay, Marine Pollution Buletin, **23**, 107-111, (1991) (wite Mishima Y. and Okaichi T.)

11. 大阪湾の富栄養化の現状と生物によるNとPの循環 沿岸海洋研究ノート，**29**, 13-27, (1991) (三島康史，岡市友利と共著)

12. 播磨灘堆積物中の核酸塩基類の水平分布. La mer, **29**, 57-61, (1991) (多田邦尚，岡市友利と共著)

13. Some characteristic features of large amorphous particles (NUTA) in Seto Inland Sea, Japan, Journal of the Oceanographical Society of Japan, **47**, 276-285, (1991) (with Mishima Y. and Okaichi T.)

14. Modification of chemical characteristics of organically enriched sedimen by *Chattonella* sp., Marine Pollution Bulletin, **26**, 375-379, (1993) (with Chareonpanich C., Tsutsumi H. and Matsuoka S.)

15. The role of NUTA (large amorphous particles) as a nutrient regenerator in Osaka Bay, Journal of Oceanography, **49**, 285-293, (1993) (with Mishima Y.)

16. Changes in chemical components and energy charge during growth cycle of *Chattonella antiqua*, Nippon Suisan Gakkaishi, **59**, 1737-1743, (1993) (with Meksumpun S., Lirdwitayaparasit T., Sakamoto H., Ochi T. and Okaichi T.)

17. Changes in cellular contents of nucleotides during the growth processes of two marine

dinoflagellates, Bulletin of Plankton Society of Japan, **40**, 105-112, (1994) (with Meksumpun S. and Okaichi T.)

5. 新入会員

（正会員）

氏 名	所属・住所	紹介者
小松輝久	〒164 東京都中野区南台1-15-1 東京大学海洋研究所漁業測定部門	竹内一郎
中嶋秀夫	〒724 広島県東広島市鏡山1-4-1 広島大学工学部共通講座環境基礎学	柳 哲雄
真鍋武彦	〒669-65兵庫県城崎郡香住町香住1852 兵庫県但馬水産事務所試験研究室	
望月敬美	〒108 東京都港区港南4-5-7 東京水産大学練習船	森永 勤

6. 住所変更

（正会員）

花本栄二 〒102 神奈川県三浦市三崎町城ケ島
神奈川県水産試験場

市川 香 〒790 愛媛県松山市文京町3
愛媛大学工学部土木海洋工学科

（賛助会員）

㈱本地郷 〒101 千代田区神田須田町2-2-4
須田町藤和ビル7F

7. 退 会

（正会員） 小牧勇蔵，青木 斌

8. 受贈図書（受領順）

海洋産業研究資料 25(5,6,7,8)
農業工学研究所ニュース 7
農業工学研究所年報 5
農業工学研究所報告 33
日本学術会議月報 35(5,6,7)
日本学術会議だより 33
養殖研究所研究報告 23
養殖研ニュース 27
養殖研究所大村支所観測記録 12
東北区水産研究所研究報告 56
しおざい 10
水産工学研究所研究報告 15
水産工学研究所技報 16
Bulltin of Marine Sciences and Fisheries Kochi University 13
日本海区水産研究所研究報告 44
Environmental Management in Aquaculture 1
NTT-R & D 43(6)
海洋観測資料カタログ 4,5
海洋研究所年報 15
海洋研究所研究報告 15
Proceedings of the International Symposium of Fisheries in Conjunction to the 30th Anniversary of the School of Marine Science and Technology, Tokai University
海産研NEWS 26
広島日仏協会報 125
日本航海学会誌 120
陸棚沿岸の高潮
海洋調査報告一覧
なつしま 131
国内海洋調査一覧
Proceedings of The Hakuho Maru Cruise KH 91-4
Chinese Science Bulletin 39 (1-10)
水産学報 18(1)
青島海洋大学学報 24 (1,2)
Aquatic Living Resources 7 (1,2,3)
Journal of the Korean Society of Oceangraphy 29 (1,2)

お詫び

前記の評議員会および総会に提出された資料の中で、平成6年度学会賞受賞候補者推薦委員会委員の氏名のうち「阿部友三郎」氏は「岸野元彰」氏の誤りでした。誠に申しわけありませんでした。お詫びして訂正させていただきます。

会長 有 賀 祐 勝

お 知 ら せ

"JECSS and CREAMS*"

I have noticed in recent publications like JOSJ and La mer that United States of America and European Oceanographic Community do not respond to calls by Japanese oceanographers or there is no indication of participations by U.S. or European oceanographers in these Japanese calls for international research program.

Of course, oceanographers of Korea, China and Japan participate. But without participation from U.S.A. and European oceanographers, the most important group of the world oceanographic community, the program will not succeed.

Takashi Ichiye
NE 855 "D" St., Pullman, WA 99163, U.S.A.

*Circulation Research of the East Asian Marginal Seas

Creams Secretary Office
Prof. Jong-Hwan Yoon, Prof. A. Ostrovskii
Research Institute for Applied mechanics
Kyushu University
6-1 Kasuga-koen, Kasuga, Fukuoka,
816 Japan
Telephone: 81-92-573-9611 ex. 755
Telefax: 81-92-582-4201 (to RIAM/Kyushu Univ.)
e-mail: e76104a@kyu-cc.cc.kyushu-u.ac.jp

第17回 理化学研究所科学講演会が開催されます

主 催：理化学研究所
後 援：科学技術庁
協 賛：日仏海洋学会，関連学・協会
日 時：平成6年10月26日（水） 10：00～17：05
会 場：ヤクルト本社ビル ヤクルトホール
〒105 東京都港区東新橋1－1－19
電話 03（3574）7255（代表）

〔プログラム〕

第I部

10：00～10：20
理研における脳・神経科学研究への取り組み
理化学研究所 国際フロンティア研究システム長
伊藤 正男

［講 演］

10：20～11：00
脳はどのように形を見分けるか
理化学研究所 国際フロンティア研究システム
思考電流研究チームリーダー
田中 啓治

11：00～11：40
脳の学習の多様性—人とネズミの動作
南カリフォルニア大学教授 神経工学センター所長
マイケル アービブ

11：40～12：20
物質科学と情報科学の相互作用による脳科学の新展開
理化学研究所 国際フロンティア研究システム
脳回路モデル研究チームリーダー
田中 繁

12：20～12：30 質疑応答

第II部

14：00～14：10
挨 拶 理化学研究所 理事長
有馬 朗人

〔講 演〕

14：10～14：50
脳と心
理化学研究所 国際フロンティア研究システム長
伊藤 正男

［14：50～15：10 休憩］

15：10～15：50
脳がつくられるしくみ
理化学研究所 分子神経生物学研究室
主任研究員 御子柴 克彦

15：50～16：30
脳とコンピューター—人工頭脳の実現に向けて
理化学研究所 国際フロンティア研究システム
情報処理研究グループ ディレクター
甘利 俊一

16：30～17：00 質疑応答

17：00～17：05
閉会 理化学研究所 副理事長
長柄 喜一郎

日仏海洋学会役員・評議員

(1994–1995年度)

顧　　問：ユーベル・ブロシェ　ジャン・デルサルト　ジャック・ロベール　アレクシス・ドランデール　ベルナール・フランク　ミシェル・ルサージュ　ローベル・ゲルムール　ジャック・マゴー　レオン・ヴァンデルメルシュ　オーギュスタン・ベルク　ユーベル・セカルディ

名誉会長：オリビエ・アンサール

会　　長：有賀　祐勝

副 会 長：高木　和徳　岡市　友利

幹　　事：（庶務）　須藤　英雄　有元　貴文
（会計）　森永　　勤　岸野　元彰
（編集）　佐藤　博雄　落合　正宏
（研究）　関　　文威　小池　勲夫
（渉外）　佐伯　和昭　隆島　史夫

監　　事：久保田　穣　辻田　時美

編集委員長：山口　征矢

評 議 員：有元　貴文　有賀　祐勝　石丸　　隆
今脇　資郎　宇野　　寛　大塚　一志
岡市　友利　奥田　邦明　落合　正宏
梶浦欣二郎　金成　誠一　鎌谷　明善
岸野　元彰　国司　秀明　久保田　穣
黒田　一紀　小池　勲夫　佐伯　和昭
坂本　　亘　佐藤　博雄　杉森　康宏
須藤　英雄　関　　文威　関根　義彦
平　　啓介　高木　和徳　隆島　史夫
高野　健三　高橋　正征　谷口　　旭
辻田　時美　寺崎　　誠　寺本　俊彦
鳥羽　良明　中田　英昭　永田　　豊
中村　重久　奈須　敬二　西沢　　敏
畑　　幸彦　半沢　正男　堀越　増興
前田　明夫　松生　　洽　松村　皐月
松山　優治　丸茂　隆三　村野　正昭
森田　良美　森永　　勤　柳　　哲雄
山口　征矢　和田　　明　渡邊　精一

賛　助　会　員

阿　部　嘉　方	東京都練馬区春日町 2-15-6
株式会社 内田老鶴圃　内田　悟	東京都文京区大塚 3-34-3
有限会社　英和出版印刷社	東京都北区中里 2-7-7
株式会社　カイジョウ	東京都西多摩郡羽村町栄町 3-1-5
㈶ 海洋生物環境研究所	東京都千代田区内神田 1-18-12　北原ビル内
株式会社　川合海苔店	東京都大田区大森本町 2-31-8
株式会社　自然・情報環境研究所	横浜市栄区桂町 1-1，3-401
新日本気象海洋株式会社	東京都世田谷区玉川 3-14-5
全日本爬虫類皮革産業連合会	東京都足立区梅田 4-3-18
株式会社　高　岡　屋	東京都台東区上野 6-7-22
株式会社東京久栄技術センター	埼玉県川口市芝鶴ケ丸 6906-10
株式会社西日本流体技研	長崎県佐世保市棚方町 283
日本アクアラング株式会社	神奈川県厚木市温水 2229-4
㈱ 三菱総合研究所 (社会情報システム部)	東京都千代田区大手町 2-3-6
㈱　本　地　郷	東京都千代田区神田須田町 2-2-4　須田町藤和ビル７F
株式会社　読売広告社	東京都中央区銀座 1-8-14
渡辺機開工業株式会社	愛知県渥美郡田原町神戸大坪 230
株式会社　渡部計器製作所	東京都文京区向丘 1-7-17

代表取締役　宮本　悟　取締役　大塚昌治

日仏海洋学会入会申込書

（正会員・学生会員）

	年度より入会	年　月　日申込
氏　名 ローマ字		年　月　日生
住　所　〒 勤務先　機関名 電　話		
自　宅　住　所　〒 電　話		
紹介会員氏名		
送付金額　円	送金方法	
会誌の送り先（希望する方に○をつける）	勤務先　自　宅	

（以下は学会事務局用）

受付	名簿 原簿	会費 原簿	あて名 カード	学会 記事

入会申込書送付先：　〒101　東京都千代田区神田駿河台 2-3

(財)日仏会館内

日仏海洋学会

郵便振替番号：00150-7-96503

投稿の手引

1. 「うみ」（日仏海洋学会機関誌；欧文誌名 La mer）は，日仏海洋学会正会員およびそれに準ずる非会員からの投稿（依頼稿を含む）を，委員会の審査により掲載する。
2. 原稿は海洋学および水産学両分野の原著論文，原著短報，総説，書評，資料などとする。すべての投稿は，本文，原図とも正副2通とする。副本は複写でよい。本文原稿用紙はすべてA4判とし，400字詰原稿用紙（和文）に，または厚手白紙にダブル・スペース（和文ワープロでは相当間隔）で記入する。表原稿および図説明原稿は，それぞれ本文原稿とは別紙とする。
3. 用語は日，仏，英3カ国語の何れかとする。ただし，表および図説明の用語は仏文または英文に限る。原著論文（前項）には約200語の英文または仏文の要旨を，別紙として必ず添える。なお，欧文論文には，上記要旨の外に，約500字の和文要旨をも添える。ただし，日本語圏外からの投稿の和文要旨については編集委員会の責任とする。
4. 投稿原稿の体裁形式は最近号掲載記事のそれに従う。著者名は略記しない。記号略号の表記は委員会の基準に従う。引用文献の提示形式は，雑誌論文，単行本分載論文(単行本の一部引用を含む)，単行本などの別による基準に従う。
5. 原図は版下用として鮮明で，縮尺（版幅または1/2版幅）に耐えられるものとする。
6. 初校に限り著者の校正を受ける。
7. 正会員に対しては7印刷ページまでの掲載を無料とする。ただし，この範囲内であっても色彩印刷を含む場合などには，別に所定の費用を著者負担とすることがある。正会員の投稿で上記限度を超える分および非会員投稿の印刷実費はすべて著者負担（10,000円/頁）とする。
8. すべての投稿記事について，1篇あたり別刷50部を無料で請求できる。50部を超える分は請求により，50部単位で作製される。別刷請求用紙は初校と同時に配布される。
9. 原稿の送り先は下記の通り。

〒108 東京都港区港南4-5-7 東京水産大学　山口征矢 気付
日仏海洋学会編集委員会

1994年8月25日 印刷
1994年8月28日 発行

うみ　第32巻 第3号

定価 ¥1,600

編集者　山口征矢
発行所　日仏海洋学会
財団法人 日仏会館内
東京都千代田区神田駿河台2-3
郵便番号：101
電話：03(3291)1141
振替番号：00150-7-96503
印刷者　佐藤一二
印刷所　㈲英和出版印刷社
東京都北区中里2—7—7
郵便番号：114
電話：03(5394)4856

(本誌出版費の一部は平成5年度文部省科学研究費補助金「研究成果公開促進費」による.)
Publication of La mer has been supported in part by a Grant-in-Aid for Publication of Scientific Research Result from the Ministry of Education, Science and Culture, Japan.

Tome 32 N° 3

SOMMAIRE

第 32 巻 第 3 号

目 次